Finite Element Analysis of Time Dependent Settlements Around Pile Structures

by

Lawrence Lo Chow

Thesis submitted to the Graduate Faculty of the
Virginia Polytechnic Institute and State University
in partial fulfillment of the requirements for the degree of
MASTER OF SCIENCE

in

Civil Engineering

APPROVED:

Dr. C. S. Desai, Chairman

Dr. R. D. Walker, Head

Dr. R. H. Plaut

June, 1977

Blacksburg, Virginia

ACKNOWLEDGEMENTS

I would like to thank , and for their advice and being my graduate committee members. During the progress of this research, gave me helpful suggestions and taught me many interesting finite element approaches and guided me.

I am also very grateful to of The Ohio State University for his suggestions on the computer program. Much appreciation is expressed to my mother for encouraging and supporting me to come to VPI & SU from the Republic of China.

Finally, I have greatly appreciated the financial support provided by the Department of Civil Engineering at VPI & SU.

TABLE OF CONTENTS

	Page
ACKNOWLEDGEMENTS	ii
LIST OF TABLES	v
LIST OF FIGURES	vi
CHAPTER	
I. INTRODUCTION	1
II. LITERATURE REVIEW	4
III. FINITE ELEMENT THEORY	7
Governing Equations	7
Time Integration	14
Matrix Formulation	16
Linear Porepressure Interpolation Over Triangular Elements	29
Coupling Matrix C	30
Boundary Quantities	30
IV. NEGATIVE SKIN FRICTION DUE TO CONSOLIDATION	32
Introduction	32
Soil Settlement Analysis	34
Proposed Method for Predicting Downdrag of Pile	35
V. FINITE ELEMENT APPLICATION FOR NEGATIVE SKIN FRICTION	37
Negative Skin Friction Due to Gravity Load	39
Negative Skin Friction Due to Backfill	54
The Influence of External Pile Load	66
The Influence of Time-Load History and Backfill	78

Page

VI. SUMMARY, CONCLUSIONS AND RECOMMENDATIONS 94

Summary 94

Conclusions and Recommendations 94

BIBLIOGRAPHY 97

VITA 100

LIST OF TABLES

Table		Page
1.	Garlanger's Table of β	6
2.	Settlements of Soil from Node 68 to 58	42
3.	Settlements between Pile (Node 51 to 41) and Soil (Node 68 to 58)	43
4.	Shear Stress of Elements near Interface	52
5a.	Settlements between Pile (Node 51 to 41) and Soil (Node 68 to 58)	58
5b.	Settlements and Rates of Settlement of Soil (from Node 68 to 58)	59
6.	The Rate of Relative Displacement ($S_{68}-S_{51}$ near top, $S_{41}-S_{58}$ near tip)	74

LIST OF FIGURES

Figure		Page
1.	Schematic Diagram of Consolidation Problem and Boundary Conditions	10
2.	Triangular Element	17
3.	Triangular or Natural Coordinates	19
4.	Global Dimensions of Element	22
4a.	Skin Friction Effect after Pile Driven	33
4b.	Skin Friction Effect after the Surrounding Soil Moves Downward Due to Consolidation	33
5.	Finite Element Mesh for Pile-Soil System	38
6.	Variation of Porepressure of Soil Section Near Pile	40
7.	Settlement History of Nodal Point 68 Due to Gravity Load	41
8.	Downdrag Force/Ultimate Bearing Capacity vs. Time	45
9.	Negative Shear Stress vs. Time	46
10.	Positive Shear Stress vs. Time	47
10a.	The Distribution of Skin Friction along the Interface (Element 24 to 20) at 301.1 days	49
10b.	Part of the Mesh Near the Interface Area	50
10c.	Backfill Loading on the Surface of FE Mesh	55
11.	Porepressure as a Function of Depth and Time	56
12.	Settlements of Node 68 and 63 Due to Backfill	57
13.	Positive Shear Stress vs. Time (Backfill Effect)	60
14.	Negative Shear Stress vs. Time (Backfill Effect)	61
15a.	Downdrag Force/Ultimate Bearing Capacity vs. Time	63

Figure		Page
15b.	Determination of Neutral Point from Relative Displacement	64
15c.	Determination of Neutral Point from Pile Axial Stress	65
16.	Skin Friction Distribution along the Interface in Different Time	67
17.	Settlements of Node 68, 51, 58 and 41 Due to 7000 psf Pile-Top Load	68
18.	Settlements of Node 68, 51, 58 and 41 Due to 21000 psf Pile-Top Load	69
19.	Settlements of Node 68, 51, 58 and 41 Due to 35000 psf Pile-Top Load	70
20.	Settlements of Node 68, 51, 58 and 41 Due to 56000 psf Pile-Top Load	71
21.	The Relative Displacement near Pile Top (S_{68}-S_{51}) and Pile Tip (S_{41}-S_{58}) vs. Time under Different External Pile-Top Load	73
22.	Skin Friction Distribution along the Interface in Different Time under 7000 psf Load	75
23.	Skin Friction Distribution along the Interface in Different Time under 21000 psf Load	76
24.	Skin Friction Distribution along the Interface in Different Time under 56000 psf Load	77
25a.	D.F./U.B.C. vs. Time (21000 psf Pile-Top Load)	79
25b.	D.F./U.B.C. vs. Time (35000 psf)	80
25c.	The Maximum Downdrag Load vs. Applied Pile-Top Load	81
26.	Time-Load History	82
27.	Settlements of Node 68, 51, 41 and 58 Due to Time-Load (7000 psf)	83
28.	Settlements of Node 68, 51, 41 and 58 Due to Time-Loading (21000 psf)	84

Figure		Page
29.	Settlements of Node 68, 51, 41 and 58 Due to Time-Loading (35000 psf)	85
30.	Skin Friction Distribution along the Interface in Different Time under 7000 psf Time-Loading	87
31.	Skin Friction Distribution along the Interface in Different Time under 21000 psf Time-Loading	88
32.	Skin Friction Distribution along the Interface in Different Time under 56000 psf Time-Loading	89
33a.	D.F./U.B.C. vs. Time (7000 psf Time Loading)	90
33b.	D.F./U.B.C. vs. Time (21000 psf Time Loading)	91
33c.	D.F./U.B.C. vs. Time (35000 psf Time Load)	92
33d.	The Maximum Downdrag Load vs. Applied Pile-Top Time-Load	93

Chapter I

INTRODUCTION

When a compressive load is applied to the surface of soil saturated with water, the volume of the soil will decrease causing expulsion of water in the pores. This phenomenon of gradual compression or settlement is called consolidation.

Terzaghi (1) has developed a one-dimensional (1 - D) theory which is mathematically consistent with the more general three-dimensional formulation. His assumption is that the consolidation in a laterally restrained column of fluid-saturated elastic soil under constant load occurs only in the vertical direction. In reality, however, just a few cases satisfy this assumption.

Rendulic (2), Schiffman (3) and Biot (4) have developed three-dimensional consolidation theories to give more satisfactory solutions to the practical situations. Among these investigations, Biot's theory has coupled deformations and pore water pressures with the progress of consolidation and has taken into account several factors which have been ignored in the previous theories. Nevertheless, Biot's formulations can be highly complex for factors such as nonhomogeneous and anisotropic media, nonlinear behavior and arbitrary geometric or boundary conditions. Thus, it is very difficult to obtain analytical solutions for practical problems.

Due to the increasing use of high speed digital computers, several numerical methods have been developed and applied to general

consolidation theories. The two commonly applied methods are the finite difference (FD) and the finite element (FE) method.

The finite difference method has been proven effective in the 1-D consolidation problem but has limitations in the two- and three-dimensional problems. On the other hand, the finite element method is more powerful and has more applications. This method has been used extensively by Desai (5), Sandhu (6,8), Sandhu and Wilson (7). Most of the previous applications of the finite element method have been, in general, for 2-D consolidations that have closed form solutions. Applications of the finite element method to problems such as negative skin friction* on (driven) piles caused by consolidation have not yet been investigated.

It is the purpose of this thesis to analyze various factors associated with negative skin friction on structures such as piles. The formulation assumes an axisymmetric idealization. Chapter II contains a review of the previous work. Chapter III gives details of the variational principle, governing equations and approximate solution methods leading to the finite element method. The effects of negative skin friction on structures such as piles are described in Chapter IV. Some practical examples are given in Chapter V. Chapter VI presents conclusions and recommendation.

---

*Negative skin friction - When pile is driven into soil foundation, part of its load is resisted by skin friction on the pile shaft. If the surrounding soil moves downward relative to the pile, the direction of the skin friction would be reversed. The reversed friction resistance is known as negative skin friction.

Scope of Investigation

It is the intent of this thesis to perform the following:

1. Review, formulate and use a theory concerning the FE method for coupled viscoelastic problems of consolidation.
2. Analyze practical problems of pile-soil systems, the relative movement and the relative settlement, velocity between soil and pile, and their effect on skin friction caused by the process of consolidation.
3. Analyze the influences of backfill, applied pile-top load and load-time history on the downdrag force, which is the total force transferred from the soil to the pile due to negative skin friction. This force which drags the pile downward is known as downdrag load.

Chapter II

LITERATURE REVIEW

Biot (4) developed a theory for three-dimensional consolidation for an ideal soil. The formulation was based on Dracy's law for water flow through soil and provided for coupling between the settlement and the pore water pressure. Biot (9,10,11 & 12) presented various applications. Schiffman et al. (13) presented various theories of consolidation.

Sandhu (6) developed a theory of mixtures applied to saturated soils and proposed a general variational principle for the coupled problem of soil deformation and fluid flow. He also formulated a finite element procedure based on Biot's theory of consolidation to obtain numerical solutions of displacement and porepressure fields for two-dimensional laminar incompressible fluid flow through linearly elastic, isotropic saturated soil. The analysis requires the solution of a series of linear algebraic equilibrium and continuity equations expressed in terms of discrete values of displacement and pore water pressure fields. The details of the formulation are given in Chapter III.

Desai and Johnson (14) developed a FE formulation based on the idealization of 1-D consolidation and found the linear model to be suitable for a 1-D analysis. Yokoo et al. (15,16) developed variational formulations allowing for an inter-element discontinuity of the field variables. Christian et al. (17) assumed the soil to

be incompressible and used Herrmann's (18) variational formulation to obtain a solution for displacement and porepressure.

In finite element approximation of the displacement and porepressure fields, in the two-dimensional domain, Sandhu and Wilson (6,7) used triangular elements with a linear interpolation function for the porepressure field. Desai (19), Asproudas and Desai (20) considers the problem of consolidation of layered media with wide differences in material properties. Desai and Saxena (21) treated consolidation in foundations involving varied clays. Martin (22) has used a triangular element for plane and axisymmetric consolidation. Ghaboussi and Wilson (23) used four-point isoparametric quadrilaterals for the porepressures and displacement. Valliappan (24) used an eight-point isoparametric interpolation for displacements and porepressures.

With respect to a special consolidation problem - the negative skin friction and downdrag load - previous research by Miller (25) described a foundation failure due to the pile downdrag. Baligh and Vivatrat (26) recommended a β-method which is defined by the relation: $f_s = \beta\ \sigma_v$ (where f_s is the negative skin friction, σ_v is the vertical effective stress, β is the empirical value as shown in Table 1). Poulos and Davis (27) used the theory of elasticity to determine the downdrag load. Begemann (28), Fellenius and Broms (29) gave the negative skin friction of a pile based on the field observations. Lambe et al. (30) gave a prediction and field evaluation of the downdrag forces on a single pile. Endo et al. (31)

gave some relations between the relative settlement and negative skin friction and suggested some useful equations to predict the downdrag forces. Most of the previous works are based essentially on many simplified assumptions and sometimes on field observation.

Table 1. Garlanger's Table of β

Soil	β
Clay	0.20 to 0.25
Silt	0.25 to 0.35
Sand	0.35 to 0.50

Chapter III

FINITE ELEMENT THEORY

The finite element method for soil consolidation problems have been published extensively (5,8). Details of the following formulation is based on the description and notation from the above papers.

Governing Equations

1. Force Equilibrium

On an infinitesimal volume, assuming small deformation neglecting inertia and body couples, Biot introduced the force balance equations as:

$$\sigma_{ij,j} + \pi_{,j}\ \delta_{ij} + \rho\ F_i = 0 \qquad (1)$$

where σ_{ij} = components of effective stress tensor

π = pore water pressure

ρ = mass density of soil

F_i = components of body force vector

δ_{ij} = Kronecker delta

the comma in $\pi_{,j}$ denotes partial derivative.

2. Equation of Continuity

2.1 Mass Continuity

For incompressible water condition, the continuity of water means saturation of the soil, i.e., the rate of the outflow from a material volume of soil skeleton equals the rate of decrease

of the volume,

$$\underline{q}_{i,i} = - \dot{e}_{ii} = - \dot{u}_{i,i} \tag{2a}$$

where $\underline{q}_i$ = fluid flux vector

e_{ij} = components of the infinitesimal stra in tensor

u_i = cartesian components u, v, and w of the displacement vector in the three-coordinate directions x_1, x_2 and x_3, Fig. 1.

2.2 Equations of Continuity of Flow

2.2.1 Diffusive Resistance

The diffusive resistance of soil and water binary mixture without inertia effect is defined (6) as:

$$\pi_i = - \pi_{,i} - \rho_w F_i = - \theta_i = - C_{ij} v_i \tag{2b}$$

where ρ_w = mass density of fluid

θ_i = vector conjugate to the flux vector

C_{ij} = components of the flow-resistivity tensor

v_i = components of the nominal relative velocity

Symmetry requirements imply

$$C_{ij} = C_{ji} \tag{2c}$$

In deformable soil and incompressible water, $v_i = \underline{q}_i$. If the resistivity tensor has an inverse - the permeability tensor K_{ij}, from (2b) we get generalized Darcy's law:

$$\underline{q}_i = K_{ij} \theta_j = K_{ij}(\pi_{,j} + \rho_w F_j) \tag{2d}$$

where $$K_{ij} = K_{ji} \tag{2e}$$

due to symmetric effect.

2.2.2 Continuity Equation

From equation (2a), (2b), (2d) continuity equation may be written as:

$$-\dot{u}_{i,i} = (K_{ji}\,\theta_j)_{,i} \tag{2f}$$

or

$$K_{ij}(\pi_{,j} + \rho_w F_j)_{,i} + \dot{u}_{i,i} = 0 \tag{2g}$$

3. Constitutive Relations

The stress-strain relation for the soil skeleton assumed to be linear and elastic can be expressed as:

$$\sigma_{ij} = C_{ijk\ell}\, e_{k\ell} \tag{3a}$$

where $C_{ijk\ell}$ = components of the elastic modal of the soil skeleton in terms of effective stress

$$e_{ij} = \frac{1}{2}(u_{i,j} + u_{j,i})$$

4. Boundary Conditions

R is the open connected region of the fluid-solid mixture. The boundary of R is defined as ∂R and its closure as R. Every function in this article defined its domain as the cartesian product $\overline{R}X[0,\infty)$ where $[0,\infty)$ means a positive interval of time.

The boundary conditions are expressed as Fig. 1.

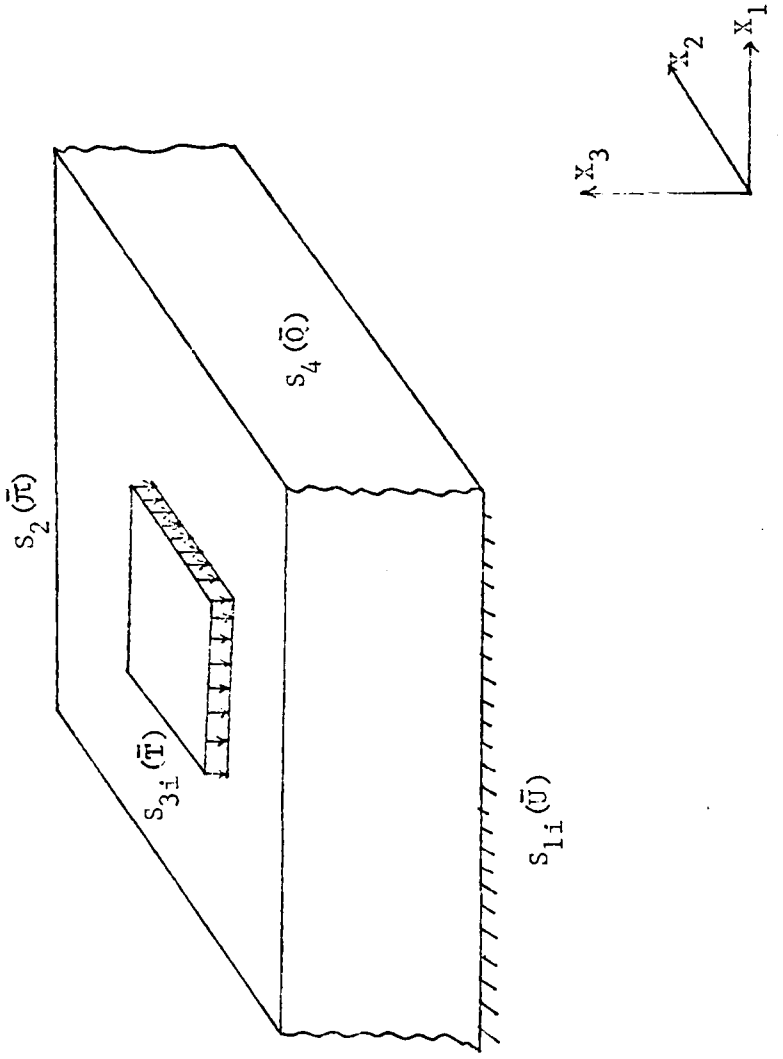

Fig. 1. Schematic Diagram of Consolidation Problem and Boundary Conditions.

4.1 Applied Displacement Boundary Conditions

$u_i(x,t) = \bar{u}_i(x,t)$ on S_{1i} X[0,∞) where S_{1i} is the subset of ∂R.

4.2 Applied Pore Water Pressure Boundary Condition

$\pi(x,t) = \bar{\pi}(x,t)$ on S_2 X[0,∞)

4.3 Applied Traction Boundary Condition

$T_i(s,t) = \bar{T}_i(x,t)$ on S_{3i} X [0,∞)

where $T_i = (\sigma_{ij} + \pi\ \delta_{ij})n_j$

S_{3i} is a subset of ∂R and complementary to S_{1i}

$\bar{S}_{1i} \cup \bar{S}_{3i} = \partial\bar{R}$ & $S_2 \cap S_4 = \phi$

4.4 Applied Flux Boundary Condition

$Q(x,t) = \bar{Q}(x,t)$ on S_4 X[0,∞)

where $Q = q_i n_i$

S_4 is a subset of ∂R complementary to S_2

$\bar{S}_2 \cup \bar{S}_4 = \partial\bar{R}$ & $S_2 \cap S_4 = \phi$

The variational principle is given by

$$A(u_i,\pi) = \int_V \left[\frac{1}{2}\sigma'_{ij} * u_{ij} - \rho\ F_i * u_i + \pi * u_{i,i} - \frac{1}{2}\, g * \underline{q}_i *(\pi_{,i} + \rho_w\ F_i)\right]dV - \int_{S_3} (\bar{T}_i * u_i)dS + \int_{S_4} (g * \bar{Q} * \pi)dS \qquad (4)$$

where * denotes convolution and is defined as

$$f_1 * f_2 = \int_0^t f_1(x_i,\tau)\ f_2(x_i,t-\tau)d\tau$$

and

$$g = 1$$

Approximation for Displacement and Pore Water Pressure

In the FE procedure, the displacements and pore water pressures are approximated by using interpolation functions, Desai and Abel (36), Desai (5) as

$$\begin{Bmatrix} u \\ v \\ w \\ \pi \end{Bmatrix} = \begin{bmatrix} [N_u] & 0 & 0 & 0 \\ 0 & [N_u] & 0 & 0 \\ 0 & 0 & [N_u] & 0 \\ 0 & 0 & 0 & [N_\pi] \end{bmatrix} \begin{Bmatrix} \{u(t)\} \\ \{v(t)\} \\ \{w(t)\} \\ \{\pi_n(t)\} \end{Bmatrix} \tag{5}$$

where $\{u(t)\}^T = [u_1, u_2, \ldots\ldots, u_n]$

$\{v(t)\}^T = [v_1, v_2, \ldots\ldots, v_n]$

$\{w(t)\}^T = [w_1, w_2, \ldots\ldots, w_n]$

$\{\pi_n(t)\}^T = [\pi_1, \pi_2, \ldots\ldots, \pi_n]$

$[N_u] = [N_{u1}, N_{u2}, \ldots\ldots, N_{un}]$

$[N_\pi] = [N_{\pi 1}, N_{\pi 2}, \ldots\ldots, N_{\pi n}]$

N_{ui} and $N_{\pi i}$ = interpolation functions

n = degrees of freedom at a node

$\{u(t)\}$ = vector of nodal displacements in the X-direction, etc.

$\{\pi_n(t)\}$ = vector of nodal pore water pressures

The notation for matrices and vectors is

Rectangular Matrix : [A]

Column Matrix (Vector) : $\{A\}$

Row Matrix (Vector) : $\{A\}^T$

According to Desai (5), substitute equation (5) and its derivative into equation (4), yields the element matrix equation, then yields the global relation as:

$$[K]\{u\} + [C]\{\pi\} = \{M_1\} - \{M_2\} + \{P_1\} \tag{6a}$$

$$[C]^T\{u\} - [\bar{K}]\{\pi\} + ([\bar{\bar{K}}] + [\bar{\bar{K}}]^T)\{\pi\} = \{M_3\} - \{P_2\} \tag{6b}$$

or

$$\begin{bmatrix} K & C \\ C^T & \tilde{K} \end{bmatrix} \begin{Bmatrix} u \\ \pi \end{Bmatrix} = \begin{Bmatrix} M_1 - M_2 + P_1 \\ M_3 - P_2 \end{Bmatrix} \tag{6c}$$

$$[K] = \sum_{e=1}^{m} \int_v [B_e]^T [C][B_e] dV$$

$$[C] = \sum_{e=1}^{m} \int_v [B_\Delta]^T \{N_\pi\} dV$$

$$[\tilde{K}] = \sum_{e=1}^{m} \int_v [B_{\underline{q}}]^T [R][B_{\underline{q}}] dV$$

$$\{M_1\} = \sum_{e=1}^{m} \int_v [B_e]^T \{\sigma_o\} dV$$

$$\{M_2\} = \sum_{e=1}^{m} \int_v [N_u]\{\rho F\} dV$$

$$\{M_3\} = \sum_{e=1}^{m} \int_v [B_{\underline{q}}]^T [R]\{\rho_w F\} dV$$

$$\{P_1\} = \sum_{e=1}^{m} \int_{S_3} [N_u]^T [N_u]\{\bar{T}\} dS$$

$$P_2 = \sum_{e=1}^{m} \int_{S_4} [N_\pi]^T [N_\pi] \{\bar{Q}\} dS$$

where various matrices and vectors are given by

strain vector $\{\varepsilon\} = [B_e]\{q\}$

effective stress vector $\{\sigma'\} = [C][B_e]\{q\} + \{\sigma_o\}$

volumetric strain vector $\{\varepsilon_v\} = [B_\Delta]\{q\}$

gradient of pore pressure vector $\frac{\partial \pi}{\partial x_i} = [B_q]\{\pi_n\}$

$\{\sigma_o\}$ = vector of initial stress

$[C]$ = stress - strain matrix

$[R]$ = matrix of permeability

Time Integration

For material properties and body forces independent of time, equation (6a) has constant $[K]$, $[C]$, $\{M_1\}$, $\{M_2\}$

$$[K]\{u(t)\} + [C]\{\pi(t)\} = \{M_1\} - \{M_2\} + \{P_1(t)\} \tag{7}$$

equation (6b) has constant $[C]^T$, in a small time interval from t_o to t, an assumed interpolation scheme will give

$$[C]^T\{u(t) - u(t_o)\} + [\tilde{K}](\alpha\pi(t) + (1 - \alpha)\pi(t_o))(t - t_o)$$

$$= \alpha\{M_3(t) - P_2(t)\}(t - t_o) + (1 - \alpha)\{M_3(t_o) - P_2(t_o)\}(t - t_o) \tag{8}$$

where α is a scalar coefficient.

Usually in linear interpolation we let $\alpha = 1/2$, $t - t_o = \Delta t$ equation (8) yields

$$[C]^T\{u(t) - u(t_o)\} + [\tilde{K}](\pi(t) + \pi(t_o))\frac{\Delta t}{2} = \frac{\Delta t}{2}\{M_3(t) + M_3(t_o)\} - \frac{\Delta t}{2}\{P_2(t) + P_2(t_o)\} \tag{9}$$

(7) & (9) can be expressed as

$$\begin{bmatrix} [K] & [C] \\ [C]^T & \frac{\Delta t}{2}[\tilde{K}] \end{bmatrix} \begin{Bmatrix} \{u\} \\ \{\pi\} \end{Bmatrix}_{t+\Delta t} = \begin{Bmatrix} \{R_u\} \\ \{R_\pi\} \end{Bmatrix} = \{R\} \tag{10}$$

where $\{R\}$ = vector of nodal forcing parameters due to loads and pore water pressures and its components are known.

These equations are solved at $t + \Delta t$ after boundary conditions are introduced, and the solution is propagated in time. The first solution is obtained at $t = \Delta t$ since $\{u\}$ and $\{\pi\}$ are known at $t = 0$.

Logarithmic interpolation has been introduced by Sandhu (8), assume a function $f(t)$ to vary logarithmically over (t_o, t_1)

For $\tau \in (t_o, t_1)$

$$f(\tau) = f(t_o) + \frac{f(t_1) - f(t_o)}{\ell n(1 + t_1 - t_o)}\ell n(1 + \tau - t_o) \tag{11}$$

Hence

$$\int_{t_o}^{t_1} f(\tau)d\tau = (\alpha\, f(t_1) + (1 - \alpha)f(t_o))(t_1 - t_o) \tag{12}$$

where

$$\alpha = 1 + \frac{1}{t_1 - t_o} - \frac{1}{\ell n(1 + t_1 - t_o)} \tag{13}$$

$$= 1 + \frac{1}{\Delta t} - \frac{1}{\ell n(1 + \Delta t)} \tag{14}$$

If we use a uniform time step (Δt is a constant), then α is constant.

As $\Delta t \to \infty$, $\alpha \to 1$.

In this case, $$\int_{t_o}^{t_1} f(\tau)d\tau = f(t_1)$$

From equation (6c) we can conclude

$$\begin{bmatrix} K & C \\ C^T & \tilde{\alpha K \Delta t} \end{bmatrix} \begin{Bmatrix} u(t_1) \\ \pi(t_1) \end{Bmatrix} = \begin{bmatrix} 0 & 0 \\ C^T & \tilde{-(1-\alpha)K\Delta t} \end{bmatrix} \begin{Bmatrix} u(t_o) \\ \pi(t_o) \end{Bmatrix} + \begin{Bmatrix} R_1 \\ R_2 \end{Bmatrix} \tag{15}$$

where

$$R_1 = M_1 - M_2 + P_1(t)$$

$$R_2 = \alpha\Delta t[M_3(t_1) - P_2(t_1)] + (1 - \alpha)\Delta t[M_3(t_o) - P_2(t_o)]$$

Matrix Formulation

Triangular elements, Fig. 2, were used for the formulation with quadratic variation for displacements and linear variation for pore water pressure.

The displacement interpolation function is

$$\{\phi_u\} = \begin{Bmatrix} L_1(2L_1 - 1) \\ L_2(2L_2 - 1) \\ L_3(2L_3 - 1) \\ 4L_1L_2 \\ 4L_2L_3 \\ 4L_3L_1 \end{Bmatrix} \tag{16}$$

The pore water pressure interpolation function is

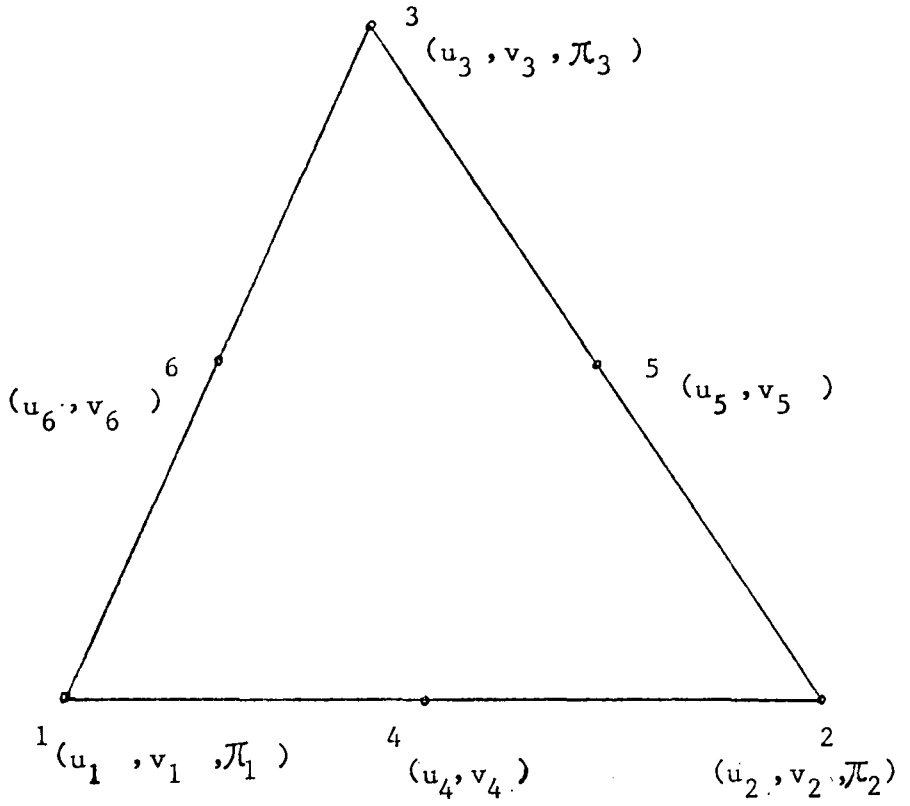

Fig. 2. Triangular Element.

1, 2, 3 = primary nodes

4, 5, 6 = secondary nodes

(Quadratic displacement fields,

Linear fluid pressure field.)

$$\{\phi_\pi\} = \begin{Bmatrix} L_1 \\ L_2 \\ L_3 \end{Bmatrix} \tag{17}$$

where $L_i = A_i/A$ and $L_1 + L_2 + L_3 = 1$

L_i are natural or triangular coordinates (Fig. 3)

$$u = \{\phi_u\}^T \{u\} \tag{18}$$

$$v = \{\phi_u\}^T \{v\} \tag{19}$$

$$\pi = \{\phi_\pi\}^T \{\pi\} \tag{20}$$

where $\{u\}$, $\{v\}$ and $\{\pi\}$ are, respectively, the radial nodal point displacement and the nodal point pore water pressure.

$$\{u\} = \begin{Bmatrix} u_1 \\ u_2 \\ u_3 \\ u_4 \\ u_5 \\ u_6 \end{Bmatrix} \qquad \{v\} = \begin{Bmatrix} v_1 \\ v_2 \\ v_3 \\ v_4 \\ v_5 \\ v_6 \end{Bmatrix} \qquad \{\pi\} = \begin{Bmatrix} \pi_1 \\ \pi_2 \\ \pi_3 \end{Bmatrix}$$

The strain-displacement relationship for axisymmetric solid is

$$\{\varepsilon\} = \begin{Bmatrix} \varepsilon_{rr} \\ \varepsilon_{zz} \\ \gamma_{rz} \\ \varepsilon_{\theta\theta} \end{Bmatrix} = [\phi_e]^T \begin{Bmatrix} u \\ v \end{Bmatrix}$$

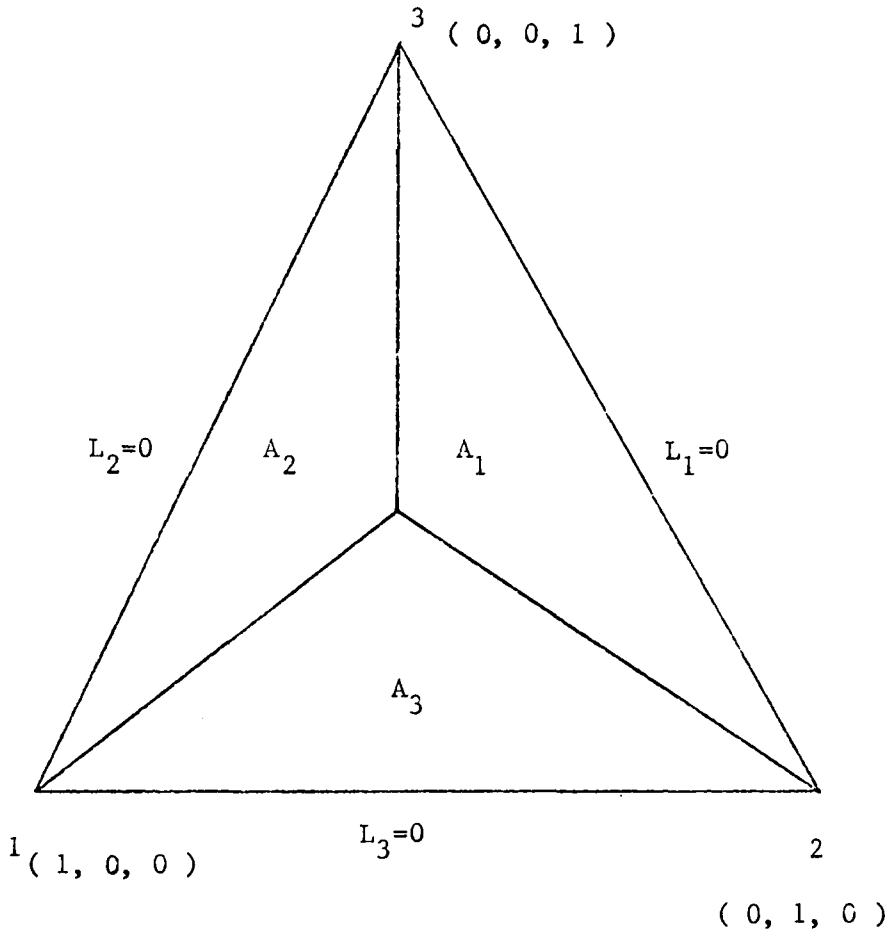

Fig. 3. Triangular or Natural Coordinates.

$$L_i = \frac{A_i}{A} \quad , \; i=1,2,3$$

$$A_1 + A_2 + A_3 = A$$

$$L_1 + L_2 + L_3 = 1$$

$$= \begin{bmatrix} \frac{\partial}{\partial r} & 0 \\ 0 & \frac{\partial}{\partial z} \\ \frac{\partial}{\partial z} & \frac{\partial}{\partial r} \\ \frac{1}{r} & 0 \end{bmatrix} \begin{Bmatrix} u \\ v \end{Bmatrix} = \begin{bmatrix} \phi^T_{u,r} & 0 \\ 0 & \phi^T_{u,z} \\ \phi^T_{u,z} & \phi^T_{u,r} \\ \frac{1}{r}\phi^T_u & 0 \end{bmatrix} \begin{Bmatrix} \underset{\sim}{u} \\ \underset{\sim}{v} \end{Bmatrix} \tag{21}$$

$$= \begin{Bmatrix} \frac{\partial u}{\partial r} \\ \frac{\partial v}{\partial z} \\ \frac{\partial u}{\partial z} + \frac{\partial v}{\partial r} \\ \frac{u}{r} \end{Bmatrix} \tag{22}$$

$$[\phi_e]^T = \begin{bmatrix} \phi^T_{u,r} & 0 \\ 0 & \phi^T_{u,z} \\ \phi^T_{u,z} & \phi^2_{u,r} \\ \frac{1}{r}\phi^T_u & 0 \end{bmatrix} \tag{23}$$

The volumetric strain $\Delta = \varepsilon_{rr} + \varepsilon_{zz} + \varepsilon_{\theta\theta}$

$$[\phi_\Delta]^T = [(\phi^T_{u,r} + \frac{1}{r}\phi^T_u) \ \phi^T_{u,z}] \tag{24}$$

$$\phi_{u,r} = \sum_{i=1}^{3} \frac{\partial \phi}{\partial L_i} \frac{\partial L_i}{\partial r} = \sum_{i=1}^{3} \frac{\partial \phi}{\partial L_i} \frac{b_i}{2A} \tag{25}$$

$$\phi_{u,z} = \sum_{i=1}^{3} \frac{\partial \phi}{\partial L_i} \frac{\partial L_i}{\partial z} = \sum_{i=1}^{3} \frac{\partial \phi}{\partial L_i} \frac{a_i}{2A} \tag{26}$$

where $a_i = r_k - r_j$

$b_i = z_j - z_k$

are shown in Fig. 4.

Because ϕ_{u,L_i} vary linearly over the element, we should separate the linearly varying ε_{rr}, ε_{zz}, γ_{rz} from the quadratically varying $\varepsilon_{\theta\theta}$.

For axisymmetric solids, the stress strain relation for linear anisotropic elasticity is $\gamma_{z\theta} = \gamma_{r\theta} = 0$, $\sigma_{z\theta} = \sigma_{r\theta} = 0$

$$\{\sigma\} = [E]\{\varepsilon\}$$

or

$$\begin{Bmatrix} \sigma_{rr} \\ \sigma_{zz} \\ \sigma_{rz} \\ \sigma_{\theta\theta} \end{Bmatrix} = \begin{bmatrix} E_{11} & E_{12} & E_{13} & E_{14} \\ E_{21} & E_{22} & E_{23} & E_{24} \\ E_{31} & E_{32} & E_{33} & E_{34} \\ E_{41} & E_{42} & E_{43} & E_{44} \end{bmatrix} \begin{Bmatrix} \varepsilon_{rr} \\ \varepsilon_{zz} \\ \gamma_{rz} \\ \varepsilon_{\theta\theta} \end{Bmatrix} \tag{27}$$

We can use subscripts r,θ to separate the r,z plane and the tangential direction respectively, that is,

$$[E] = \begin{bmatrix} E_{rr} & E_{r\theta} \\ E_{\theta r} & E_{\theta\theta} \end{bmatrix} \tag{28}$$

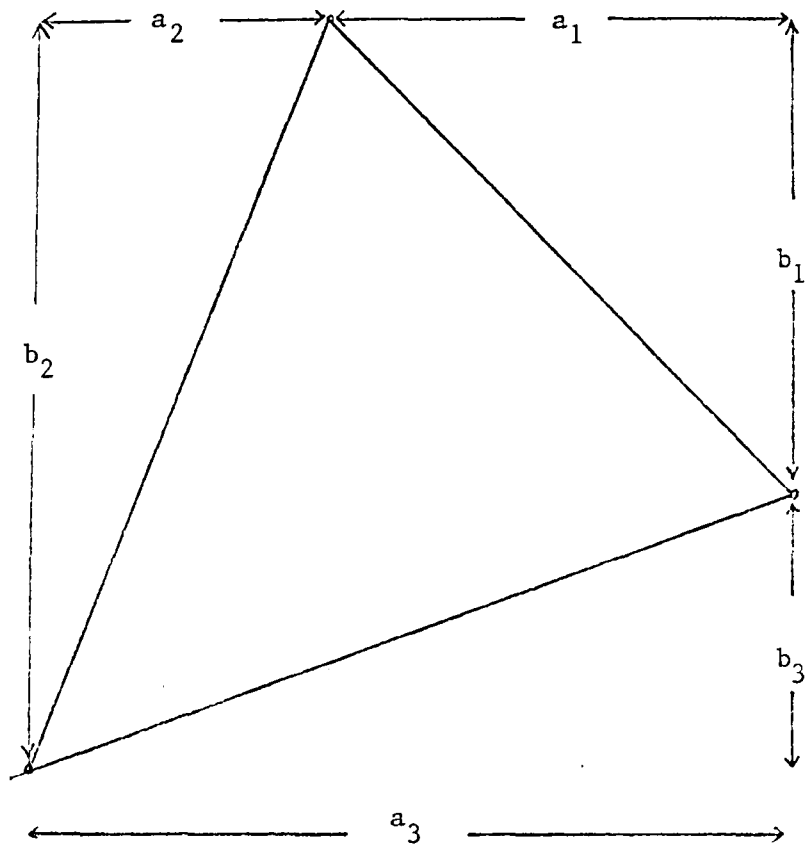

$2A = a_3 b_2 - a_2 b_3$ etc.

Fig. 4. Global Dimensions of Element.

The element stiffness matrix is

$$[K] = \int_{R_e} [\phi_e][E][\phi_e]^T dR_e$$

$$= \int_{R_e} [\phi_{er} \; \phi_{e\theta}] \begin{bmatrix} E_{rr} & E_{r\theta} \\ E_{\theta r} & E_{\theta\theta} \end{bmatrix} \begin{Bmatrix} \phi_{er}^T \\ \phi_{e\theta}^T \end{Bmatrix}$$

$$= \int_{R_e} [\phi_{er}E_{rr}\phi_{er}^T + \phi_{er}E_{r\theta}\phi_{e\theta}^T + \phi_{e\theta}E_{\theta r}\phi_{er}^T + \phi_{e\theta}E_{\theta\theta}\phi_{e\theta}^T] dR_e$$

$$= [K_{rr}] + [K_{r\theta}] + [K_{\theta r}] + [K_{\theta\theta}] \tag{29}$$

From equation (16), (25) & (26) we get

$$\{\phi_{u,r}\} = \frac{1}{2A} \begin{Bmatrix} (4L_1 - 1)b_1 \\ (4L_2 - 1)b_2 \\ (4L_3 - 1)b_3 \\ 4(L_2b_1 + L_1b_2) \\ 4(L_3b_2 + L_2b_3) \\ 4(L_1b_3 + L_3b_1) \end{Bmatrix} \tag{30}$$

$$\{\phi_{u,z}\} = \frac{1}{2A} \begin{Bmatrix} (4L_1 - 1)a_1 \\ (4L_2 - 1)a_2 \\ (4L_3 - 1)a_3 \\ 4(L_2a_1 + L_1a_2) \\ 4(L_3a_2 + L_2a_3) \\ 4(L_1a_3 + L_3a_1) \end{Bmatrix} \tag{31}$$

When we evaluate $\{\phi_{u,r}\}$, $\{\phi_{u,z}\}$ at the three nodal points (1,0,0) (0,1,0) and (0,0,1) of the element, we get

$$[u] = \begin{bmatrix} 3b_1 & -b_2 & -b_3 & 4b_2 & 0 & 4b_3 \\ -b_1 & 3b_2 & -b_3 & 4b_1 & 4b_3 & 0 \\ -b_1 & -b_2 & 3b_3 & 0 & 4b_2 & 4b_1 \end{bmatrix} \tag{32}$$

$$[V] = \begin{bmatrix} 3a_1 & -a_2 & -a_3 & 4a_2 & 0 & 4a_3 \\ -a_1 & 3a_2 & -a_3 & 4a_1 & 4a_3 & 0 \\ -a_1 & -a_2 & 3a_3 & 0 & 4a_2 & 4a_1 \end{bmatrix} \tag{33}$$

$$\{\varepsilon\} = [N_\varepsilon]\{\varepsilon_n\} \tag{34}$$

where

$$\{\varepsilon_n\} = \begin{Bmatrix} \varepsilon_{rr1} \\ \varepsilon_{rr2} \\ \varepsilon_{rr3} \\ \varepsilon_{zz1} \\ \varepsilon_{zz2} \\ \varepsilon_{zz3} \\ \gamma_{rz1} \\ \gamma_{rz2} \\ \gamma_{rz3} \end{Bmatrix} \tag{35}$$

$$[N_\varepsilon] = \begin{bmatrix} \{N_1\}^T & \{0\}^T & \{0\}^T \\ \{0\}^T & \{N_1\}^T & \{0\}^T \\ \{0\}^T & \{0\}^T & \{N_1\}^T \end{bmatrix} \tag{36}$$

$$\{N_1\}^T = [L_1 \quad L_2 \quad L_3] \tag{37}$$

$$\{\varepsilon_n\} = \begin{bmatrix} u & 0 \\ 0 & v \\ v & u \end{bmatrix} \begin{Bmatrix} u \\ \sim \\ v \\ \sim \end{Bmatrix} \tag{38}$$

From equation (32) through (38)

$$\begin{Bmatrix} \varepsilon_{rr} \\ \varepsilon_{zz} \\ \gamma_{rz} \end{Bmatrix} = \frac{1}{2A} \begin{bmatrix} N_1^T & 0 & 0 \\ 0 & N_1^T & 0 \\ 0 & 0 & N_1^T \end{bmatrix} \begin{bmatrix} u & 0 \\ 0 & v \\ v & u \end{bmatrix} \begin{Bmatrix} u \\ \sim \\ v \\ \sim \end{Bmatrix} \tag{39}$$

$$[K_{rr}] = \int_{R_e} \frac{1}{2A} \begin{bmatrix} U^T & 0 & V^T \\ 0 & V^T & U^T \end{bmatrix} \begin{bmatrix} N_1 & 0 & 0 \\ 0 & N_1 & 0 \\ 0 & 0 & N_1 \end{bmatrix} \begin{bmatrix} E_{11} & E_{12} & E_{13} \\ E_{21} & E_{22} & E_{23} \\ E_{31} & E_{32} & E_{33} \end{bmatrix} \cdot \frac{1}{2A} \cdot$$

$$\begin{bmatrix} N_1^T & 0 & 0 \\ 0 & N_1^T & 0 \\ 0 & 0 & N_1^T \end{bmatrix} \begin{bmatrix} U & 0 \\ 0 & V \\ V & U \end{bmatrix} dR_e \tag{40}$$

$$= \int_{R_e} \frac{1}{4A^2} \begin{bmatrix} N_1 & 0 & 0 \\ 0 & N_1 & 0 \\ 0 & 0 & N_1 \end{bmatrix} \begin{bmatrix} E_{11} & E_{12} & E_{13} \\ E_{21} & E_{22} & E_{23} \\ E_{31} & E_{32} & E_{33} \end{bmatrix} \begin{bmatrix} N_1^T & 0 & 0 \\ 0 & N_1^T & 0 \\ 0 & 0 & N_1^T \end{bmatrix} dR_e$$

$$= \int_{R_e} \frac{1}{4A^2} \begin{bmatrix} E_{11}N_1N_1^T t & E_{12}N_1N_1^T t & E_{13}N_1N_1^T t \\ E_{21}N_1N_1^T t & E_{22}N_1N_1^T t & E_{23}N_1N_1^T t \\ E_{31}N_1N_1^T t & E_{32}N_1N_1^T t & E_{33}N_1N_1^T t \end{bmatrix} dA \tag{41}$$

Hence the thickness

$$t = r = [L_1,\ L_2,\ L_3]\begin{Bmatrix} r_1 \\ r_2 \\ r_3 \end{Bmatrix}$$

where r_i is the radial distance of the ith corner of the element

$$\int_A N_1 N_1^T t dA = \int_A \begin{bmatrix} L_1^2 & L_1L_2 & L_1L_3 \\ L_2L_1 & L_2^2 & L_2L_3 \\ L_3L_1 & L_3L_2 & L_3^2 \end{bmatrix} [L_1 \quad L_2 \quad L_3] \begin{Bmatrix} r_1 \\ r_2 \\ r_3 \end{Bmatrix} dA \qquad (42)$$

$$\int_A L_1^p\, L_2^q\, L_3^r\, dA = \frac{p\,!\,q\,!\,r\,!}{(p+q+r+2)!}\, 2A \qquad (43)$$

equation (42) becomes

$$\int_A N_1 N_1^T t dA = A \cdot \frac{1}{60} \begin{bmatrix} 6r_1+2r_2+2r_3 & 2r_1+2r_2+r_3 & 2r_1+r_2+2r_3 \\ 2r_1+2r_2+r_3 & 2r_1+6r_2+2r_3 & r_1+2r_2+2r_3 \\ 2r_1+r_2+2r_3 & r_1+2r_2+2r_3 & 2r_1+2r_2+6r_3 \end{bmatrix} \qquad (44)$$

From equation (40), (41) & (44)

$$[K_{rr}] = \frac{1}{4A} \begin{bmatrix} U^T & 0 & V^T \\ 0 & V^T & U^T \end{bmatrix} \begin{bmatrix} E_{11}^Q & E_{12}^Q & E_{13}^Q \\ E_{21}^Q & E_{22}^Q & E_{23}^Q \\ E_{31}^Q & E_{32}^Q & E_{33}^Q \end{bmatrix} \begin{bmatrix} U & 0 \\ 0 & V \\ V & U \end{bmatrix} \qquad (45)$$

$$= \begin{bmatrix} K_{11} & K_{12} \\ K_{21} & K_{22} \end{bmatrix}_{rr}$$

where

$$K_{11} = E_{11}U^TQU + E_{13}(U^TQV + V^TQU) + E_{33}V^TQV$$
$$K_{12} = K_{21}^T = E_{12}U^TQV + E_{13}U^TQU + E_{32}V^TQV + E_{33}V^TQU$$
$$K_{22} = E_{22}V^TQV + E_{23}(V^TQU + U^TQV) + E_{33}U^TQU$$

From equation (29), (27) & (39)

$$[K_{r\theta}] = \int_{R_e} \frac{1}{2A} \begin{bmatrix} U^T & 0 & V^T \\ 0 & V^T & U^T \end{bmatrix} \begin{bmatrix} N_1 & 0 & 0 \\ 0 & N_1 & 0 \\ 0 & 0 & N_1 \end{bmatrix} \begin{bmatrix} E_{14} \\ E_{24} \\ E_{34} \end{bmatrix} [\phi_U^T \quad 0] \frac{1}{r} dR_e \qquad (46)$$

$$dR_e = tdA = rdA$$

and

$$\int_A \frac{1}{2A} \{N_1\}[\phi_U]^T dA = [\bar{Q}]$$
$$= \frac{1}{120} \begin{bmatrix} 2 & -1 & -1 & 8 & 4 & 8 \\ -1 & 2 & -1 & 8 & 8 & 4 \\ -1 & -1 & 2 & 4 & 8 & 8 \end{bmatrix} \qquad (47)$$

$$[K_{r\theta}] = \begin{bmatrix} U^T & 0 & V^T \\ 0 & V^T & U^T \end{bmatrix} \begin{bmatrix} E_{14}\bar{Q} & 0 \\ E_{24}\bar{Q} & 0 \\ E_{34}\bar{Q} & 0 \end{bmatrix}$$

$$= \begin{bmatrix} E_{14}U^T\bar{Q} + E_{34}V^T\bar{Q} & 0 \\ E_{24}V^T\bar{Q} + E_{34}U^T\bar{Q} & 0 \end{bmatrix} \qquad (48)$$

Hence

$$[K_{r\theta}] + [K_{\theta r}] = [K_{r\theta}] + [K_{r\theta}]^T$$

$$= \begin{bmatrix} E_{14}(U^T\overline{Q} + \overline{Q}^T U) + E_{34}(V^T\overline{Q} + \overline{Q}^T V) & E_{24}\overline{Q}^T V + E_{34}\overline{Q}^T U \\ E_{24}V^T\overline{Q} + E_{34}U^T\overline{Q} & 0 \end{bmatrix} \tag{49}$$

$$[K_{\theta\theta}] = \int_{R_e} \begin{bmatrix} \phi_u \\ 0 \end{bmatrix} E_{44} [\phi_U^T \quad 0] \frac{1}{r^2} dR_e \tag{50}$$

$$dR_e = tdA = rdA$$

$$[K_{\theta\theta}] = \int_A \begin{bmatrix} E_{44}\phi_u\phi_u^T & 0 \\ 0 & 0 \end{bmatrix} \frac{1}{r} dA \tag{51}$$

From numerical integration

$$[K] = \int_{R_e} [\phi_e][E][\phi_e]^T dR$$

$$= \int_{R_e} [\phi_e][E][\phi_e]^T rdA$$

$$= A \cdot \sum_{j=1}^{n} \sum_{i=1}^{n} H_{ij}[\phi_e(n_i,n_j)][E(n_i,n_j)] \cdot$$

$$[\phi_e(n_i,n_j)]^T \cdot r(n_i,n_j) \tag{52}$$

where n_i, n_j are coordinates of Gauss points

H_{ij} are the weights

n is the number of integration points in each dimension

Linear Porepressure Interpolation Over Triangular Elements

From equation (17) porepressure interpolation is

$$\{\phi_\pi\} = \begin{Bmatrix} L_1 \\ L_2 \\ L_3 \end{Bmatrix}$$

The pressure gradients are

$$\begin{Bmatrix} g_x \\ g_y \end{Bmatrix} = \begin{bmatrix} \phi_{\pi,r}^T \\ \phi_{\pi,z}^T \end{bmatrix} \{\pi\} \tag{53}$$

or

$$[g] = [\phi_\theta]^T \{\pi\} \tag{54}$$

where

$$[\phi_\theta]^T = \frac{1}{2A} \begin{bmatrix} b_1 & b_2 & b_3 \\ a_1 & a_2 & a_3 \end{bmatrix} \tag{55}$$

$$\{\pi\} = \begin{Bmatrix} \pi_1 \\ \pi_2 \\ \pi_3 \end{Bmatrix}$$

The Generalized Darcy's law is

$$\begin{Bmatrix} q_r \\ q_z \end{Bmatrix} = \begin{bmatrix} K_{11} & K_{12} \\ K_{21} & K_{22} \end{bmatrix} \begin{Bmatrix} g_r + \rho_2 f_r \\ g_z + \rho_2 f_z \end{Bmatrix} \tag{56}$$

$$[\bar{K}]_e = \int_{R_e} [\phi_\theta][K][\phi_\theta]^T dR_e$$

$$= \int_{R_e} [\phi_\theta][K][\phi_\theta]^T r dA$$

$$= \frac{r_o}{4A} \begin{bmatrix} b_1 & a_1 \\ b_2 & a_2 \\ b_3 & a_3 \end{bmatrix} \begin{bmatrix} K_{11} & K_{12} \\ K_{21} & K_{22} \end{bmatrix} \begin{bmatrix} b_1 & b_2 & b_3 \\ a_1 & a_2 & a_3 \end{bmatrix} \tag{57}$$

where $r_o = \frac{r_1+r_2+r_3}{3}$ is the radial coordinate of the centroid of the cross section of the ring element.

Coupling Matrix C

$$[C] = \int_{R_e} \{\phi_\Delta\}\{\phi_\pi\}^T dR_e$$

$$= \int_{R_e} \begin{Bmatrix} \phi_{u,r} + \frac{1}{r}\phi_u \\ \phi_{u,z} \end{Bmatrix} \{\phi_\pi\}^T dR_e \tag{58}$$

$$= \int_{R_e} \begin{Bmatrix} \phi_{u,r} + \frac{1}{r}\phi_u \\ \phi_{u,z} \end{Bmatrix} \{\phi_\pi\}^T r dA$$

Boundary Quantities

The surface of a segment of the axisymmetric ring involves the tangential dimension if the specified boundary quantity varies along the boundary with varying distance from the axis.

$$\{p_1\} = \int \{\phi_u\}\{\phi_t\}[\hat{t}] d\ell$$

where t_r, t_z are the components of applied traction at arbitrary point along the boundary.

If we assume a linear interpolation condition in tractions along the boundary, let L_1, L_2 be non-dimensional coordinates of a point x from i.

$$L_1 = 1 - x/\ell \qquad L_2 = x/\ell$$

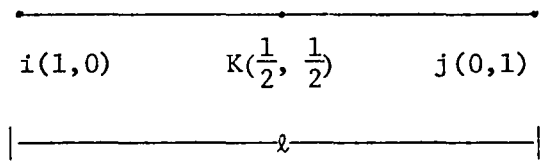

$$\hat{t}_r = [L_1 \quad L_2]\begin{Bmatrix} \hat{t}^i_r \\ \hat{t}^j_r \end{Bmatrix}$$

$$\{P_1\}_{,r} = \int_i^j \begin{Bmatrix} L_1(2L_1 - 1) \\ L_2(2L_2 - 1) \\ L_3(2L_3 - 1) \end{Bmatrix} [L_1 \quad L_2] \begin{Bmatrix} \hat{t}^i_r \\ \hat{t}^j_r \end{Bmatrix} r\,dz$$

$$= \frac{Z_j - Z_i}{60} \begin{bmatrix} 9r_i+r_j & r_i-r_j \\ -r_i+r_j & r_i+9r_j \\ 12r_i+8r_j & 8r_i+12r_j \end{bmatrix} \begin{Bmatrix} \hat{t}^i_r \\ \hat{t}^j_r \end{Bmatrix}$$

$$= \frac{Z_j - Z_i}{60} \begin{bmatrix} 5(r_i+r_j)+4(r_i-r_j) & r_i-r_j \\ -r_i+r_j & 5(r_i+r_j)+4(r_j-r_i) \\ 10(r_i+r_j)+2(r_i-r_j) & 10(r_i+r_j)+2(r_j-r_i) \end{bmatrix} \begin{Bmatrix} \hat{t}^i_r \\ \hat{t}^j_r \end{Bmatrix} \tag{59}$$

Chapter IV

NEGATIVE SKIN FRICTION DUE TO CONSOLIDATION

1. Introduction

When a foundation system is not strong enough to support a structure, it is required to transmit the load of superstructure to a more suitable material at a greater depth by means of piles. A friction pile which moves downward relative to the soil will transfer load from the pile to the soil. Part of the load is resisted by an upward or positive skin friction, Q_s, along the pile shaft and the remaining load is supported by the point bearing Q_p, at the tip of the pile as shown in Fig. 4a. When the pile is driven into soft normally consolidated clay, the clay close to the pile is remolded and displaced causing a build-up of large excess porepressure. After some time the gradual reconsolidation of the clay and dissipation of the excess porepressure will cause some additional settlement of the clay. As a consequence, the surrounding soil will move downward relative to the pile and reverse the direction of the skin friction. The reversed skin friction is known as negative skin friction, as shown in Fig. 4b. The total force transferred from the soil to the pile due to this negative skin friction drags the pile downward, thereby increasing the load transferred to the stratum beneath the pile tip. This may cause failure of the pile if the soil bearing capacity is exceeded by this additional frictional force.

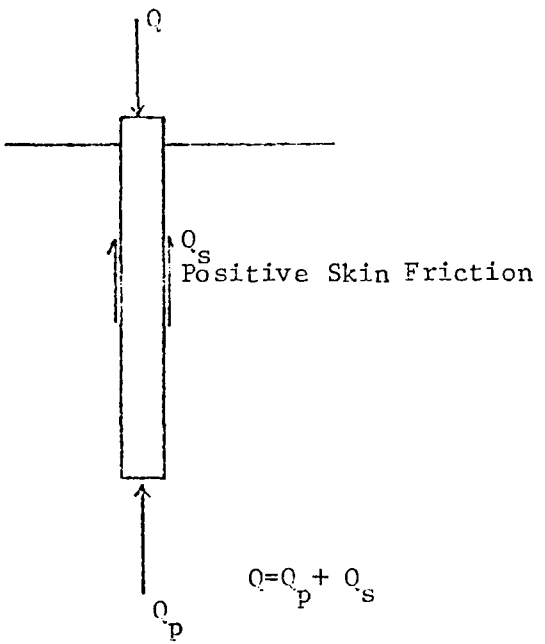

Fig. 4a. Skin Friction Effect after Pile Driven

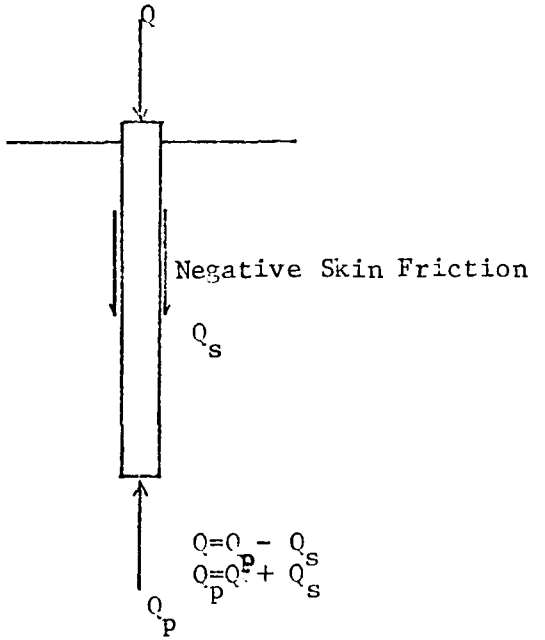

Fig. 4b. Skin Friction Effect after the Surrounding Soil Moves Downward Due to Consolidation.

2. Soil Settlement Analysis

Since the downdrag load on a pile is the result of a downward movement of the surrounding soil with respect to the pile, we can examine the predicted or measured settlement in order to investigate the downdrag problem in the pile foundation. According to a recent paper given by Baligh and Vivatrat (25), the most common cases of downdrag on piles consist of:

(a) piles driven through settling ground,

(b) piles driven through freshly placed fill overlying compressible materials,

(c) the consolidation settlement due to pile driving.

The type of problem in case (a) is the soil undergoing consolidation due to its own weight or ground water table lowering. Usually one can estimate the expected additional settlement by measuring the pore water pressure.

In case (b), the base level of a pile-supported structure which is raised to the design elevation by the placement of fill on the surface will cause the downdrag on the pile.

A pile driven through compressible soil will cause excess pore water pressure. The dissipation of the excess pore water will cause a consolidation settlement of the soil, which is case (c).

Existing information from Winterkorn and Fang (31) indicates that the relative movement required to mobilize friction rarely exceeds a value of about 1 cm. Lambe et al. (29) indicates that the development of full frictional resistance by a relative movement is about 1/4 inch (0.6 cm). Beyond that value, the negative skin

friction remains at a constant maximum value.

3. Proposed Method for Predicting Downdrag of Pile

Before predicting the downdrag force, we should find the maximum skin friction on the pile surface. Fellenius (32) suggests that the maximum negative skin friction is equal to the shear stress carried by the surrounding soil.

To calculate the maximum downdrag force, there are three methods suggested by various workers:

(a) Terzaghi and Peck's Method (33):

$$F_n = \pi \cdot D \cdot h \cdot s \tag{60}$$

where F_n = maximum downdrag force

D = diameter of the pile

h = depth of the pile in the compressible soil

s = average shear stress in the compressible soil

(b) Winterkorn and Fang's Method (31):

$$F_n = \pi \cdot D \cdot h \cdot s \tag{61}$$

where F_n, D and h are the same as equation (60)

s = average value of the undrained shear strength of the undisturbed soft soil or $s = \sigma_u/2$

(c) Baligh and Vivatrat's (25) Method (β-Method):

The β-Method is an empirical method, usually applicable only when the soil settlement between soil and pile is large; if otherwise used it will overestimate the downdrag load. Another

assumption is that the negative skin friction is fully mobilized along the length of the pile.

In this method,

$$f_s = \bar{\sigma}_h \cdot \tan \bar{\phi}_\alpha \tag{62}$$

where f_s = maximum frictional resistance

$\bar{\sigma}_h$ = effective horizontal stresses

$\bar{\phi}_\alpha$ = angle of friction between soil and pile

$$\bar{\sigma}_h = K \bar{\sigma}_v \tag{63}$$

where K = coefficient of lateral earth pressure

$\bar{\sigma}_v$ = vertical effective stress

$$\bar{\sigma}_v = \sigma_v - u \tag{64}$$

where σ_v = total vertical stress

u = pore water pressure

By substituting equation (63) into equation (62), we obtain the following equation:

$$\begin{aligned} \bar{\sigma}_h &= K \cdot \tan \bar{\phi}_\alpha \cdot \bar{\sigma}_v \\ &= \beta \cdot \bar{\sigma}_v \end{aligned} \tag{65}$$

where β is given in Table 1.

Therefore, the maximum downdrag force is

$$F_n = f_s \cdot \pi \cdot D \cdot h \tag{66}$$

where F_n, D and h are the same as in equation (60).

Chapter V

FINITE ELEMENT APPLICATION FOR NEGATIVE SKIN FRICTION

An analysis of negative skin friction on the pile-soil interface is a complex mechanics problem. Previous work in this field has been based on field observations through the installation of various devices in the test piles and in the surrounding soil. These devices include strain gauges, pressure gauges and pore pressure gauges. Such field observations may not be reliable in obtaining satisfactory predictions, since the measuring instruments are easily damaged during the driving process and are influenced by the local site conditions. On the other hand, the FE method has been found to be effective for approximate solutions of time-dependent boundary value problems. Besides, this method can generate histories of deformations (horizontal and vertical displacements), stresses and porepressures.

In order to study the details of the pile downdrag problem in this thesis, a pile was assumed to be driven into the soil. The pile-soil system was idealized as axisymmetric. The soil mass and the pile were discretized into a number of sets of FE meshes with 187 nodes and 80 elements, Fig. 5. A few numerical quantities of settlement, skin friction and porepressures caused by the gravity load and backfill were studied. Then the influences of applied pile-top load and time-load history were evaluated, and finally the importance of backfill was examined.

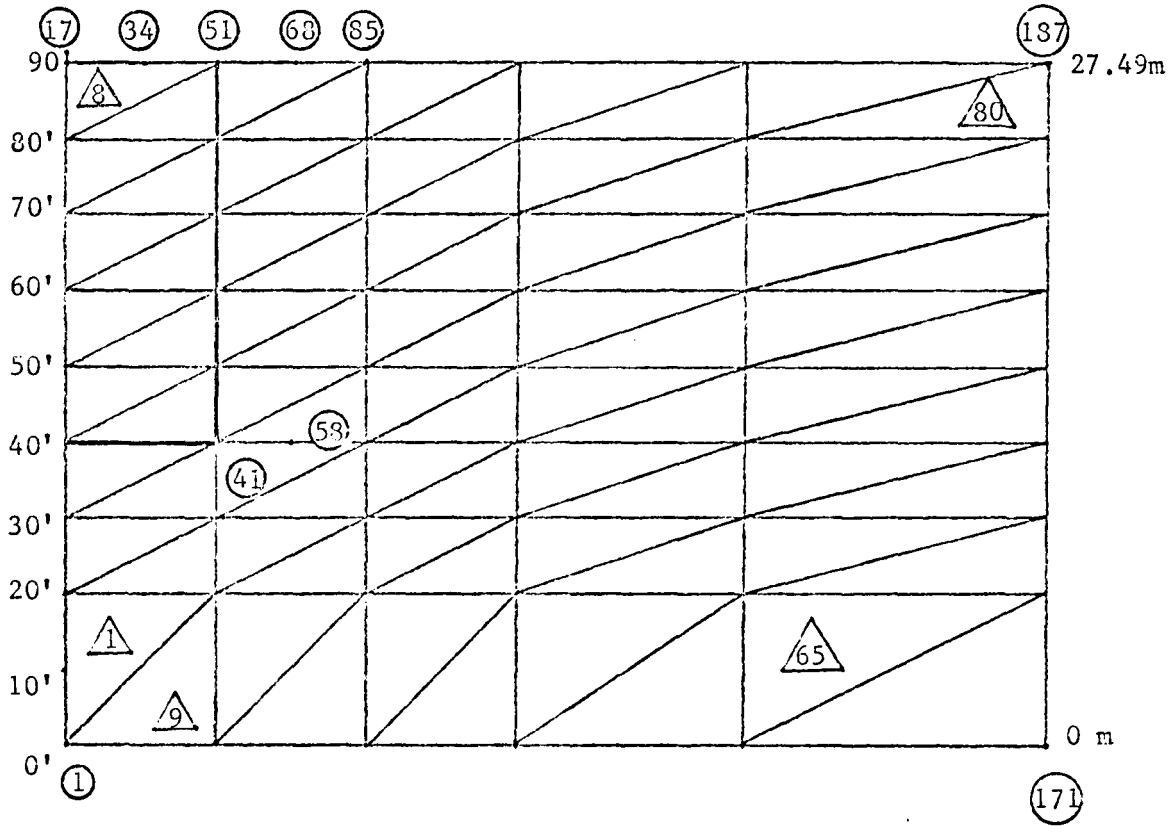

Fig.5. Finite Element Mesh for Pile-Soil System

The material properties of the soil and pile are listed below:

Soil: elastic modulus, E = 44,100 lb/ft^2 (214,767 Kg/m^2), Poisson's ratio, ν = 0.45, permeability $K_x = K_y = 0.638 \times 10^{-4}$ ft/day (0.1948×10^{-4} m/day), unit weight, γ = 110 lb/ft^3 (1.755.6 Kg/m^3), soil adhesion Ca = 490 lb/ft^2 (2,386.3 Kg/m^2)

Pile: elastic modulus, E = 432,000,000 lb/ft^2 (2.10384×10^9 Kg/m^2), Poisson's ratio, ν = 0.25, permeability, $K_x = K_y = 0.638 \times 10^{-6}$ ft/day (0.1948×10^{-6} m/day), unit weight, γ = 150 lb/ft^3 (2,394 Kg/m^3).

Negative Skin Friction Due to Gravity Load

The soil was allowed to undergo consolidation by its own weight, and the variation of porewater pressure with respect to line observed along the depth from nodal point 69 to 83, Fig. 6. In the figure we can see that after 316 days, the consolidation process was 90% complete. (Every node from 52 to 68 was found to have the same gravity load and their vertical settlements along this section were the same.) The vertical settlement for nodal point 68 vs. time is shown in Fig. 7. In the figure the rate of settlement (slope of the settlement curve) decreased as time increased. Table 2 gives the settlement and rate of settlement at section along nodes 68 to 58 of the soil at different depths and time periods. From the table, it can be seen that the rate of settlement gradually decreased as time increased, consistent with the result from Fig. 7.

Table 3 gives the values of ground settlement of the pile face and the surrounding soil as a function of time and depth. The

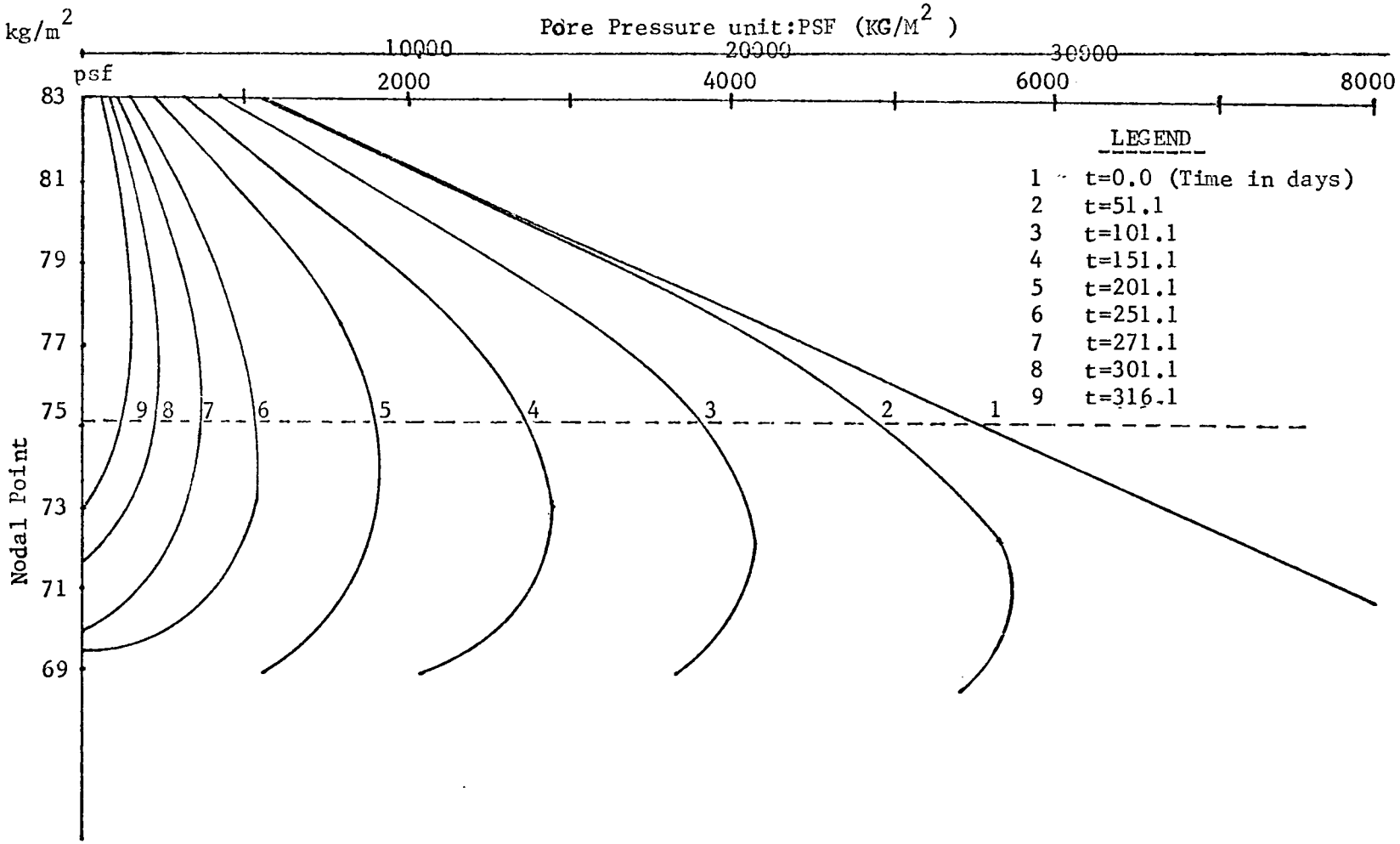

Fig. 6. Variation of Porepressure of Soil Section Near Pile

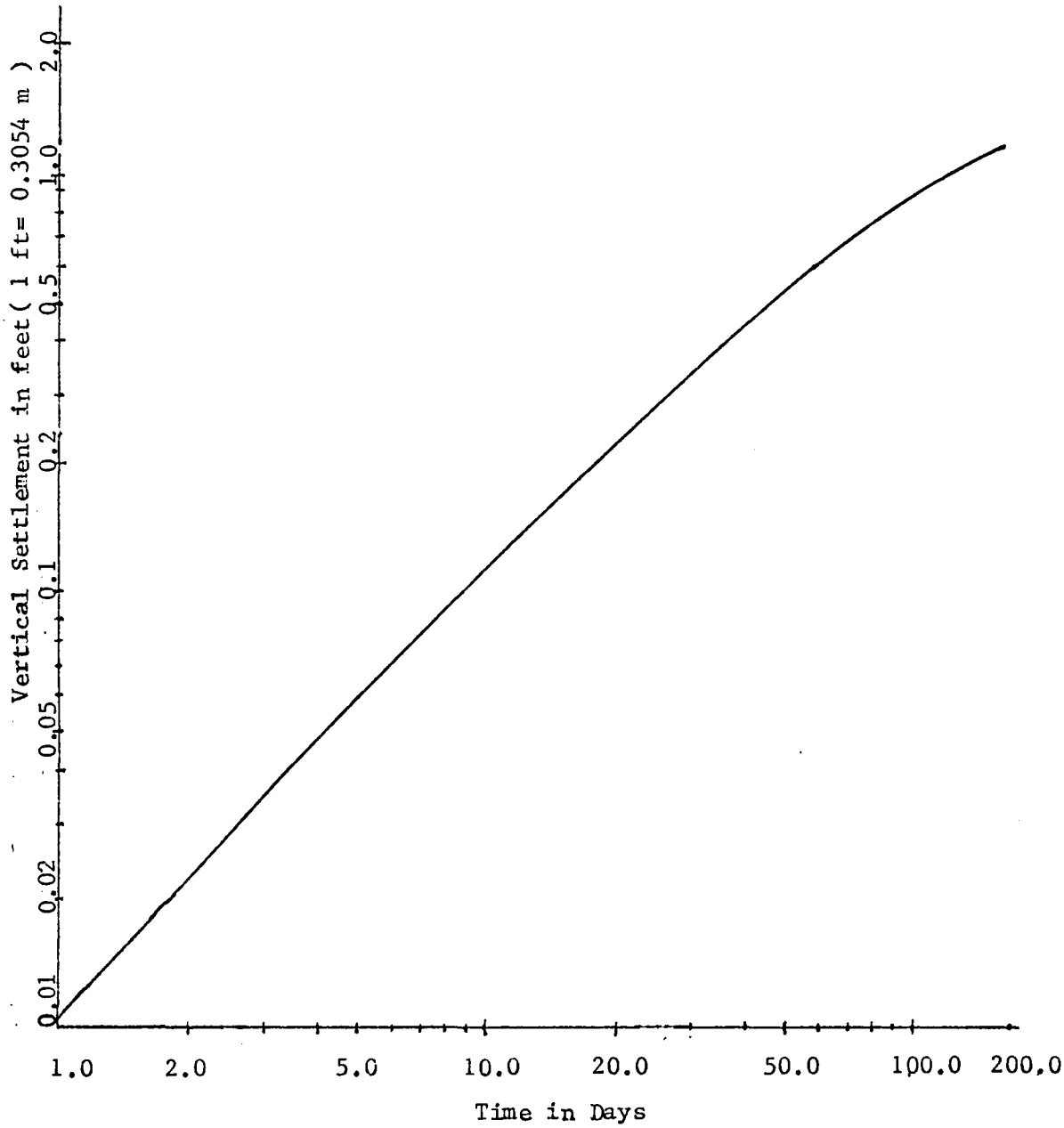

Fig. 7. Settlement History of Nodal Point 68 Due to Gravity Load

Table 2. Settlements of Soil from Node 68 to 58.

Settlement in feet(cm), Rate of Settlement in feet/month(cm/month)

Depth	1st. Peridd		2nd. Period		3rd. Period		4th. Period		5th. Period	
	1.1day-10.1day		10.1day-31.1day		31.1day-101.1day		101.1day-201.1day		201.1day-301.1day	
	Settle-ment	Rate of Settle-ment	Settle-ment	Rate of Settle-ment	Settle-ment	Rate of Settle-ment	Settle-ment	Rate of Settle-ment	Settle-ment	Rate of Settle-ment
0'	0.01 (0.3054)	0.33 (10.0)	0.2315 (7.07)	0.32 (9.77)	0.696 (21.26)	0.298 (9.10)	0.76 (23.21)	0.228 (6.96)	0.54 (16.49)	0.162 (4.95)
10'	0.01 (0.3054)	0.33 (10.0)	0.2314 (7.06)	0.32 (9.77)	0.695 (21.25)	0.297 (9.07)	0.756 (23.09)	0.227 (6.93)	0.539 (16.46)	0.162 (4.95)
20'	0.01 (0.3054)	0.33 (10.0)	0.2314 (7.06)	0.32 (9.77)	0.690 (21.07)	0.295 (9.01)	0.75 (22.90)	0.225 (6.87)	0.534 (16.31)	0.160 (4.89)
30'	0.01 (0.3054)	0.33 (10.0)	0.2314 (7.06)	0.32 (9.77)	0.684 (20.89)	0.293 (8.95)	0.74 (22.60)	0.222 (6.78)	0.527 (16.09)	0.158 (4.83)
40'	0.01 (0.3054)	0.33 (10.0)	0.2309 (7.05)	0.318 (9.71)	0.676 (20.65)	0.289 (8.83)	0.726 (22.17)	0.218 (6.66)	0.517 (15.79)	0.155 (4.73)
50'	0.01 (0.3054)	0.33 (10.0)	0.228 (6.96)	0.31 (9.47)	0.652 (19.91)	0.279 (8.52)	0.695 (21.23)	0.208 (6.35)	0.495 (15.12)	0.148 (4.52)

Table 3. Settlements between Pile(Node 51 to 41) and Soil(Node 68 to 58)
in feet (cm)

Time / Depth	1.1 day		10.1 day		27.1 day		31.1 day		101.1 day		201.1 day		301.1 day	
	Pile	Soil	Pile	Soil	Pile	Soil	Pile	Soil	Pile	Soil	Pile	Soil	Pile	Soil
0'	0.1219 (3.72)	0.1218 (3.72)	0.1121 (3.42)	0.112 (3.41)	0.299 (9.155)	0.2998 (9.16)	0.3433 (10.48)	0.3435 (10.49)	1.027 (31.4)	1.039 (31.7)	1.768 (54.0)	1.799 (54.9)	2.296 (70.1)	2.340 (71.5)
10'	0.1219 (3.72)	0.1218 (3.72)	0.1121 (3.42)	0.112 (3.41)	0.299 (9.155)	0.2998 (9.16)	0.3432 (10.48)	0.3435 (10.49)	1.027 (31.4)	1.037 (31.67)	1.768 (54.0)	1.793 (54.76)	2.295 (70.1)	2.332 (71.2)
20'	0.1219 (3.72)	0.1218 (3.72)	0.1121 (3.42)	0.112 (3.41)	0.299 (9.155)	0.2998 (9.16)	0.3432 (10.48)	0.3435 (10.49)	1.027 (31.4)	1.034 (31.6)	1.767 (54.0)	1.785 (54.51)	2.294 (70.06)	2.332 (71.2)
30'	0.1219 (3.72)	0.1218 (3.72)	0.1121 (3.42)	0.112 (3.41)	0.299 (9.155)	0.300 (9.16)	0.3432 (10.48)	0.3435 (10.49)	1.026 (31.3)	1.028 (31.4)	1.765 (53.9)	1.769 (54.0)	2.291 (69.97)	2.319 (70.8)
40'	0.1219 (3.72)	0.1218 (3.72)	0.1121 (3.42)	0.112 (3.41)	0.299 (9.155)	0.2999 (9.16)	0.3432 (10.48)	0.3432 (10.48)	1.025 (31.3)	1.019 (31.1)	1.763 (53.8)	1.745 (53.3)	2.288 (69.88)	2.184 (69.1)
50'	0.1219 (3.72)	0.1218 (3.72)	0.1121 (3.42)	0.112 (3.41)	0.299 (9.155)	0.2999 (9.16)	0.3431 (10.48)	0.3413 (10.42)	1.024 (31.3)	0.994 (30.4)	1.761 (53.8)	1.689 (51.6)	2.286 (69.8)	2.184 (66.7)

settlements pertain to nodes on pile such as 51, 49 and so on and nodes in the soil such as 68, 66 and so on. The relative displacement between the pile and the soil at different times influenced the kind of skin friction along the pile-soil interface. Before about 27.1 days, the pile settled more than the soil. After 27.1 days, the soil began to settle more than the pile. After this period, the soil gradually settled faster than the pile. The difference between their settlement grew slowly and reached its maximum value of 0.04 ft. or 0.48 inches (1.22 cm) around 301.1 days. These results are essentially in agreement with the criterion by Winterkorn and Fang (31), which requires about 1 cm (0.4 inches) relative settlement for development of maximum skin friction.

Fig. 8 shows the downdrag force divided by the ultimate bearing capacity, vs. time. Before 27.1 days, there was no downdrag load as depicted in Table 3. After day 27.1 the downdrag load increased gradually and reached its maximum value on day 301.1, which was 39% of the ultimate bearing capacity.

Fig. 9 shows the negative skin friction distribution in a number of elements in the vicinity of the pile-soil interface vs. time, while Fig. 10 shows the positive skin friction distribution along the same section (element 20 to 24). From Table 3 and Fig. 9 and 10, it can be seen that whenever the soil settled more than the pile, negative skin friction occurred; otherwise positive skin friction developed. After 27.1 days, elements 22, 23 and 24 experience negative skin friction, while elements 20 and 21 had

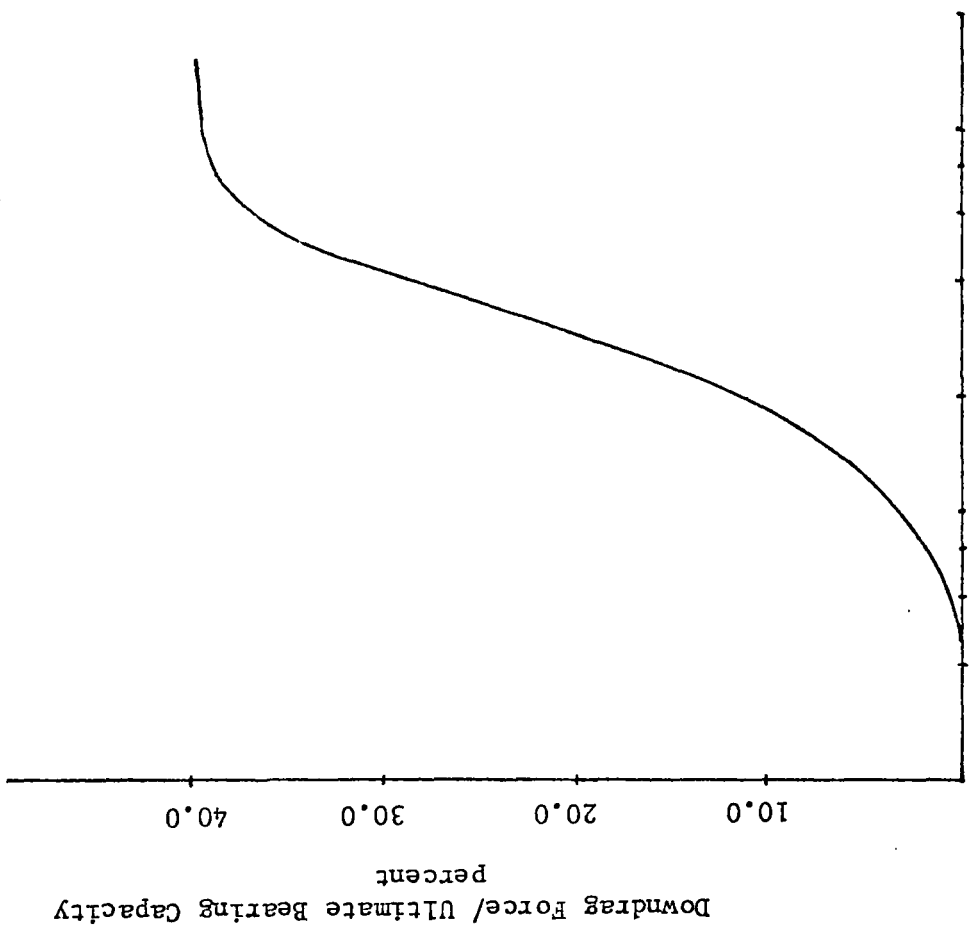

Fig. 8. Downdrag Force/ Ultimate Bearing Capacity vs. Time

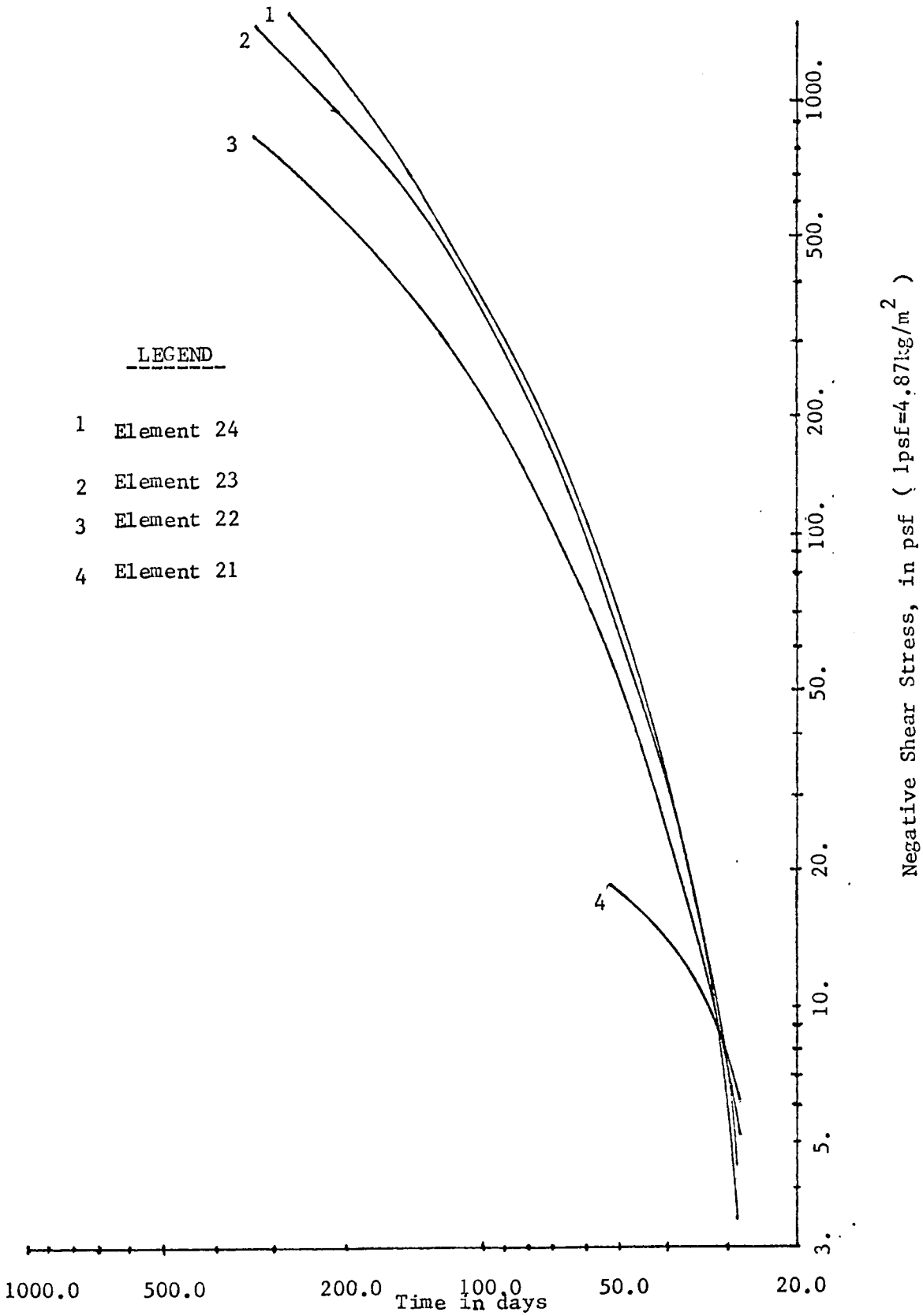

Fig.9. Negative Shear Stress vs. Time

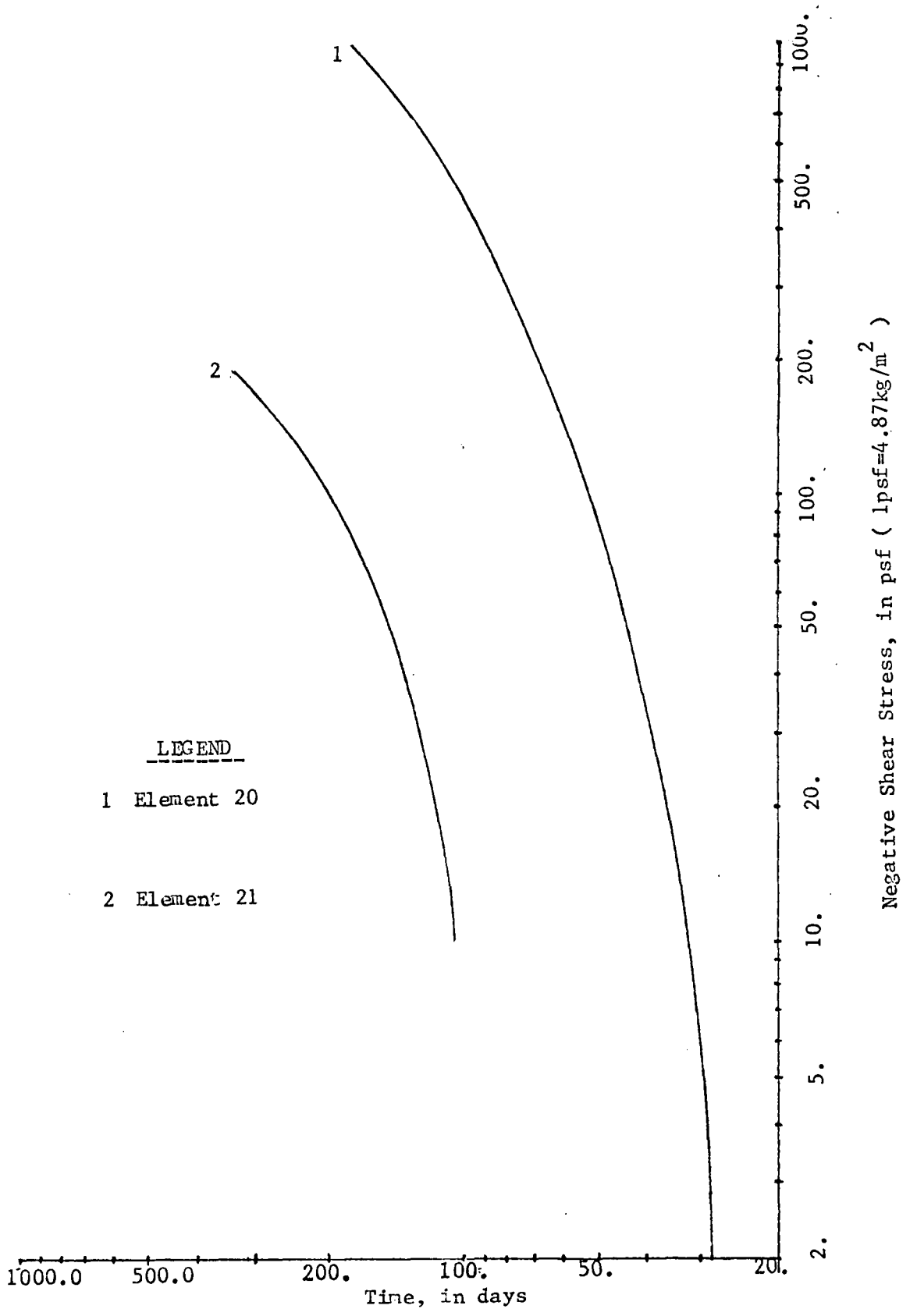

Fig. 10. Positive Shear Stress vs. Time

positive skin friction, Fig. 10a. Thus we can define a neutral point on the pile above which negative skin friction occurs. The ratio of the depth from the surface to the neutral point in relation to the length of the pile is 0.6. However, Endo et al. (30) had estimated this value to be 0.73 to 0.78. If pile were divided into more elements, the computed value can be different.

In determining the maximum downdrag load, it is assumed that the negative skin friction is the average shear stress of the surrounding soil near the pile-soil interface. Often, use of the triangular element may introduce unbalance or skewness. To avoid this and to obtain symmetry, the number of elements were doubled as shown in Fig. 10b. The shear stress, f_s, was then computed as an average of shear stresses in the four triangular elements. For example, at a depth of 25 feet (7.635 m) from the top, it was found as

$$f_s = (\tau_{rz}(22) + \tau_{rz}(30) + \tau_{rz}(102) + \tau_{rz}(110))/4 \qquad (67)$$

where τ_{rz} = shear stress and the number in the parenthesis denotes an element

Then the total drag force, F_n, was evaluated as

$$F_n = \sum_{i=1}^{N} f_{s_i} \cdot \pi \cdot D \cdot \Delta h \qquad (68)$$

where f_s = average shear stress near the pile-soil interface at section i

D = diameter of the pile (0.667' in this problem)

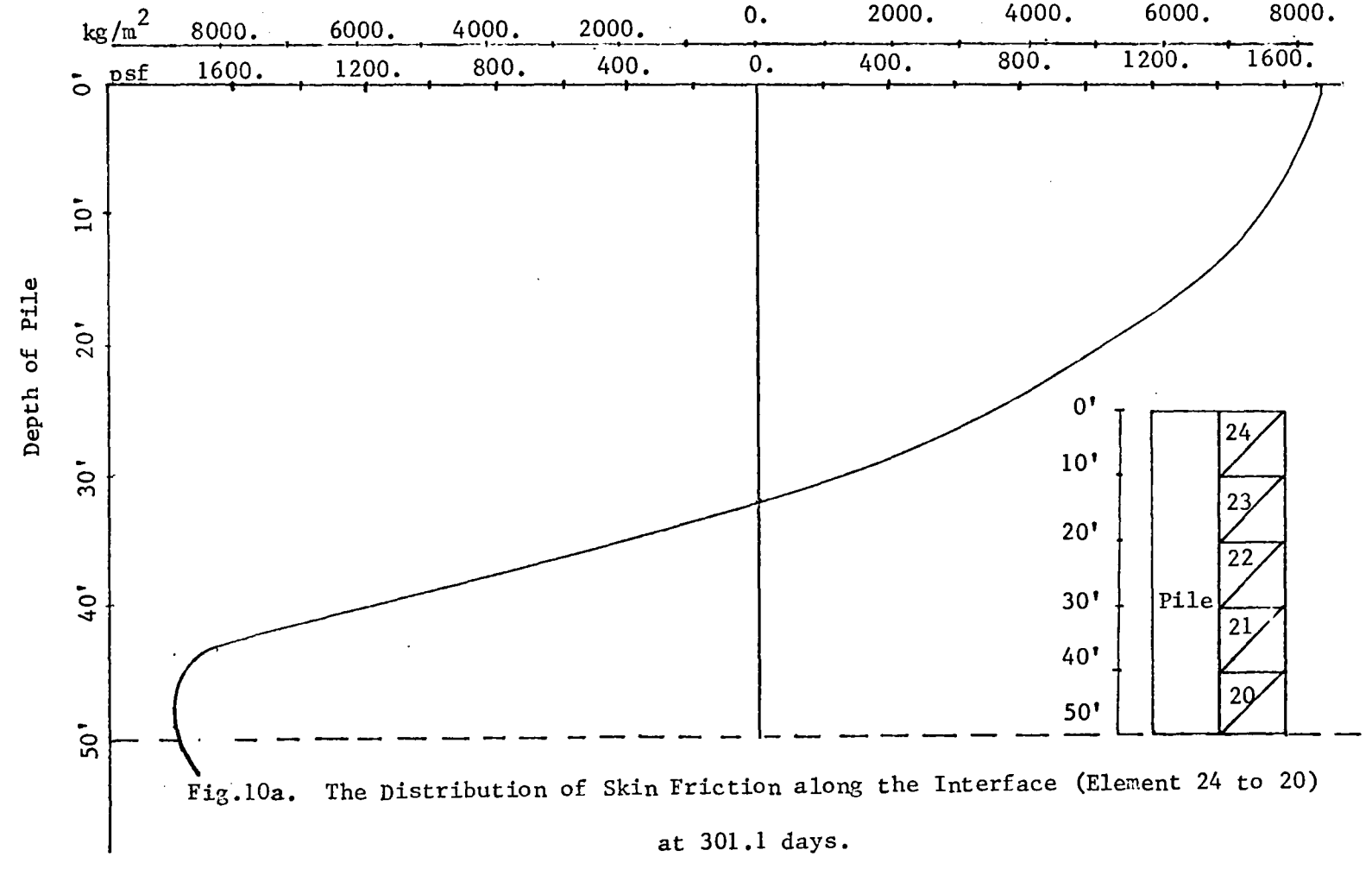

Fig.10a. The Distribution of Skin Friction along the Interface (Element 24 to 20) at 301.1 days.

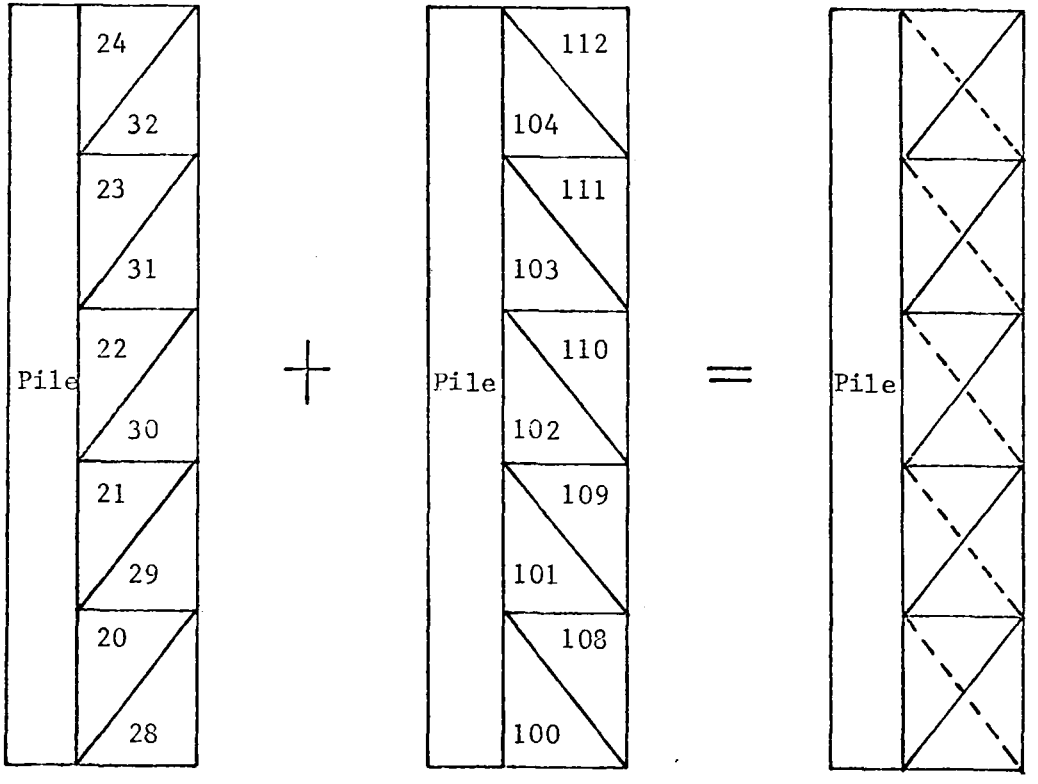

Fig. 10b. Part of the Mesh Near the Interface Area.

Δh = height of the pile surrounding the section

(10 ft (3.054 m) in this problem)

and N = total number of sections

The computed values of the shear stress of the elements near the interface are shown in Table 4.

Substituting the values in Table 4 into equation (67) and (68), we determine an approximate value of the downdrag force to be equal to 43,670 lb. (19,850 Kg). Endo et al. (30) gives a formula for the maximum estimated downdrag as:

$$F_{max} = \eta \cdot \psi \cdot \alpha \int_0^{\beta \ell} \sigma'_{vz} \cdot dZ \qquad (69)$$

where η : coefficient which depends on the type of the pile point (1.0 for closed point pile and 0.6 for open point pile)

α : K tan ϕ_a (0.3 to 0.35)

β : $\ell n/\ell > 1/2$ relative depth of the neutral point (0.73 to 0.78)

ℓn : distance between pile top and neutral point

ℓ : length of pile in compressible strata

ψ : perimeter of pile

For this problem using a closed-point pile, we adopt these values:

$\eta = 1$

$\alpha = 0.35$

$\beta = 0.6$ or 0.7

$\ell = 50'$

Table 4. Shear Stress of Elements near Interface

in psf (kg/m^2)

Element 20	1870.	(9106.9)
Element 21	197.5	(961.8)
Element 22	- 914.7	(-4454.6)
Element 23	-1572.	(-7655.6)
Element 24	-1992.	(-9701.0)
Element 28	2612.	(12720.4)
Element 29	572.1	(2786.1)
Element 30	- 477.3	(- 2324.5)
Element 31	-1130.	(- 5503.1)
Element 32	-1422.	(- 6925.1)
Element		
100	2925.	(14244.8)
101	639.7	(3115.3)
102	- 630.6	(- 3071.)
103	-1418.	(- 6950.7)
104	-1723.	(- 8391.)
Element		
108	1556.	(7577.7)
109	129.8	(632.1)
110	- 716.3	(- 3488.4)
111	-1284.	(- 6253.1)
112	-1521.	(- 7407.3)

$$\psi = 2 \cdot \pi \cdot (0.667') = 4.2'$$

For $\beta = 0.6$, only the top three elements (24, 23 and 22) have negative skin friction, as shown in Fig. 10a.

vz 20 : -3,191 lb/ft^2

vz 21 : -2,159 lb/ft^2

vz 22 : -1.367 lb/ft^2

vz 23 : -730.5 lb/ft^2

vz 24 : -197.2 lb/ft^2

$$F_{max} = \eta \cdot \psi \cdot \alpha \int_0^{0.6\ell} \sigma'_{vz} \cdot dZ$$

$$= \eta \cdot \psi \cdot \alpha \sum_{i=1}^{3} \sigma'_{vz_i} \cdot \Delta\ell$$

$$= 1 \cdot (4.2) \cdot (0.35) \cdot (1,367 + 730.5 + 197.2) \cdot 10$$

$$= 33,730 \text{ lb}$$

$$= 16.87 \text{ ton}$$

For = 0.7

$$F_{max} = 1 \cdot (4.2) \cdot (0.35) \cdot [(1,367 + 730.5 + 197.2) \cdot 10 + (0.5) \cdot (2,159) \cdot 10]$$

$$= 49,560 \text{ lb}$$

$$= 24.78 \text{ ton}$$

Hence, the average value using Endo's method is approximately 41,650 lb. or 20.8 ton. This value is very close to the computed value of 43,670 lb.

Negative Skin Friction Due to Backfill

In this case, a pile was assumed to be driven in a homogeneous compressible material. The same finite element mesh as in the first case (Fig. 5) was used. Freshly placed fill of about 35 ft (10.69 m) high was placed on the surface starting from 0.667 ft from the pile-soil interface up to the right-hand boundary, Fig. 10c. Assuming a density for fill equal to about 110 lb/ft^3 (1,755.6 Kg/m^3), this created an equivalent uniform applied load of about 4,000 lb/ft^2 (19,480 Kg/m^2).

The variation of porepressure along the depth at 1.33 ft (0.4 m) from the interface vs. time is shown in Fig. 11. In the initial stages, the consolidation process was found to be not quite stable, as indicated by the curves at time t = 0, t = 1.1 and t = 5.1 days. Gradually the process became steadier and after 1,050 days, the consolidation was almost 95% complete. The vertical settlement along the depth for two nodal points, 63 (near the center) and 68 (at the surface) vs. time is shown in Fig. 12. The figure indicates that the surface soil settled more than the central and lower layers in the initial stage, but they converged to a stable value of 0.65 ft (0.2 m) near the completion of the consolidation process.

The movements between pile and soil was calculated as a function of time and depth, Table 5a. Table 5b shows the rates of settlement of soil near the pile-soil interface as a function of time. Fig. 13 shows the variations of positive skin friction for the elements in the pile vicinity with respect to time, while Fig. 14 shows the

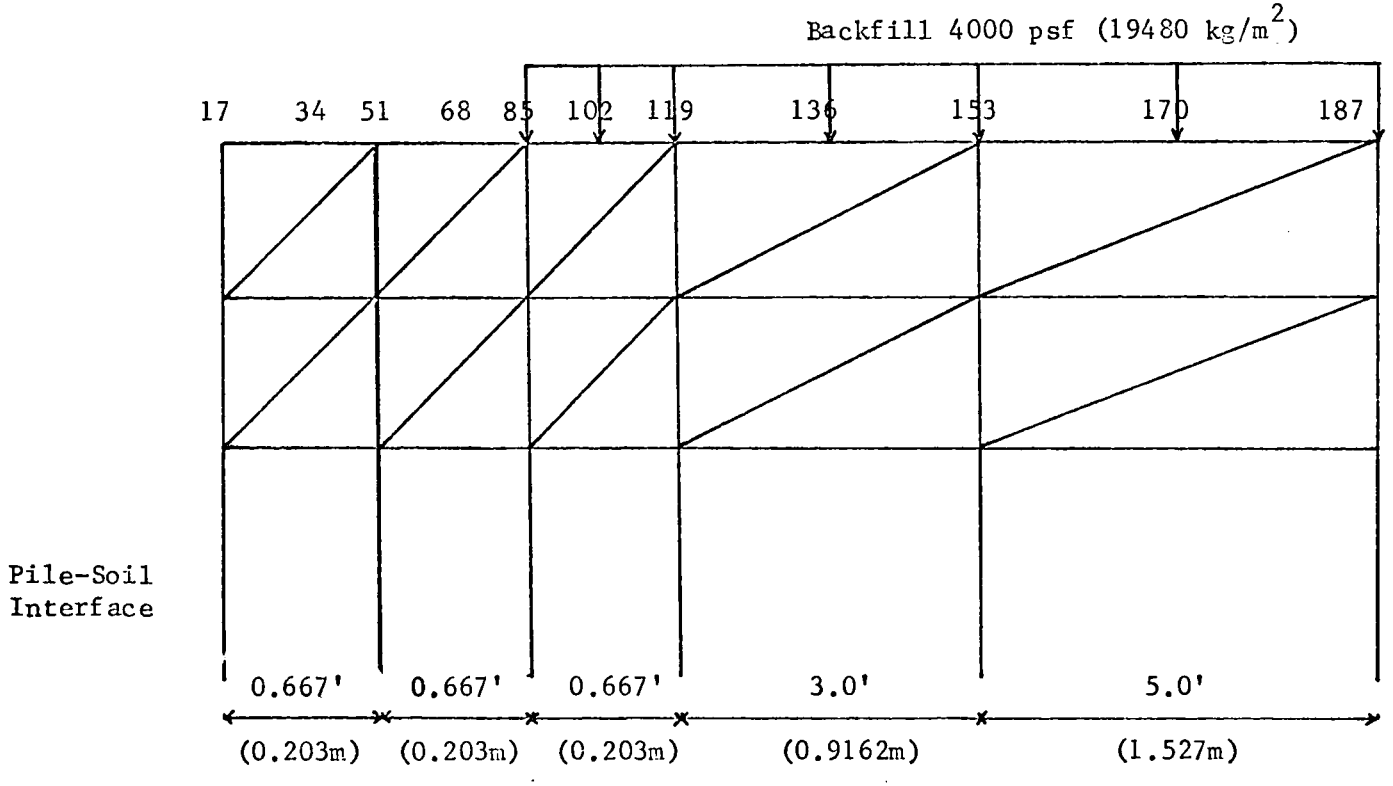

Fig. 10c. Backfill Loading on the Surface of FE Mesh

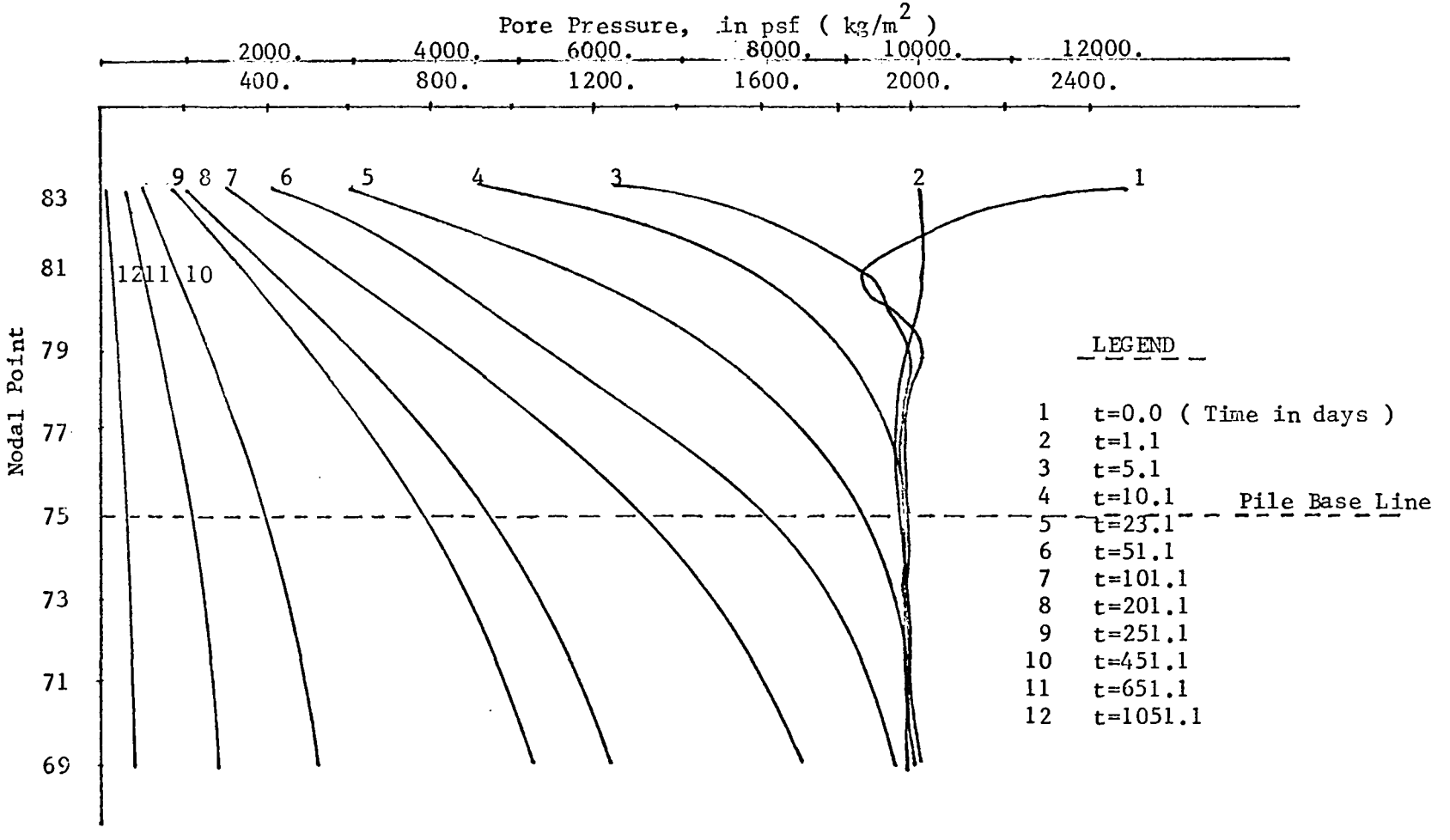

Fig. 11. Porepressure as a Function of Depth and Time

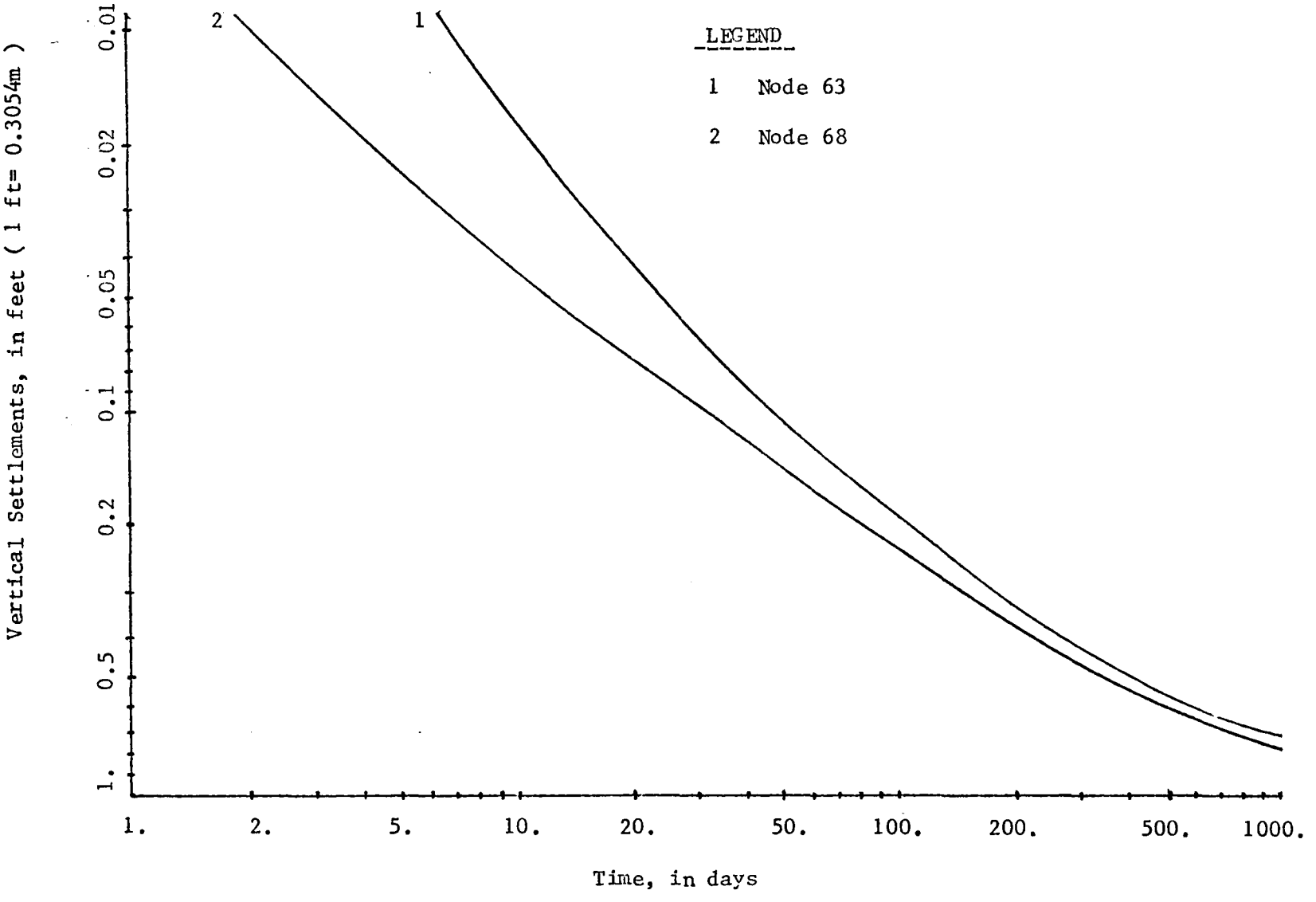

Fig. 12. Settlements of Node 68 and 63 Due to Backfill

Table 5a. Settlements between Pile(Node 51 to 41) and Soil(Node 68 to 58)						Unit: ft(cm)	
50'	40'	30'	20'	10'	0'	Depth	Time
0.01898 (0.580)	0.01909 (0.583)	0.01932 (0.590)	0.01966 (0.600)	0.02004 (0.612)	0.02025 (0.618)	Pile	10.1
0.01547 (0.472)	0.01549 (0.473)	0.01588 (0.485)	0.01810 (0.553)	0.02539 (0.775)	0.04183 (1.277)	Soil	day
0.05695 (1.739)	0.05724 (1.748)	0.05780 (1.765)	0.05854 (1.788)	0.05926 (1.810)	0.05960 (1.820)	Pile	27.1
0.04459 (1.362)	0.04895 (1.495)	0.05235 (1.599)	0.05902 (1.802)	0.07065 (2.158)	0.08976 (2.741)	Soil	day
0.1977 (6.038)	0.1983 (6.056)	0.1994 (6.090)	0.2007 (6.129)	0.2017 (6.160)	0.2.22 (6.175)	Pile	101.1
0.1708 (5.216)	0.1845 5.635)	0.1935 (5.909)	0.2052 (6.267)	0.2202 (6.725)	0.2415 (7.375)	Soil	day
0.3368 (10.286)	0.3375 (10.307)	0.3388 (10.347)	0.3403 (10.393)	0.3416 (10.432)	0.3422 (10.450)	Pile	201.1
0.3014 (9.205)	0.3214 (9.816)	0.3333 (10.179)	0.3470 (10.597)	0.3633 (11.095)	0.3854 (11.770)	Soil	day
0.5329 (16.275)	0.5339 (16.305)	0.5356 (16.357)	0.5374 (16.412)	0.5389 (16.458)	0.5395 (16.476)	Pile	451.1
0.4863 (14.852)	0.5147 (15.719)	0.5305 (16.201)	0.5470 (16.705)	0.5648 (17.249)	0.5879 (17.954)	Soil	day
0.6417 (19.598)	0.6428 (19.631)	0.6446 (19.686)	0.6466 (19.747)	0.6482 (19.796)	0.6489 (19.817)	Pile	851.1
0.5889 (17.068)	0.6219 (18.993)	0.6398 (19.539)	0.6578 (20.089)	0.6765 (20.660)	0.7001 (21.381)	Soil	day
0.6602 (20.162)	0.6613 (20.196)	0.6632 (20.254)	0.6652 (20.315)	0.6668 (20.364)	0.6675 (20.385)	Pile	1051.1
0.6063 (18.516)	0.6402 (19.552)	0.6584 (20.108)	0.6766 (20.663)	0.6955 (21.241)	0.7192 (21.964)	Soil	day

Table 5b. Settlements and Rates of Settlement of Soil (from node 68 to 58) in feet(cm) and feet/month(cm/month)

Depth	10.1day -31.1dqy		31.1day -101.1day		101.1day - 201.1day		201.1day-451.1day		451.1day-1051.1day	
	Settlement	Rate of Settlement	S.	R.	S.	R.	S.	R.	S.	R.
0'	0.058 (1.771)	0.0828 2.529)	0.1417 (4.328)	0.0607 (1.854)	0.1439 (4.395)	0.0432 (1.319)	0.2025 (6.184)	0.0243 (0.742)	0.1313 (4.010)	0.00656 (0.200)
10'	0.055 (1.680)	0.0785 (2.397)	0.1398 (4.269)	0.0599 (1.829)	0.1431 (4.370)	0.0429 (1.310)	0.2014 (6.151)	0.0241 (0.736)	0.1306 (3.989)	0.00653 (0.199)
20'	0.050 (1.527)	0.0714 (2.181)	0.1370 (4.184)	0.0587 (1.793)	0.1418 (4.331)	0.0425 (1.298)	0.1999 (6.105)	0.0239 (0.730)	0.1296 (3.958)	0.00648 (0.198)
30'	0.0451 (1.377)	0.0644 (1.967)	0.1325 (4.047)	0.0567 (1.732)	0.1397 (4.266)	0.0419 (1.280)	0.1966 (6.004)	0.0236 (. 21)	0.1284 (3.921)	0.00642 (0.196)
40'	0.0415 (1.267)	0.0592 (1.808)	0.1276 (3.897)	0.0546 (1.667)	0.1368 (4.178)	0.0410 (1.252)	0.1933 (5.903)	0.0231 (0.705)	0.1252 (3.824)	0.00626 (0.191)
50'	0.0374 (1.142)	0.0534 (1.631)	0.1189 (3.631)	0.0509 (1.554)	0.1306 (3.989)	0.0392 (1.197)	0.1849 (5.647)	0.0221 (0.675)	0.1199 (3.662)	0.00599 (0.183)

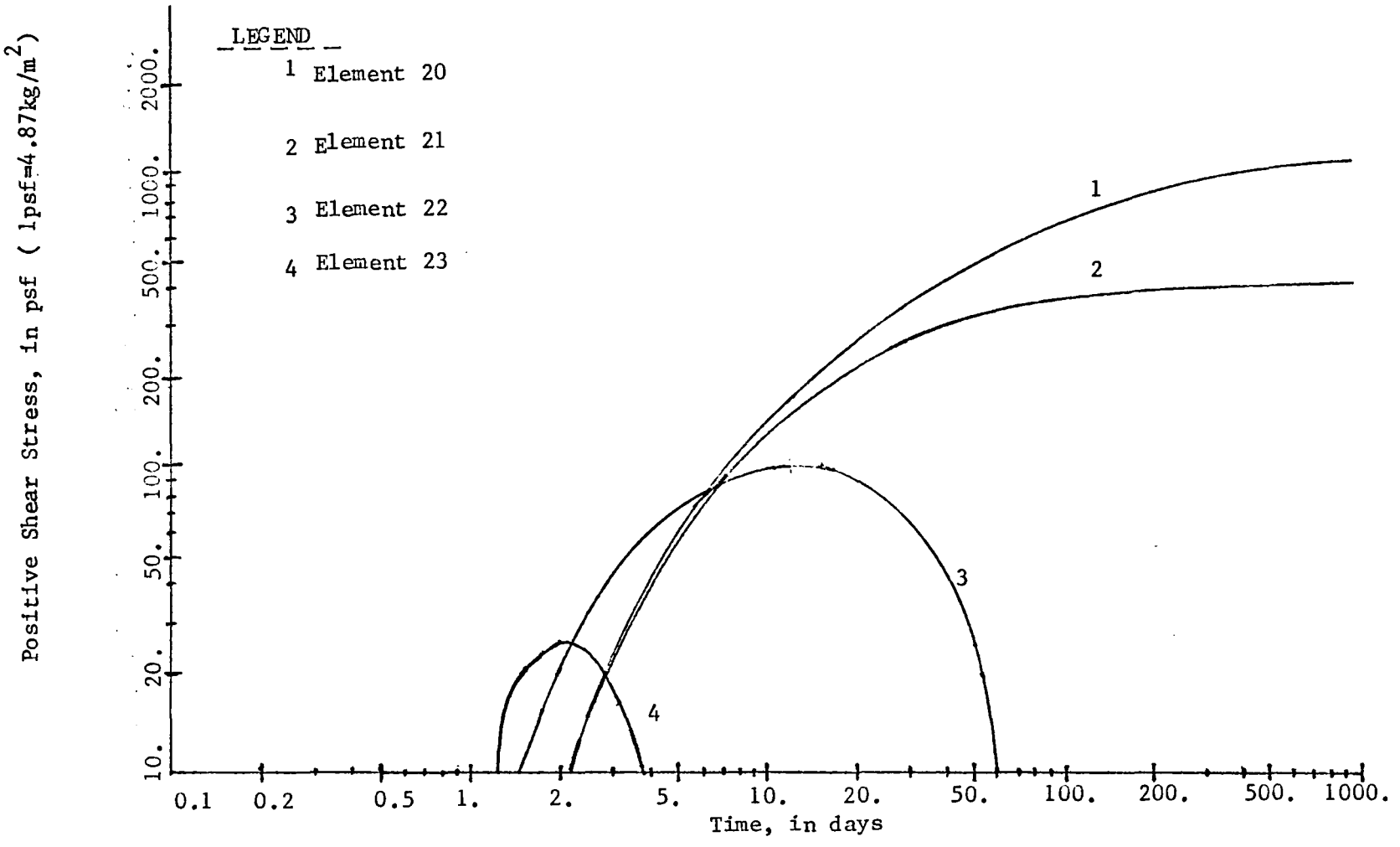

Fig. 13. Positive Shear Stress vs. Time (Backfill Effect)

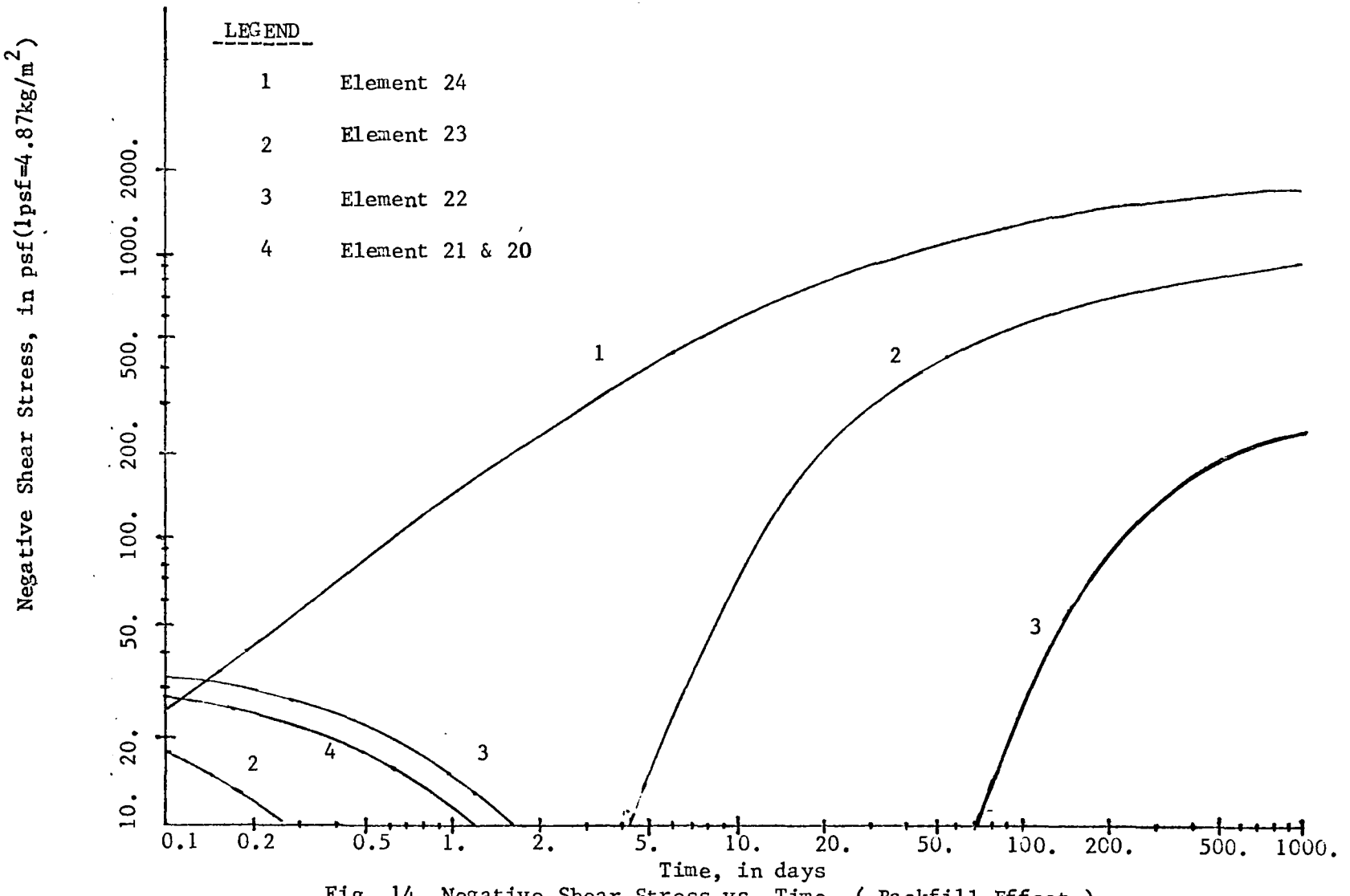

Fig. 14. Negative Shear Stress vs. Time. (Backfill Fffect)

negative skin friction variations. Comparing Figs. 13 & 14 with Table 5, it is obvious that when the soil settled more than the pile, negative skin friction occurred (Fig. 14); otherwise positive skin friction occurred as in Fig. 13.

Fig. 15a gives the percentage of computed maximum downdrag load with respect to the ultimate bearing capacity* vs. time. The maximum value is seen to be about 24% of the ultimate bearing capacity of the pile. Fig. 15b shows the existence of a neutral point which is defined as the point at which the soil and the pile move together. The results show the neutral point at about 30 ft below the ground surface.

Fig. 15c suggests another method used by Endo et al. (31) to estimate the neutral point. The figure plots the vertical axial stress distribution vs. pile depth as a function of time. The neutral point occurs at the maximum axial stress. In this figure, at maximum downdrag this point is about 30 ft (9.16 m) below the ground surface.

---

*The ultimate bearing capacity was computed as

$$UBC = \int_0^L C \cdot Ca \cdot dZ + q \cdot A_b$$

where c = circumference

Ca = adhesion (and friction) at interface between pile and soil = (490 lb/ft^2) or (2,386.3 Kg/m^2)

q_o = bearing capacity at base = $C_a N_c + (\gamma - 62.5)$

N_c = 9

UBC = $2 \cdot (3.1416) \cdot (0.667) \cdot (490) \cdot 50 + [490.9 + (110 - 62.5)] \cdot \pi \cdot (0.667)^2$ = 108,900 lb

= 49,500 Kg.

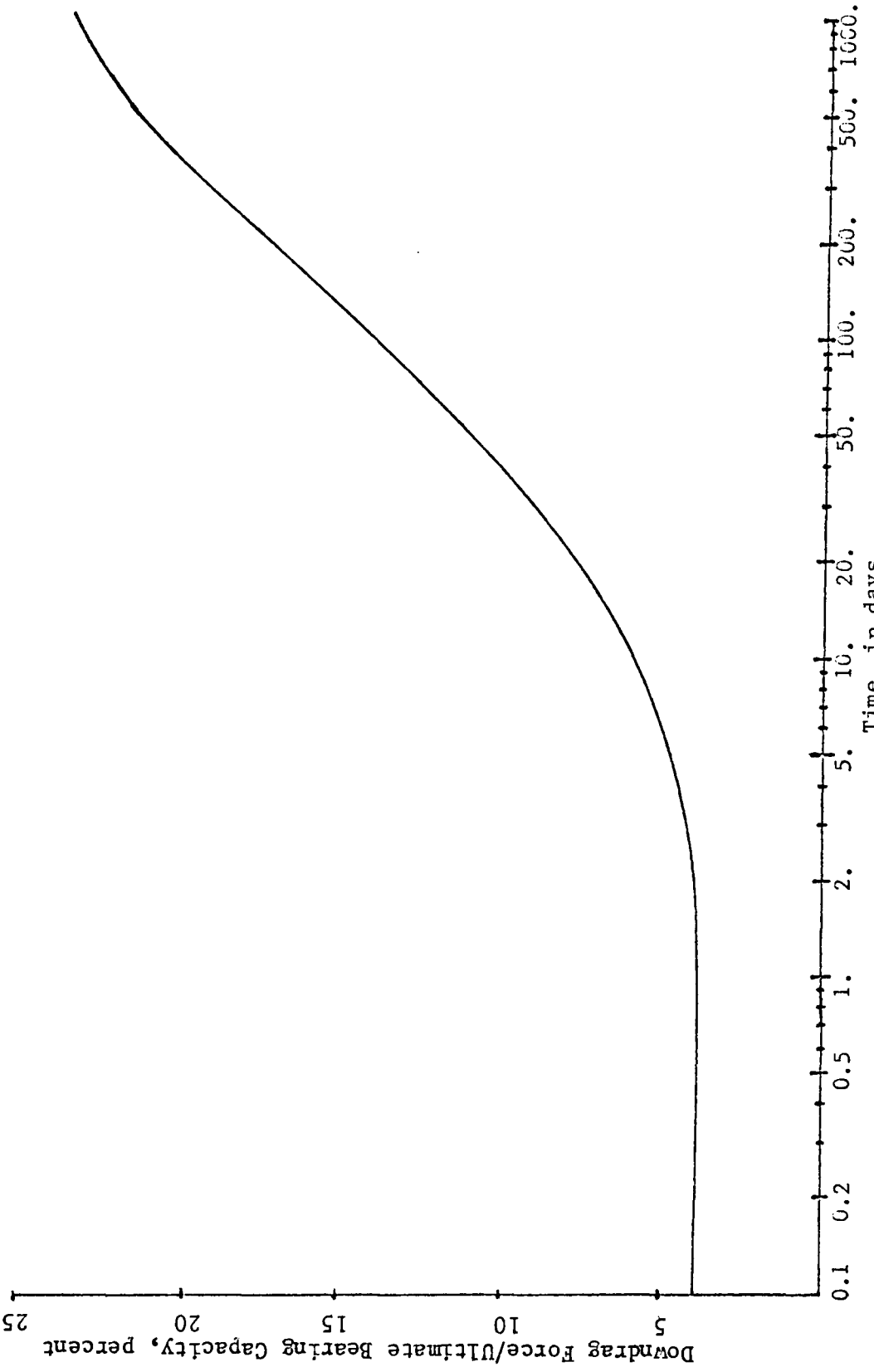

Fig. 15a. Downdrag Force/ Ultimate Bearing Capacity vs. Time

Fig. 15b. Determination of Neutral Point from

Relative Displacement
Settlements of Pile (node 51 to 41) and Soil (node 68 to 58), in ft. (cm)

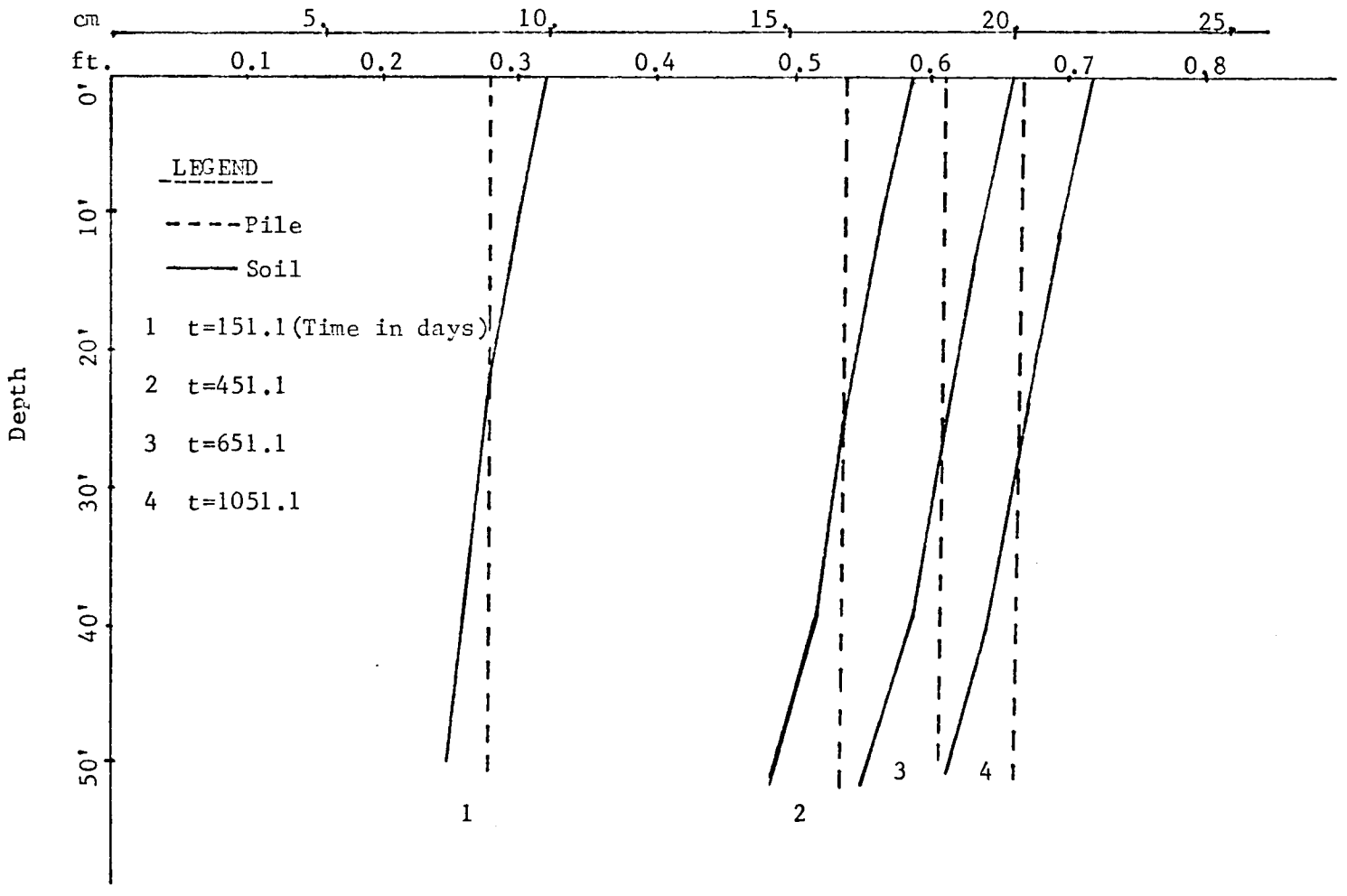

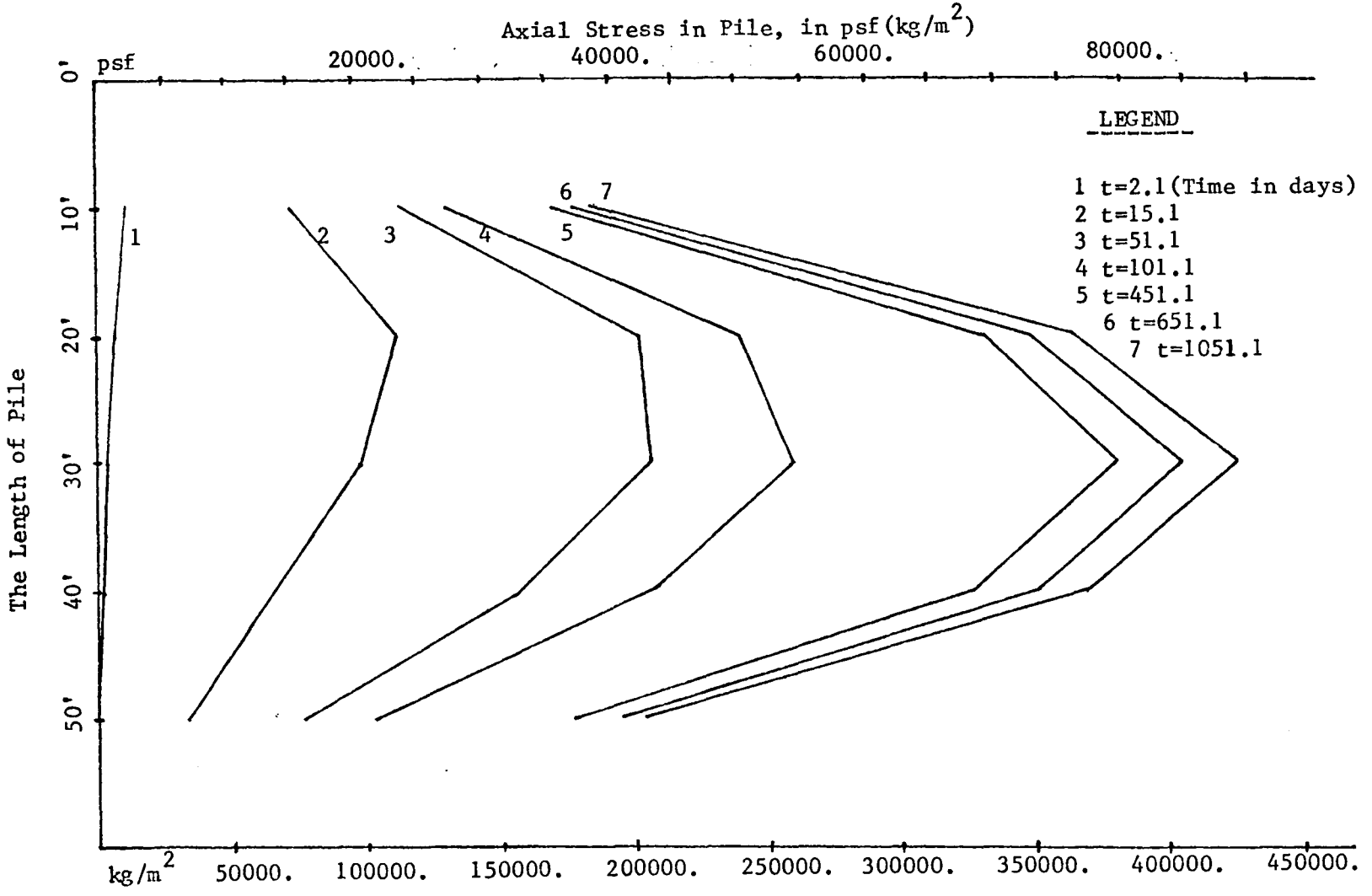

Fig. 15c. Determination of Neutral Point from Pile Axial Stress.

Fig. 16 shows the skin friction distributions along the section at 0.333 ft (0.1 m) from the pile face at different time levels. The net downdrag load is the difference between the negative skin friction and the positive skin friction times the surface area of the pile. Thus, the maximum downdrag load of 26,000 lb (11,820 Kg) was computed.

The Influence of External Pile Load

In the previous examples we have discussed the relationship between porepressure, relative settlement and skin friction for consolidation due to gravity and due to fill. For the effect of loads applied to the pile top, the same FE mesh as shown in Fig. 5 was used. A load of 7,000 lb/ft^2 (34.090 Kg/m^2) was applied at nodal points 51, 34 and 17, and the equivalent backfill load, 4,000 lb/ft^2 (19,480 Kg/m^2), no nodal points 187, 170, 153, 136, 119, 102 and 85. The settlement of the pile (at node 51 on top, node 41 on the bottom), and the surrounding soil settlements (node 68 near the pile top, node 58 near the pile tip) vs. time are shown in Fig. 17. At the upper part of the pile, the soil settled more than the pile and created negative skin friction as in the previous problems. At the lower part of the pile, the soil settled less than the pile, causing positive skin friction.

Next, a load of 21,000 lb/ft^2 (102,270 Kg/m^2) was applied on the pile-top, the results are shown in Fig. 18. The pile-top loading was increased with loads of 35,000 lb/ft^2 (170,450 Kg/m^2) and 56,000 lb/ft^2 (272,720 Kg/m^2), and the results are shown in Fig. 19 and 20, respectively.

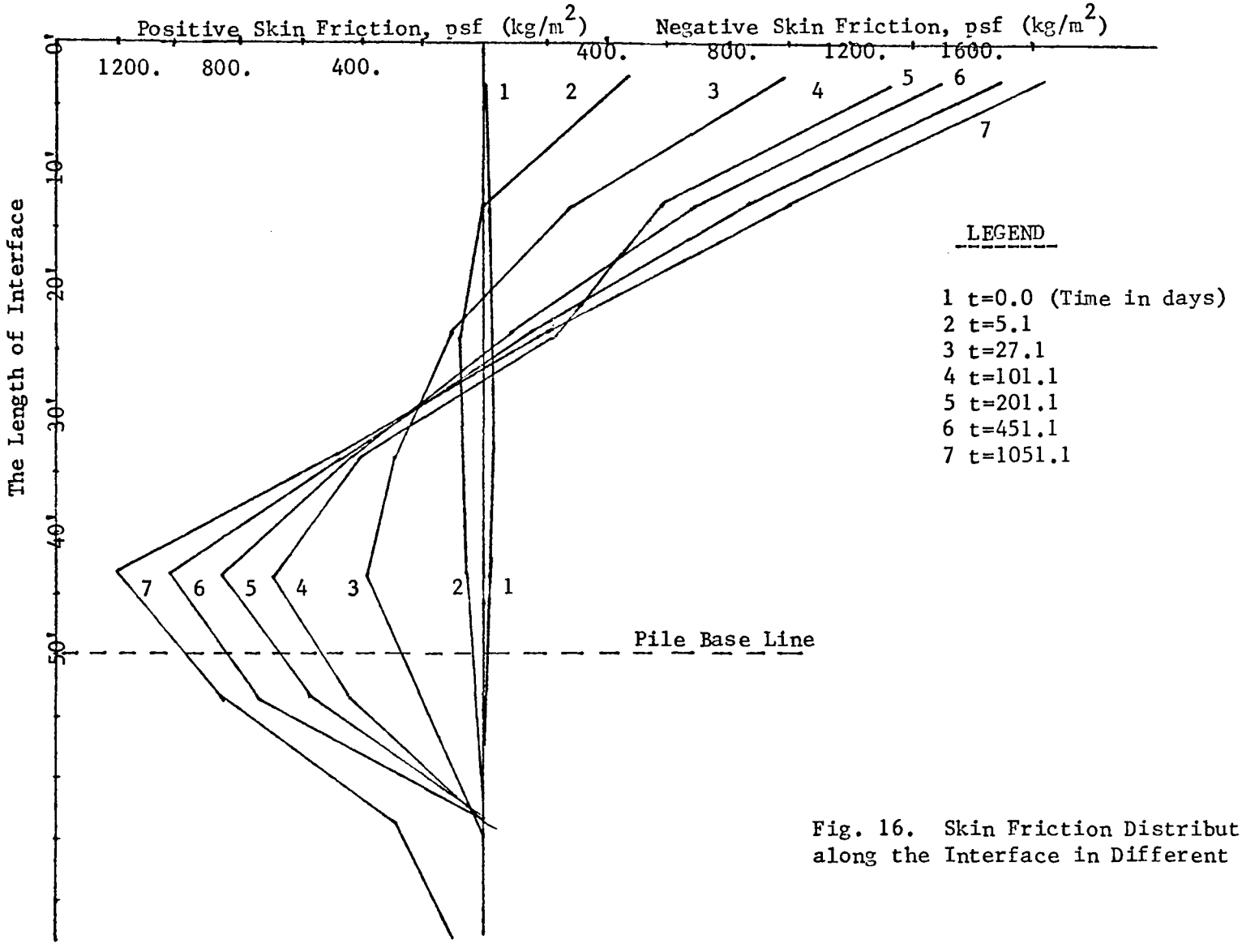

Fig. 16. Skin Friction Distribution along the Interface in Different Time.

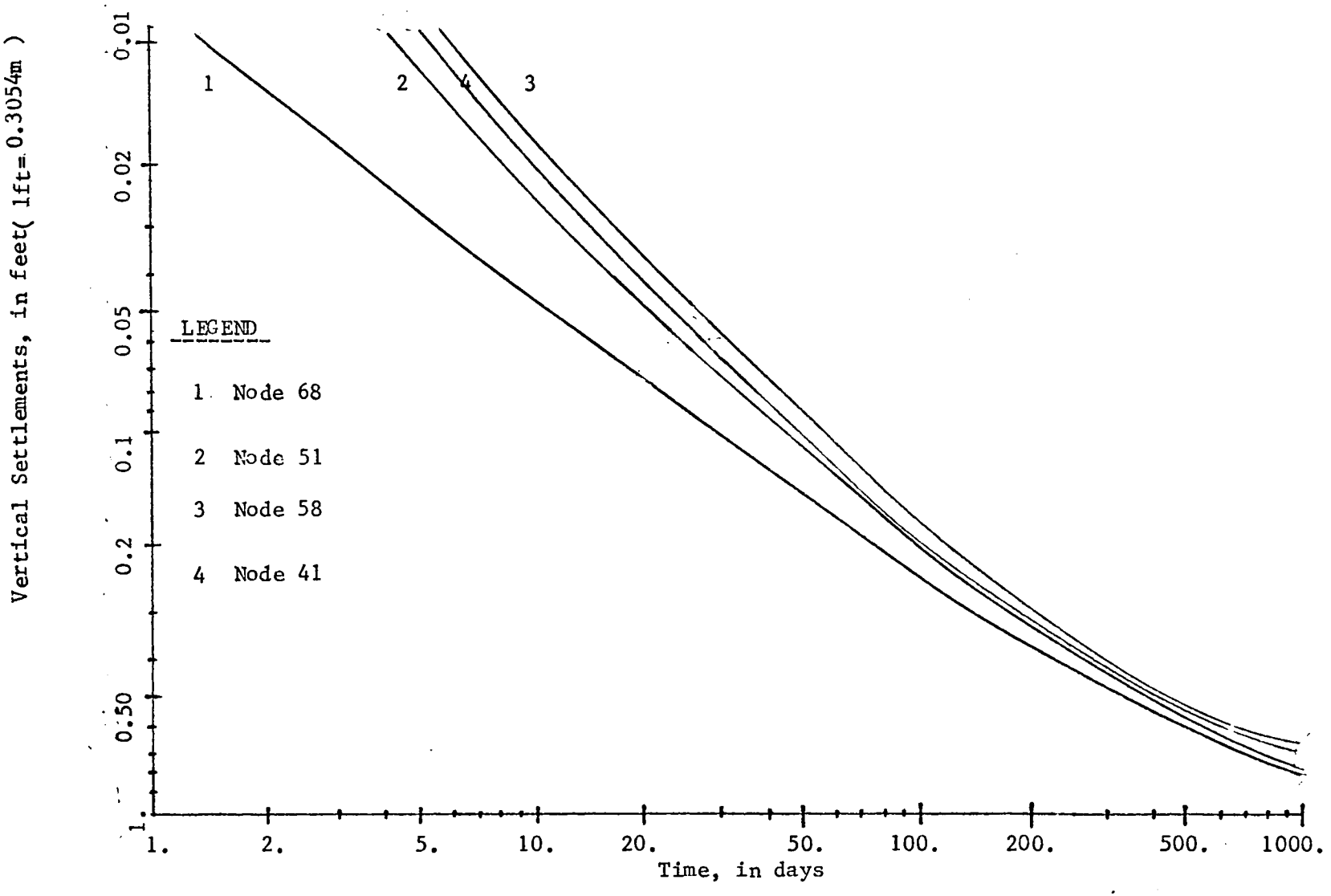

Fig. 17. Settlements of Node 68, 51, 58 and 41 Due to 7000 psf Pile-Top Load.

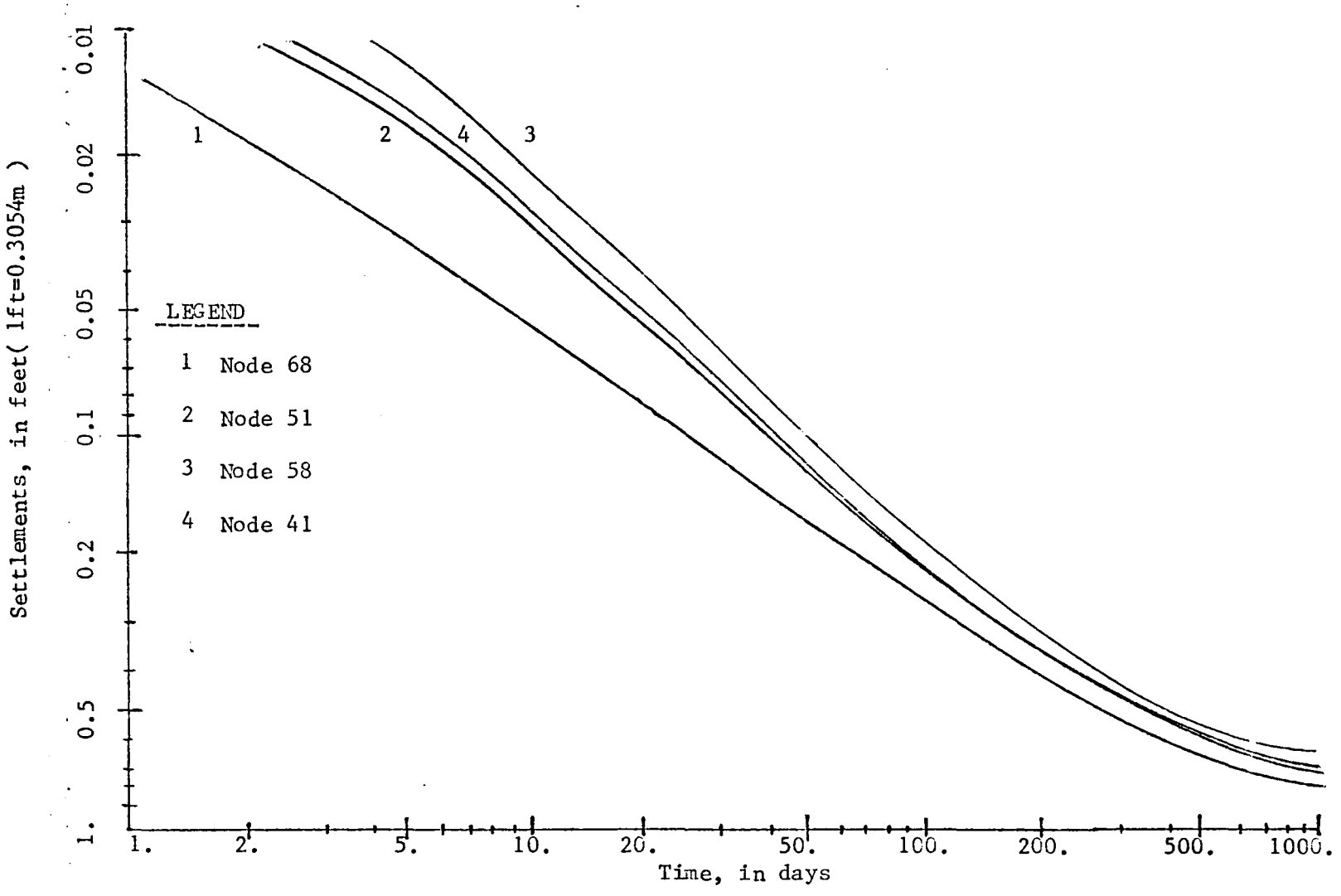

Fig. 18. Settlements of Node 68, 51, 58 and 41 Due to 21000 psf Pile-Top Load.

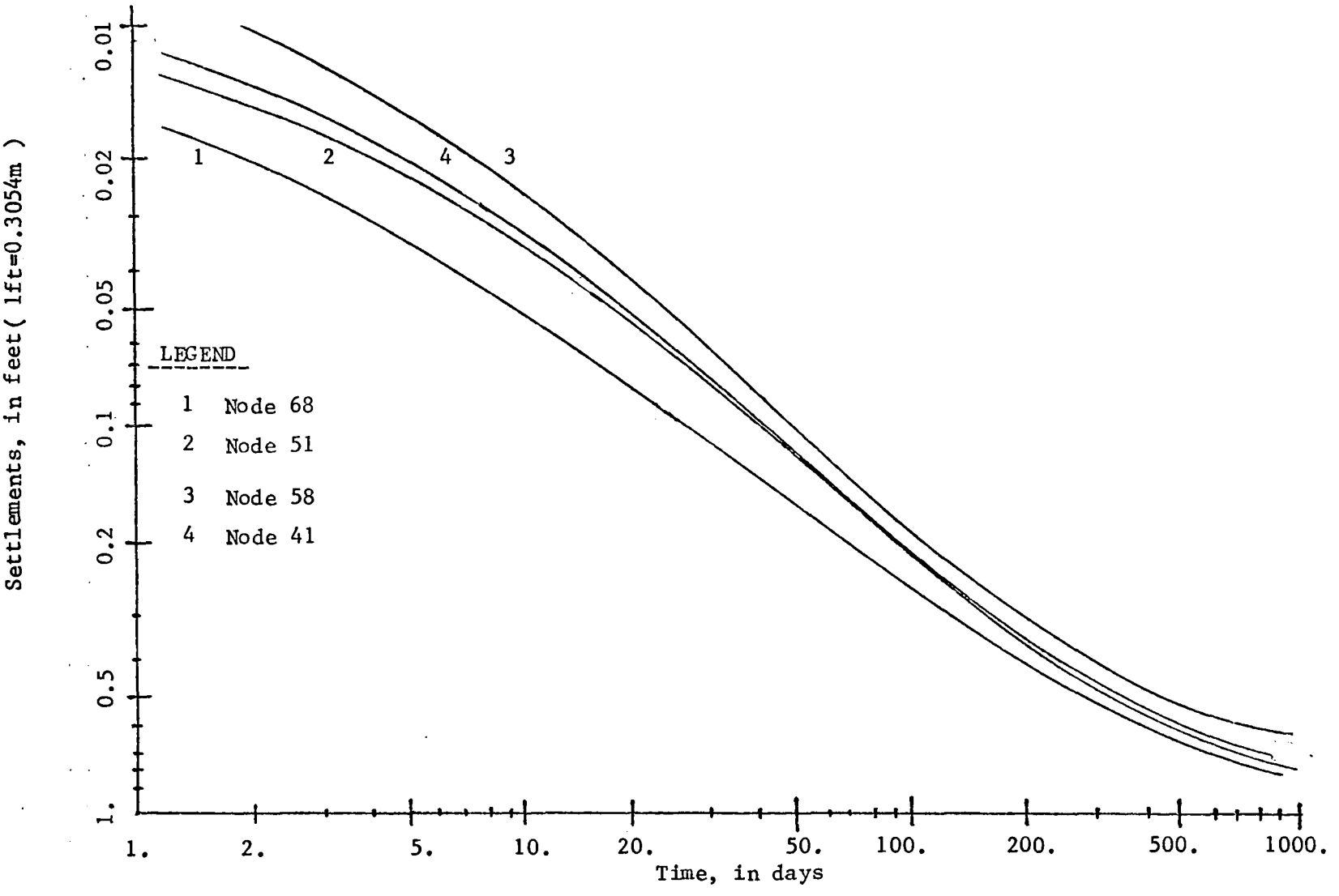

Fig. 19. Settlements of Node 68, 51, 58 and 41 Due to 35000 psf Pile-Top Load.

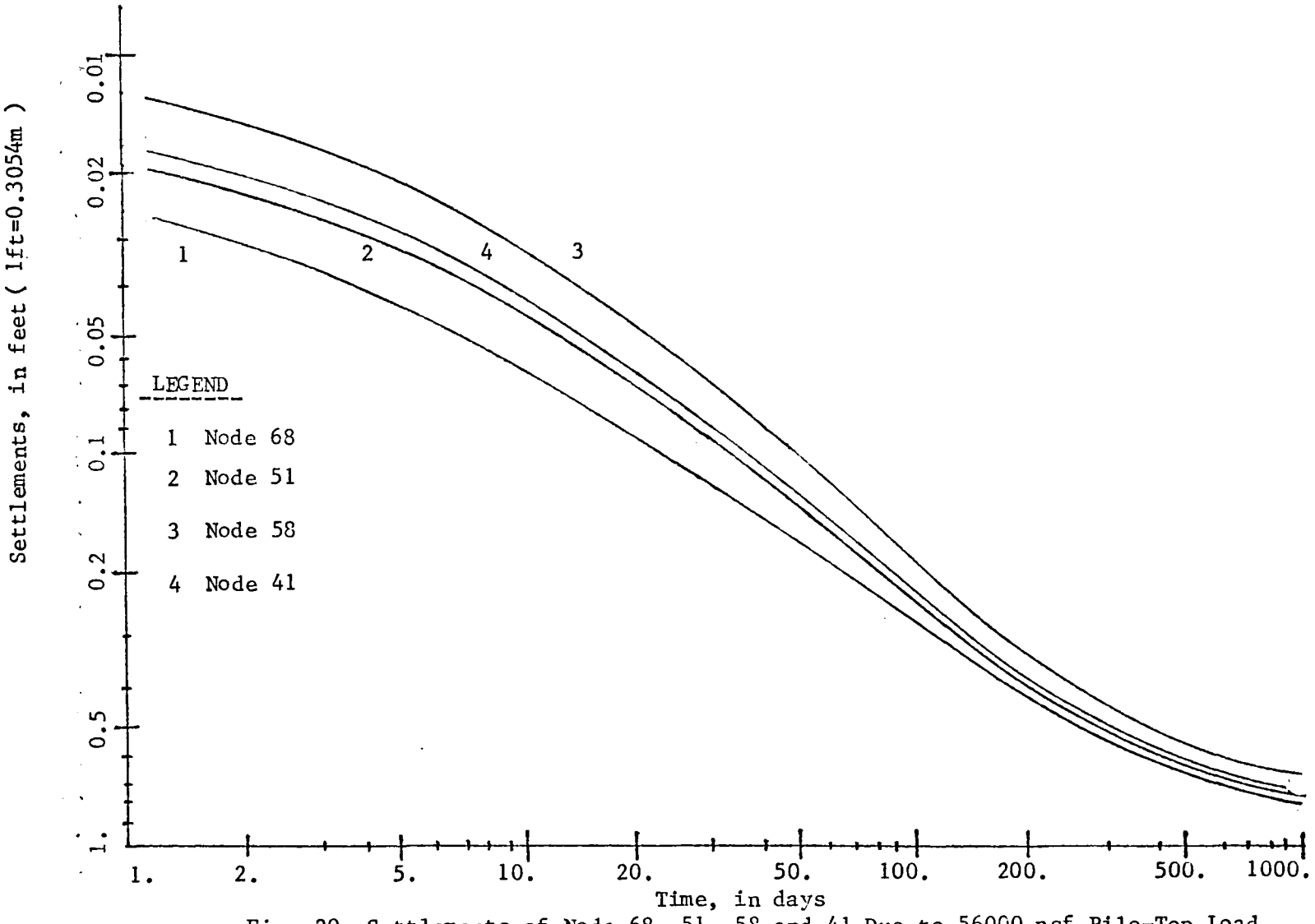

Fig. 20. Settlements of Node 68, 51, 58 and 41 Due to 56000 psf Pile-Top Load.

From Fig. 17 to Fig. 20, it is obvious that the relative displacements between the pile and the soil for each different loading condition were quite different. Fig. 21 shows the relative displacement variations with respect to time for each loading condition. The relative displacement was found as the difference between the settlement of a node on pile and of the node in the vicinity in the soil. Near the pile top, the relative displacement (S_{68} minus S_{51}) decreased when the applied pile-top load increased. In contrast, the relative displacement (S_{41} minus S_{58}) near the pile tip increased with the increase of the applied load.

Table 6 gives the rate of relative displacements of three different loading conditions for different time periods. In condition 1 (7,000 lb/ft^2), 2 (21,000 lb/ft^2), and 3 (56,000 lb/ft^2), after 51.1 days the rate of relative displacement near the pile tip increased when the applied load increased. Compared with the skin friction variations along the pile-soil interface in Fig. 22, 23 and 24 for 7,000, 21,000 and 56,000 lb/ft^2 loads respectively, the positive skin friction along the lower part of the pile increased as the load increased. On the other hand, the negative skin friction along the upper part of the pile decreased as the load increased.

This phenomenon further demonstrates the relationship between relative settlement of pile and soil and the resulting skin friction. As the load is increased on the pile-top, on the basis of the results of soil-pile settlement variations and distributions of skin friction along the pile-soil interface, it can be concluded that the downdrag

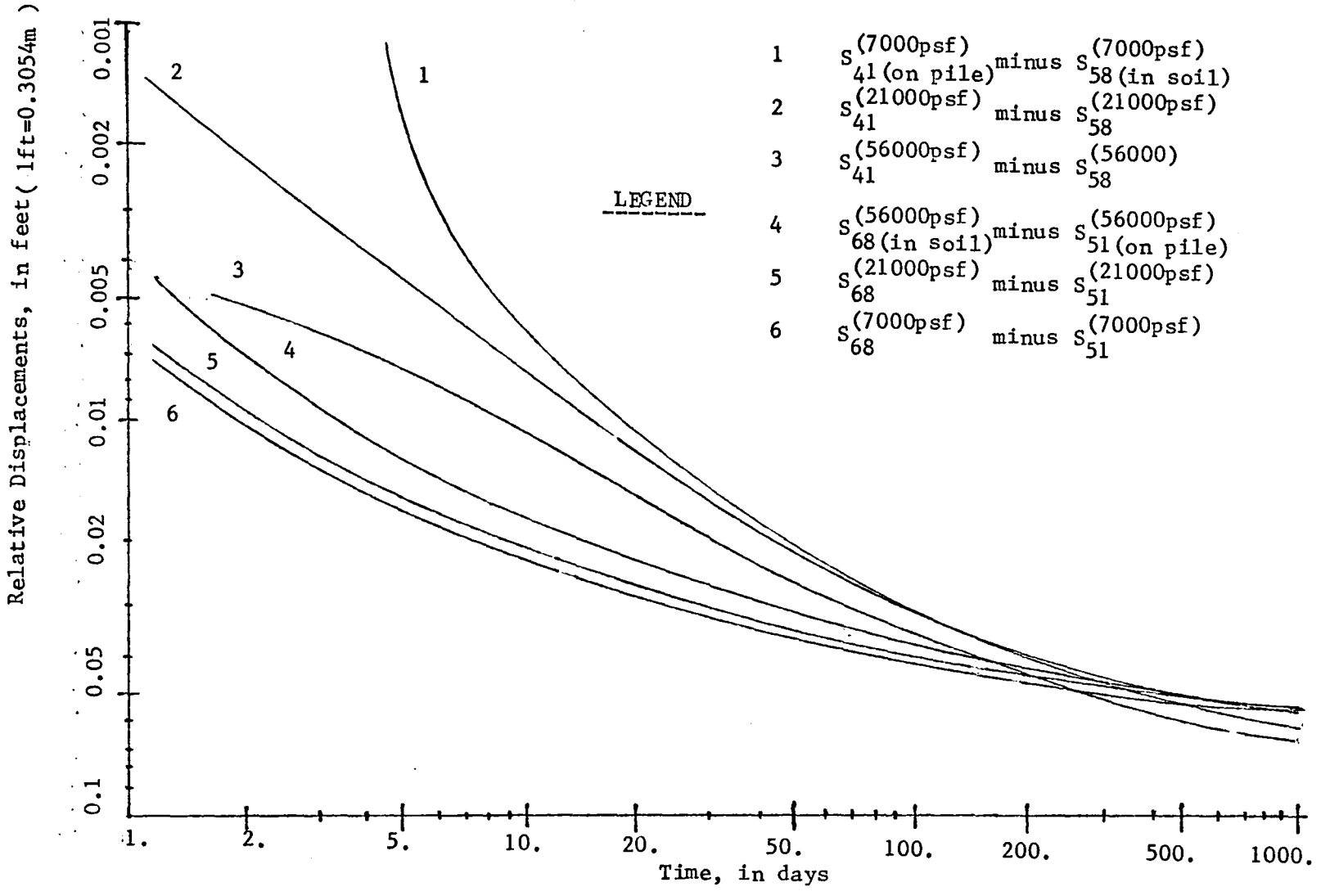

Fig. 21. The Relative Displacement near Pile Top (S_{68}-S_{51}) and Pile Tip (S_{41}-S_{58}) vs. Time under Different External Pile-Top Load.

Table 6. The Rate of Relative Displacement (S_{68}-S_{51} near top, S_{41}-S_{58}near tip)

Cond.	Time / Rate	ft/month (cm/month) 2.1 - 6.1day	6.1-10.1	10.1 - 31.1	31.1 - 51.1	51.1 - 101.1	101.1-651.1	651.1-1051.1
1.	Top	0.05775 (1.764)	0.0375 (1.145)	0.0107 (0.327)	0.00525 (0.160)	0.0042 (0.128)	0.0006 (0.018)	0.0002 (0.006)
(7000)	Tip	0.0045 (0.137)	0.00945 (0.289)	0.0106 (0.324)	0.0105 (0.321)	0.006 (0.183)	0.00109 (0.033)	0.00024 (0.007)
2.	Top	0.0525 (1.603)	0.03 (0.916)	0.0105 (0.321)	0.00521 (0.159)	0.003 (0.092)	0.000560 (0.017)	0.00015 (0.005)
(21000)	Tip	0.0225 (0.687)	0.015 (0.458)	0.01275 (0.389)	0.009 (0.275)	0.0062 (0.190)	0.0025 (0.076)	0.00035 (0.011)
3.	Top	0.04875 (1.489)	0.0275 (0.840)	0.0101 (0.308)	0.0345 (1.054)	0.0029 (0.089)	0.00042 (0.013)	0.00012 (0.004)
(56000)	Tip	0.023 (0.702)	0.017 (0.519)	0.012 (0.366)	0.0105 (0.321)	0.0065 (0.194)	0.0027 (0.082)	0.00041 (0.013)

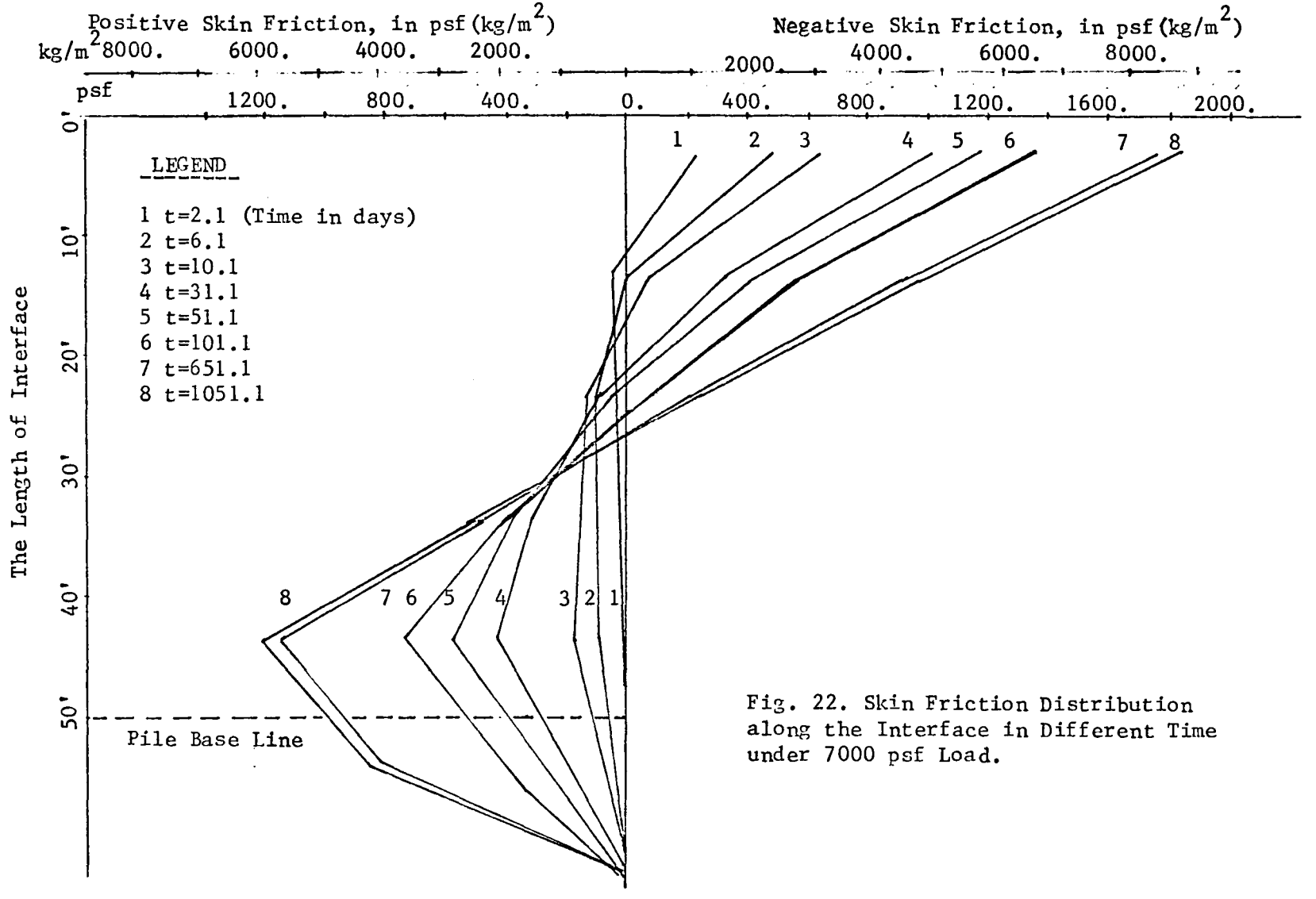

Fig. 22. Skin Friction Distribution along the Interface in Different Time under 7000 psf Load.

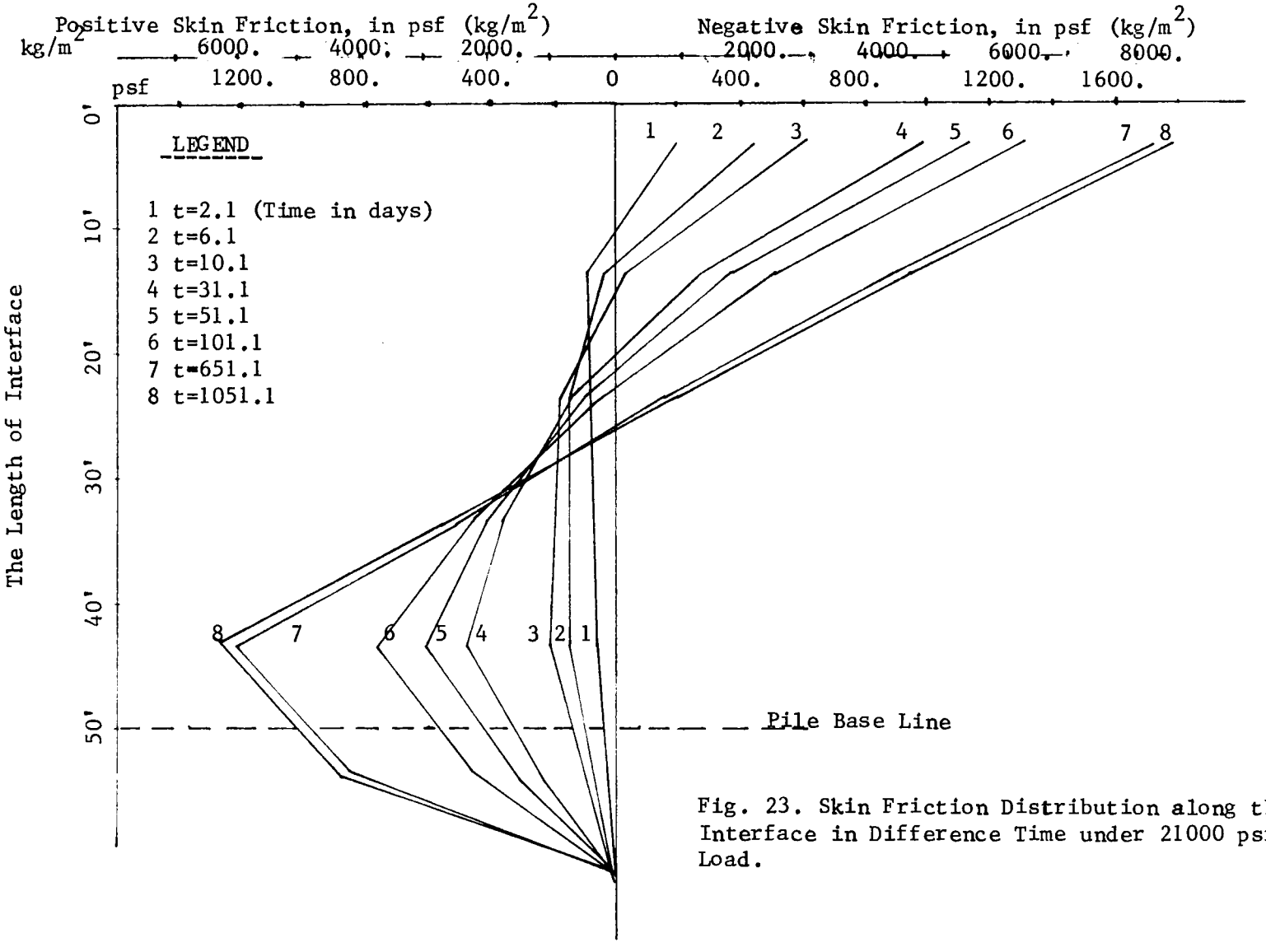

Fig. 23. Skin Friction Distribution along the Interface in Difference Time under 21000 psf Load.

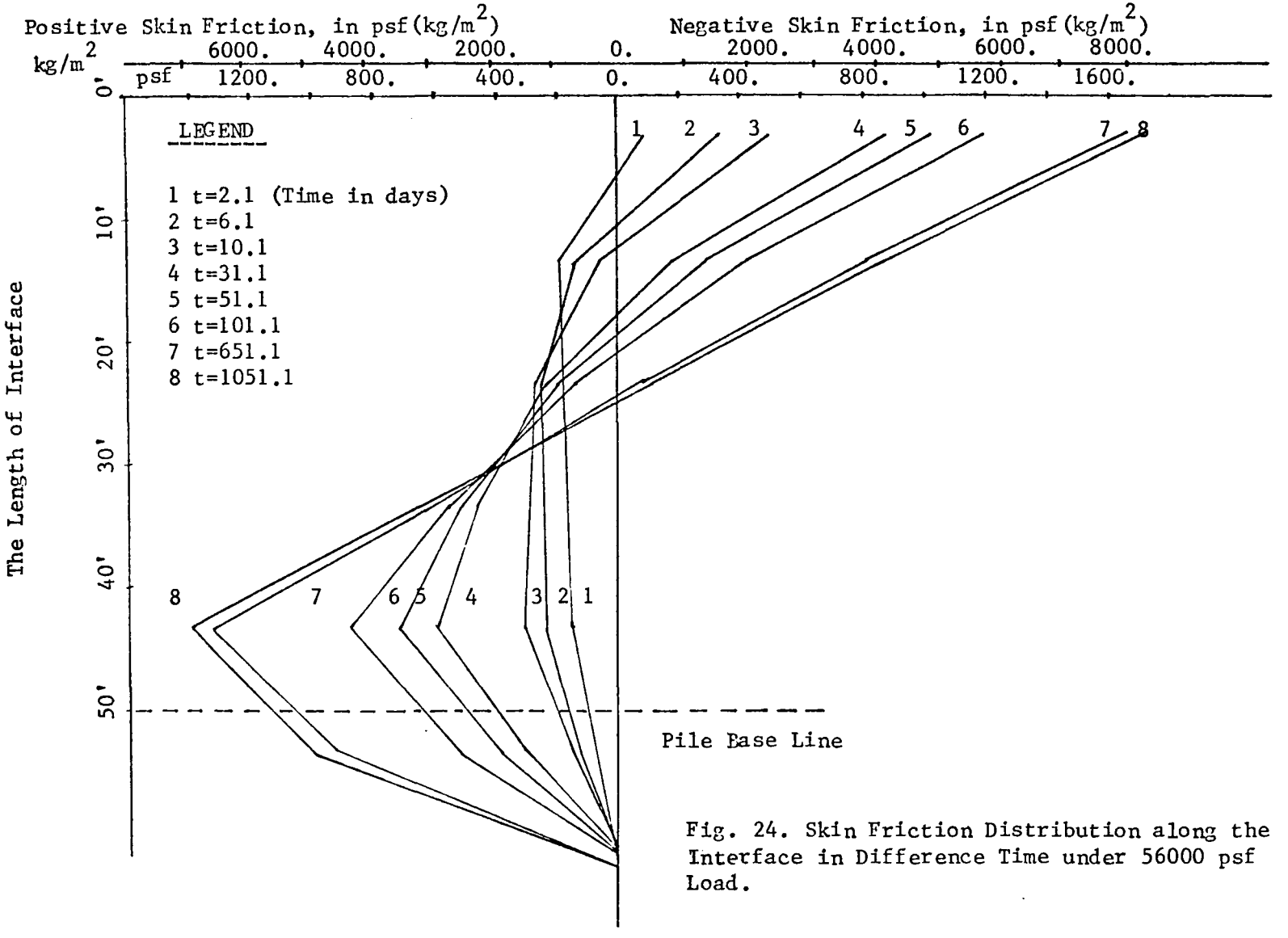

Fig. 24. Skin Friction Distribution along the Interface in Difference Time under 56000 psf Load.

load on the pile decreases with the increasing load, since negative skin friction on the pile becomes smaller whereas positive skin friction becomes larger. This conclusion is indicated in Fig. 25c. which shows the influence of the applied load on the downdrag load. It is interesting to find that there is no downdrag load beyond an applied load about 52,000 lb/ft^2 (253,240 Kg/m^2).

The Influence of Time-Load History and Backfill

During construction procedure, the applied load and backfill are usually increased gradually within given time periods. To account for the effect of time-load history, the pile-top load was allowed to vary linearly within 31.1 days, from a value of zero to 7,000 lb/ft^2 (34,090 Kg/m^2), and then it may maintain at the value of 7,000 lb/ft^2. The consolidation was permitted for 220 days and then the backfill increased linearly within a 20 day period (from 251.1 days to 271.1 days) from zero to 4,000 lb/ft^2 (19,480 Kg/m^2), Fig. 26. The settlement near the pile top (node 68 for soil, node 51 for pile) and pile tip (node 58 for soil, node 41 for pile) is shown in Fig. 27. In the initial stage, the pile settled more than the soil. After the backfill was applied, the pile and soil abruptly settled by a large amount, and in the upper zones, the soil settled somewhat more than the pile. With the same loading procedure but with different pile-top loads (21,000 and 56,000 lb/ft^2), the results were plotted, Figs. 28 and 29, respectively. The effect of the backfill caused a significant, sudden settlement and sudden change in the relative displacement in the upper part of the pile. But the effect of the

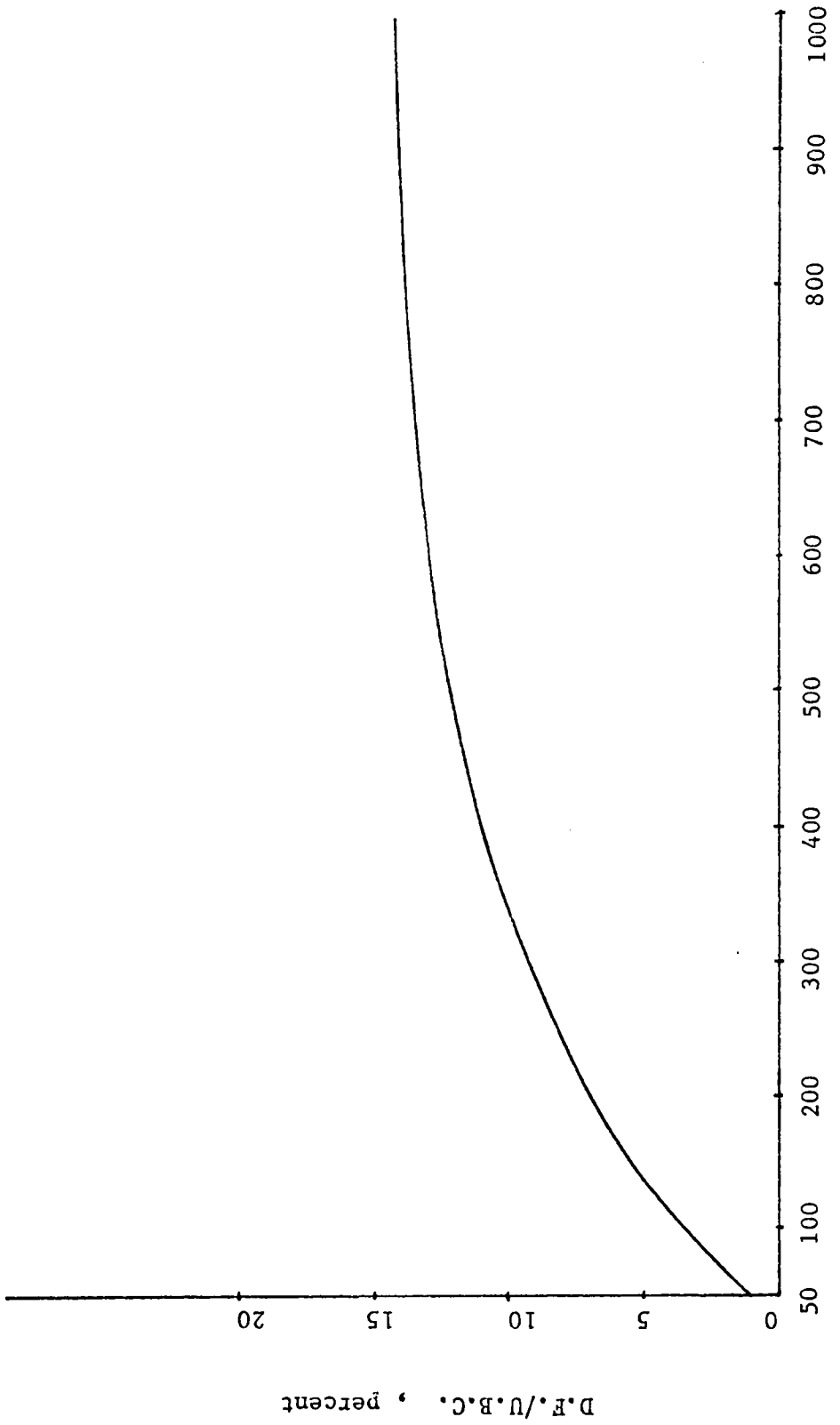

Fig. 25a. D.F./U.B.C. vs. Time (21000 psf Pile-Top Load)

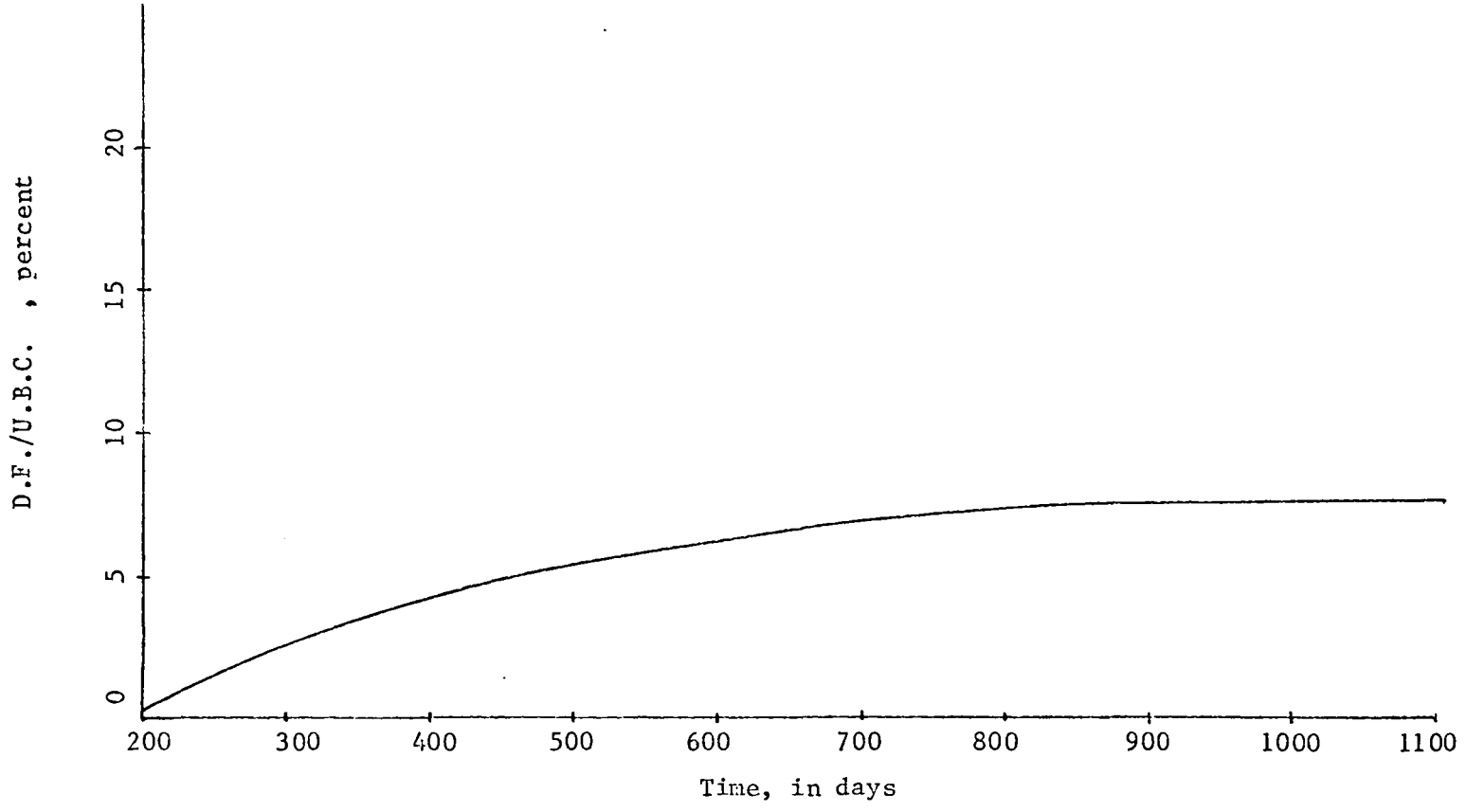

Fig. 25b. D.F./ U.B.C. vs. Time. (35000 psf)

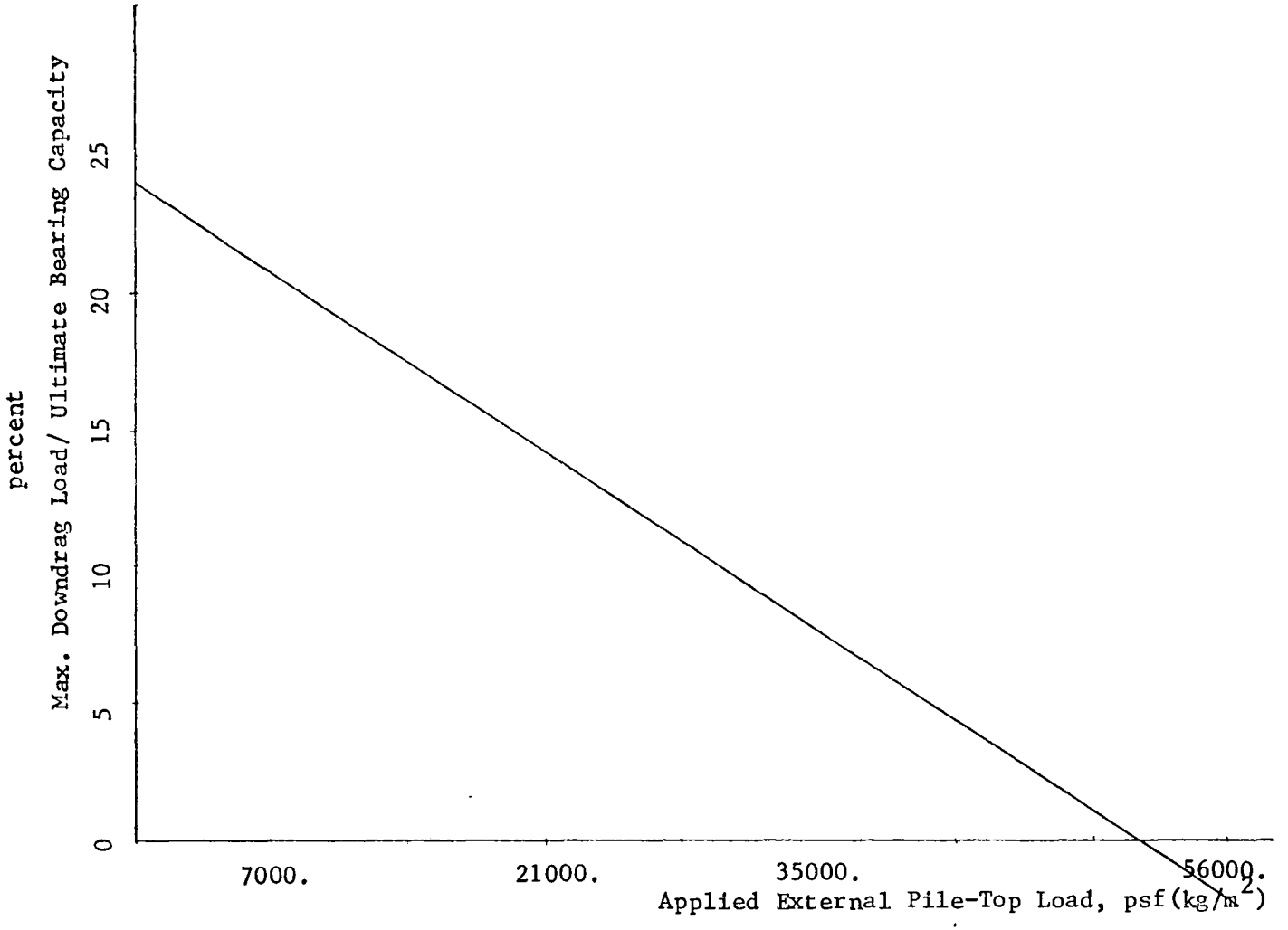

Fig. 25c. The Maximum Downdrag Load vs. Applied Pile-Top Load.

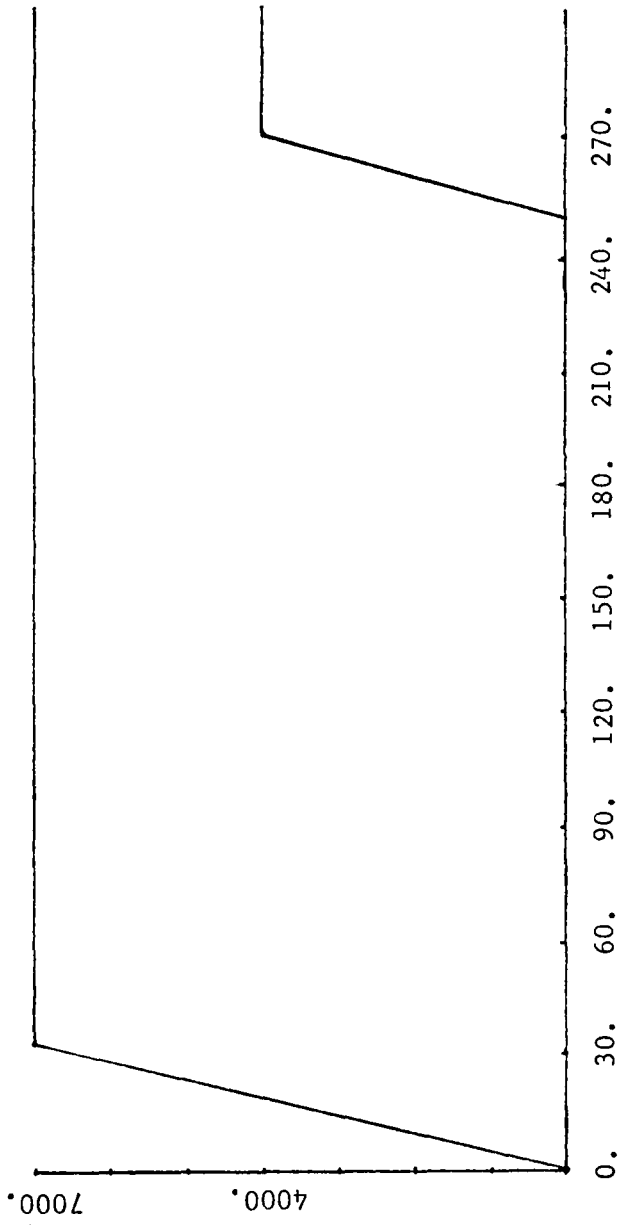

Fig. 26. Time-Load History

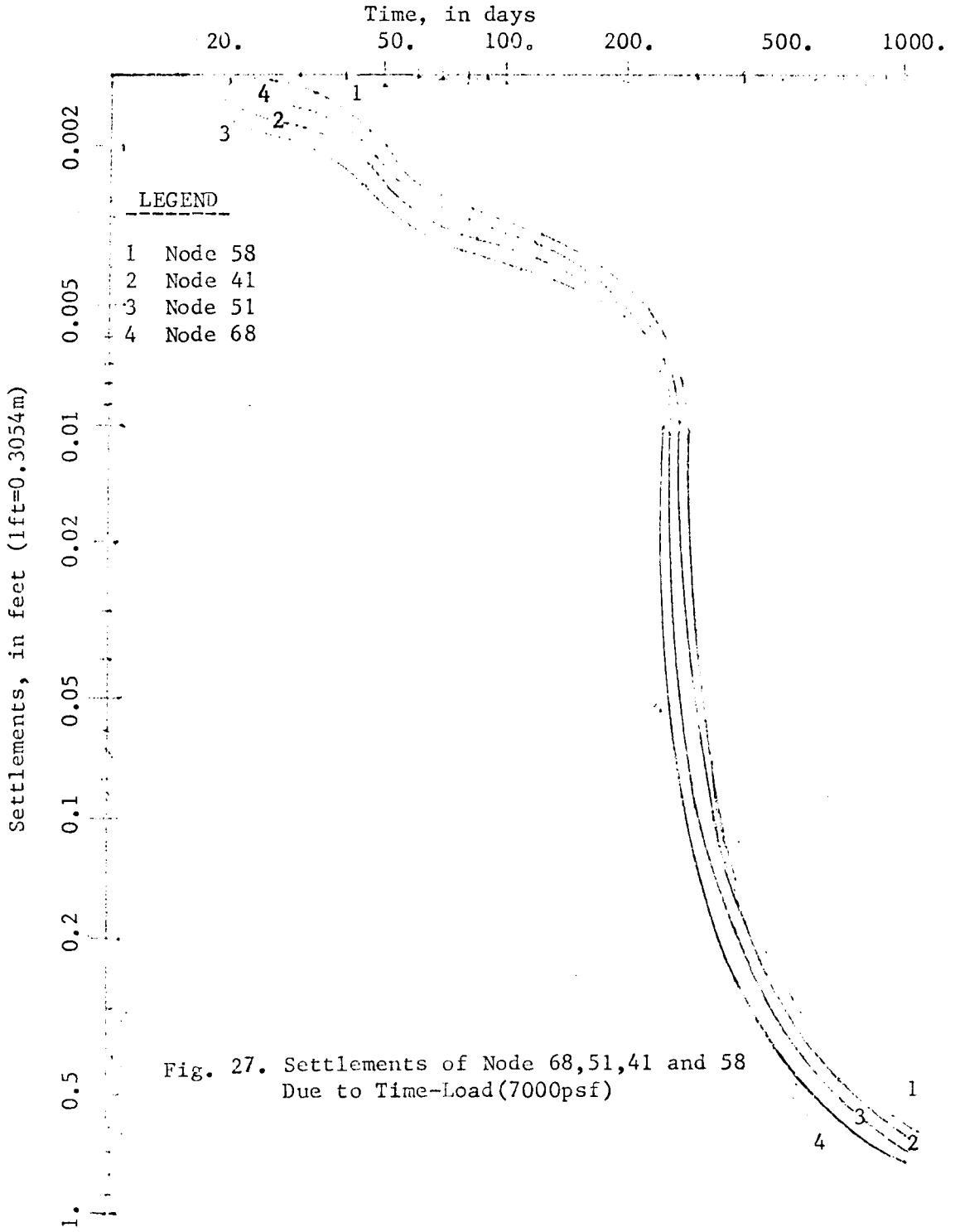

Fig. 27. Settlements of Node 68,51,41 and 58
Due to Time-Load(7000psf)

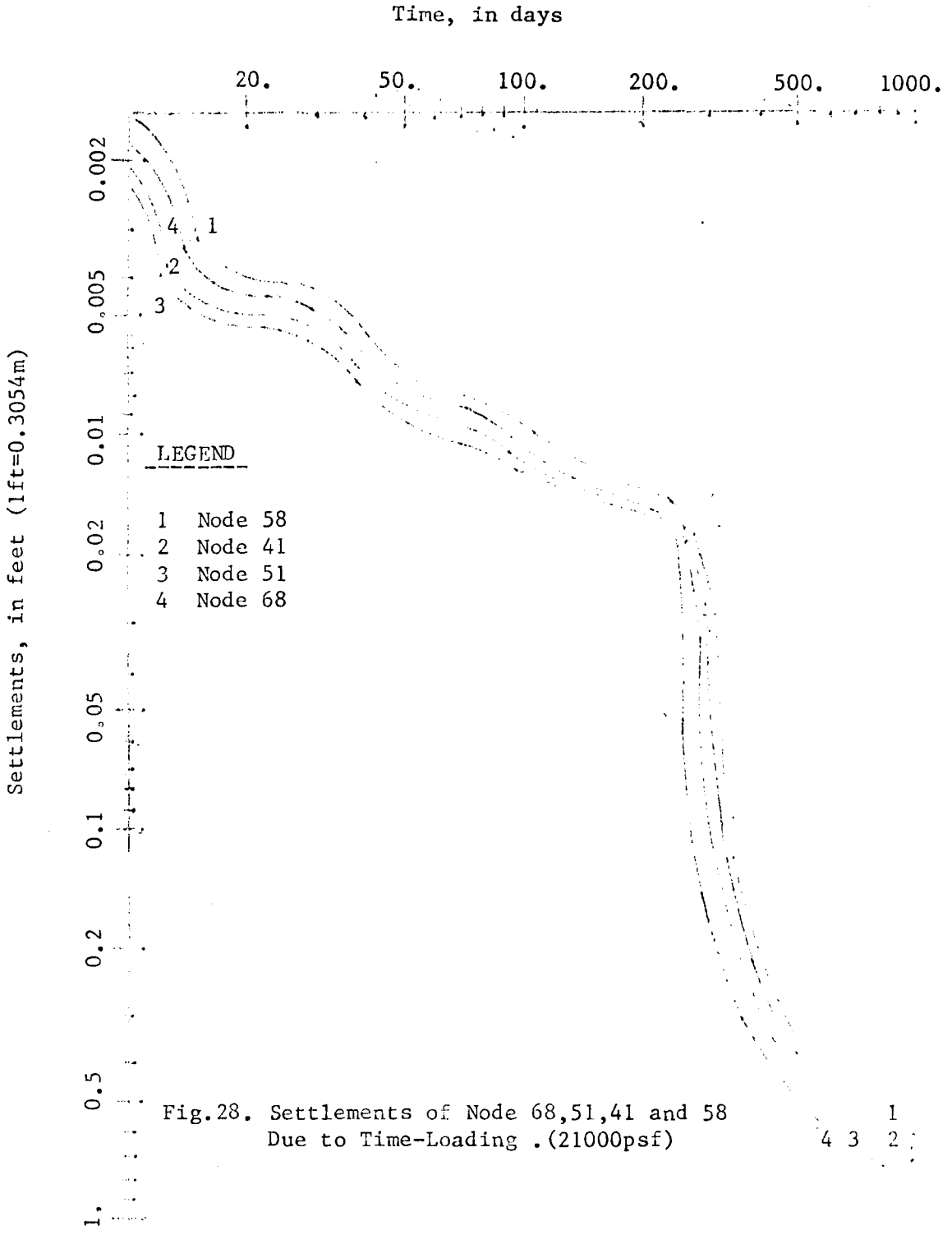

Fig.28. Settlements of Node 68,51,41 and 58 Due to Time-Loading .(21000psf)

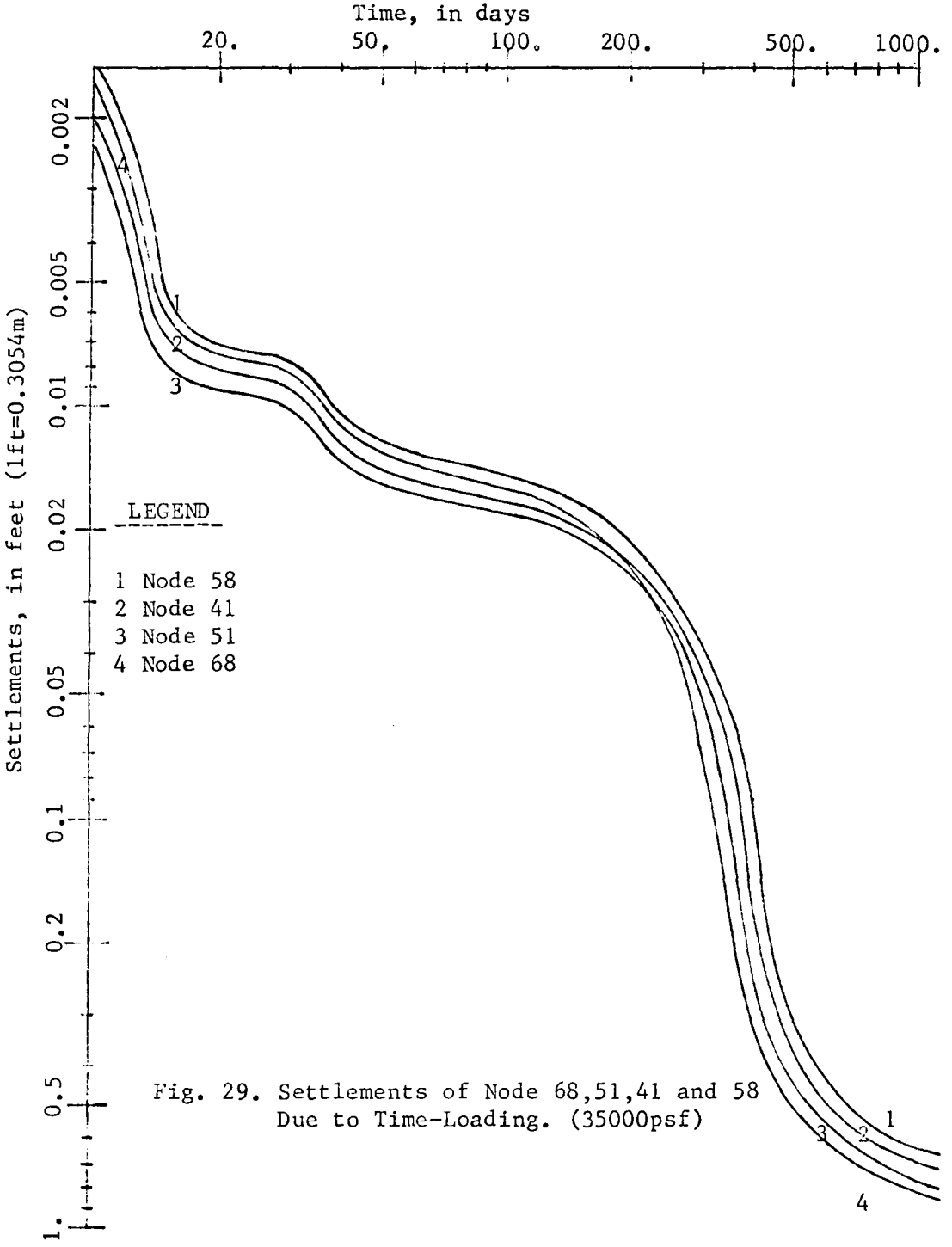

Fig. 29. Settlements of Node 68,51,41 and 58 Due to Time-Loading. (35000psf)

applied backfill diminished as the pile-top load increased.

The skin friction distributions along the pile-soil interface with different pile-top loads (7,000, 21,000 and 56,000 lb/ft^2) are as shown in Figs. 30, 31 and 32, respectively. Before the backfill was applied, positive skin friction occurred almost along the whole pile-soil interface. After the backfill was applied, negative skin friction started to occur in the upper parts of the pile.

We can conclude that the backfill plays an important role in causing negative skin friction. This friction caused by the backfill appears to disappear when the applied pile-top load was very large. Fig. 33d shows that when the applied pile-top load exceeded 52,000 lb/ft^2 (253,240 Kg/m^2), there was no downdrag load. The results were approximately the same when the pile-top load and backfill were applied simultaneously. In spite of the different loading conditions, (as indicated in Figs. 12, 17, 18, 19, 20, 26, 27 and 28 with the same backfill 4,000 lb/ft^2), the results of the final soil settlement at pt. 68 are the same. However, the variations of downdrag loads and the rates of settlements are influenced significantly if the time history of loading is included.

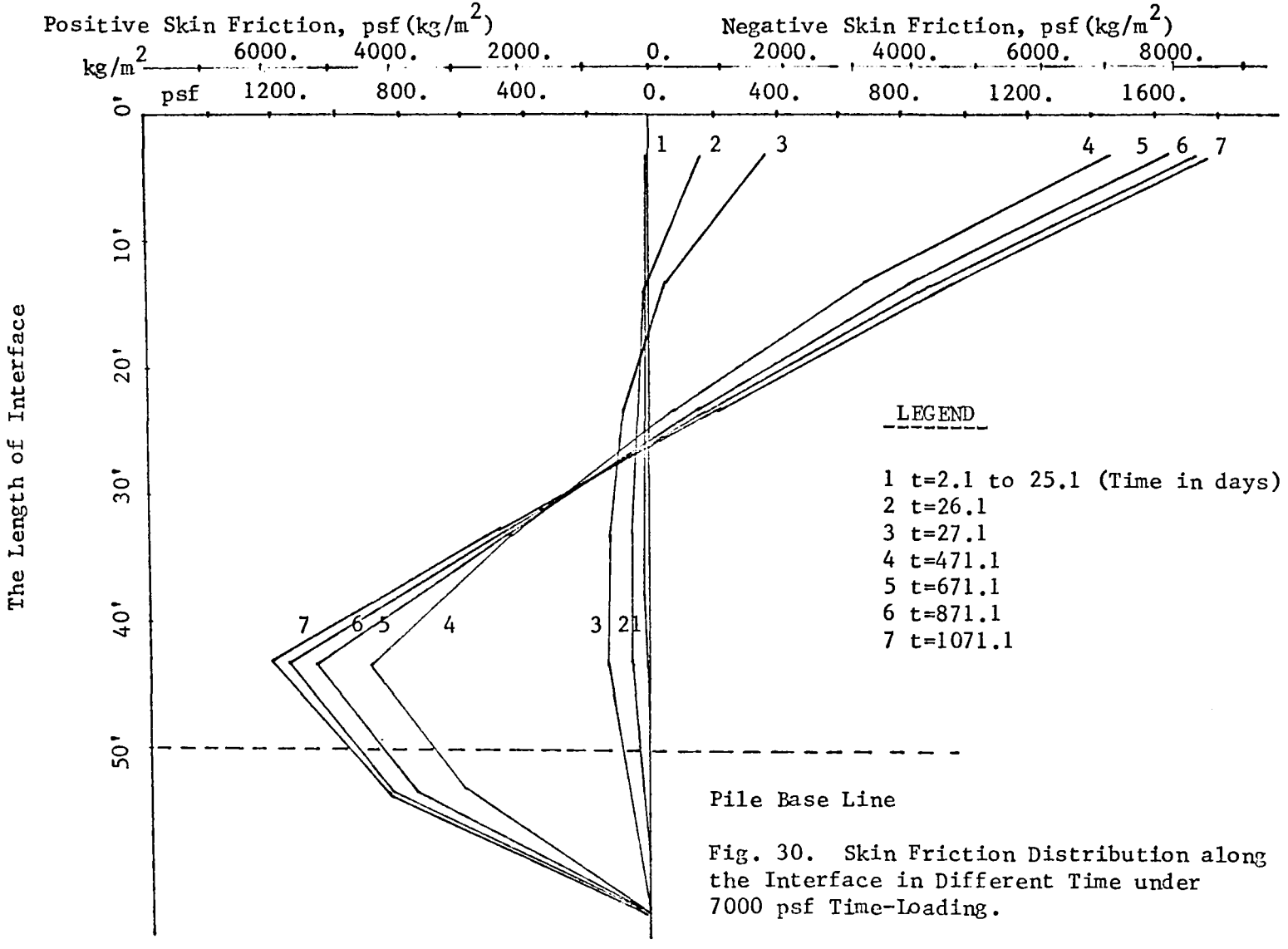

Fig. 30. Skin Friction Distribution along the Interface in Different Time under 7000 psf Time-Loading.

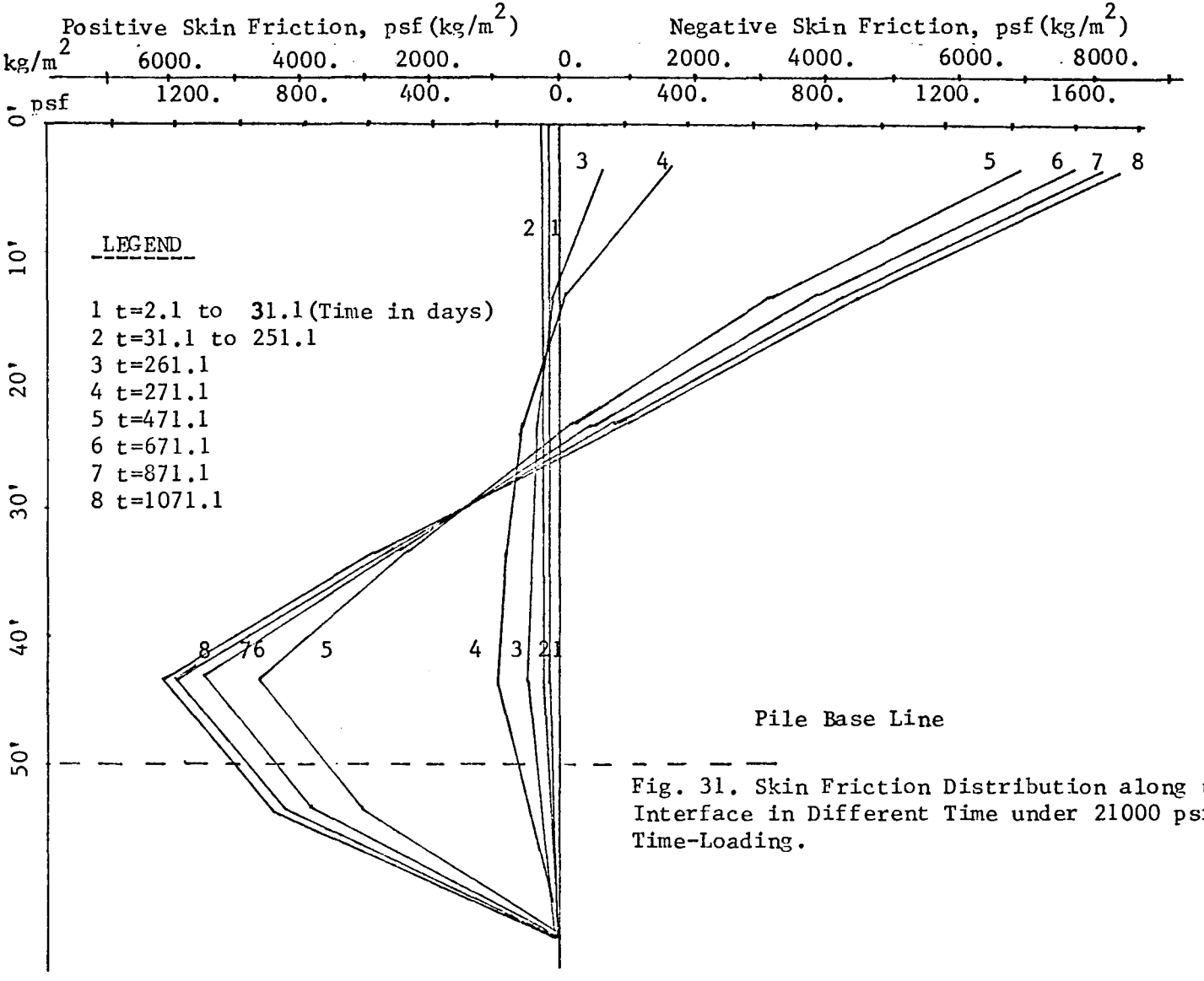

Fig. 31. Skin Friction Distribution along the Interface in Different Time under 21000 psf Time-Loading.

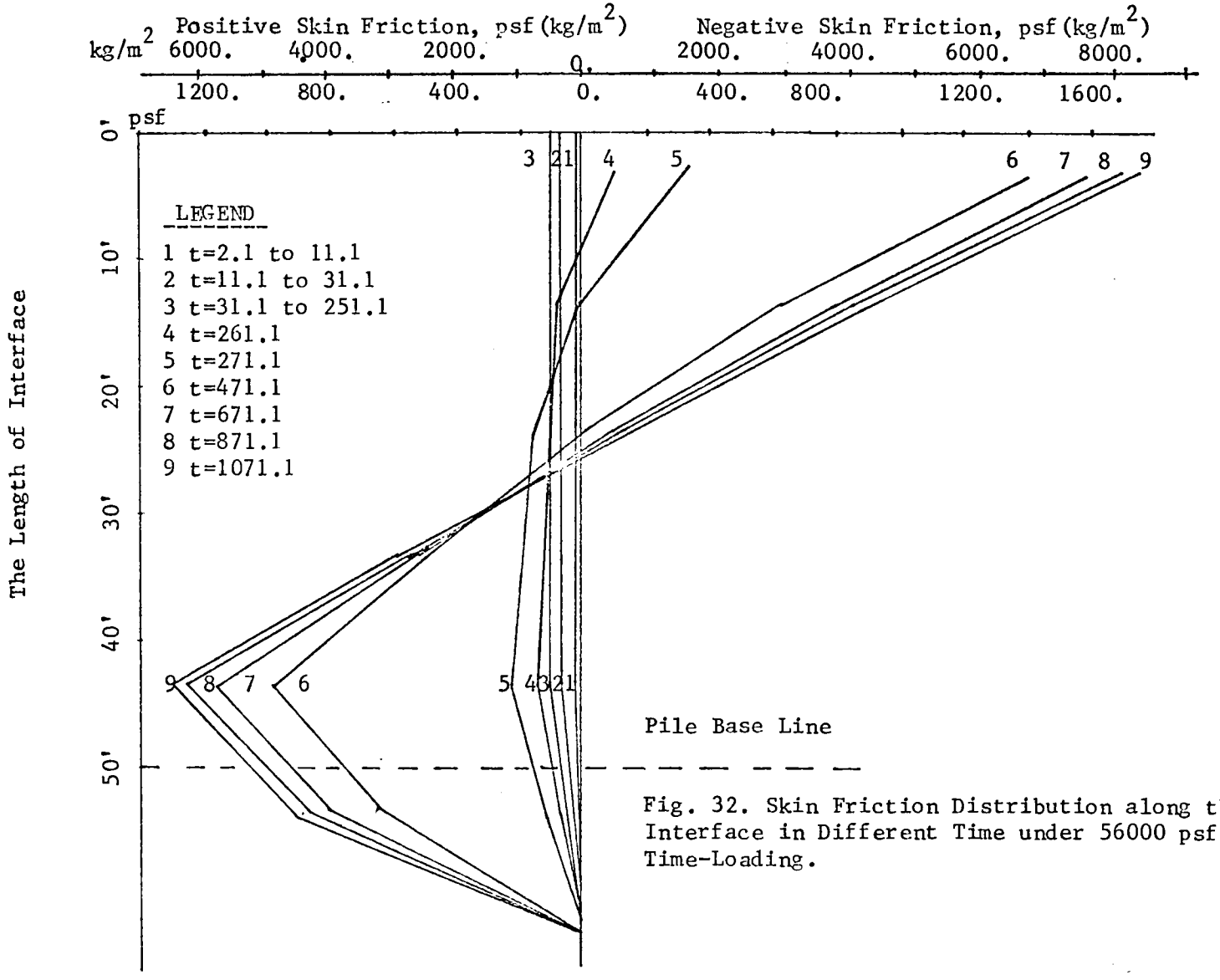

Fig. 32. Skin Friction Distribution along the Interface in Different Time under 56000 psf Time-Loading.

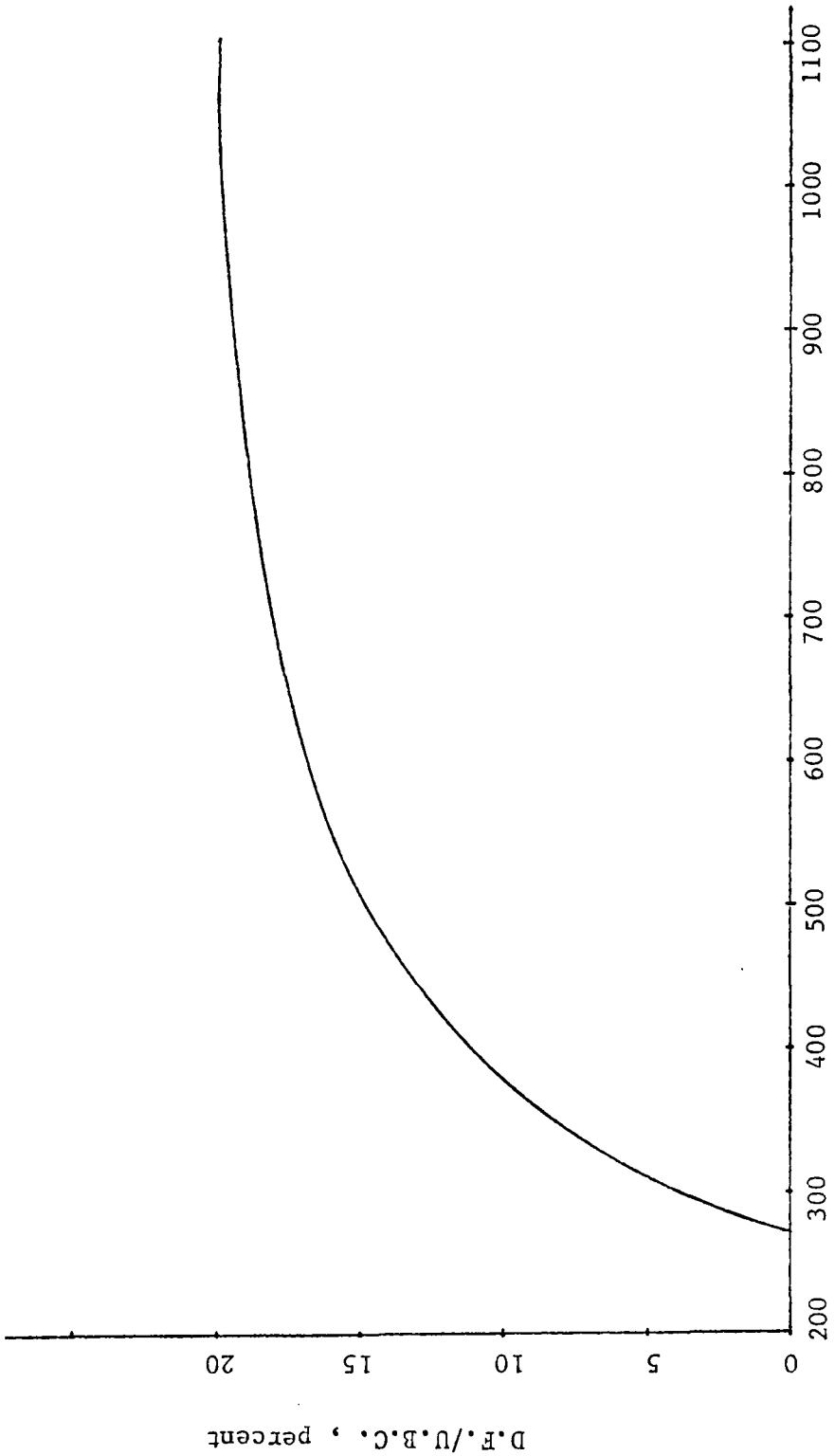

Fig. 33a. D.F./U.B.C. vs. Time.(7000 psf Time Loading)

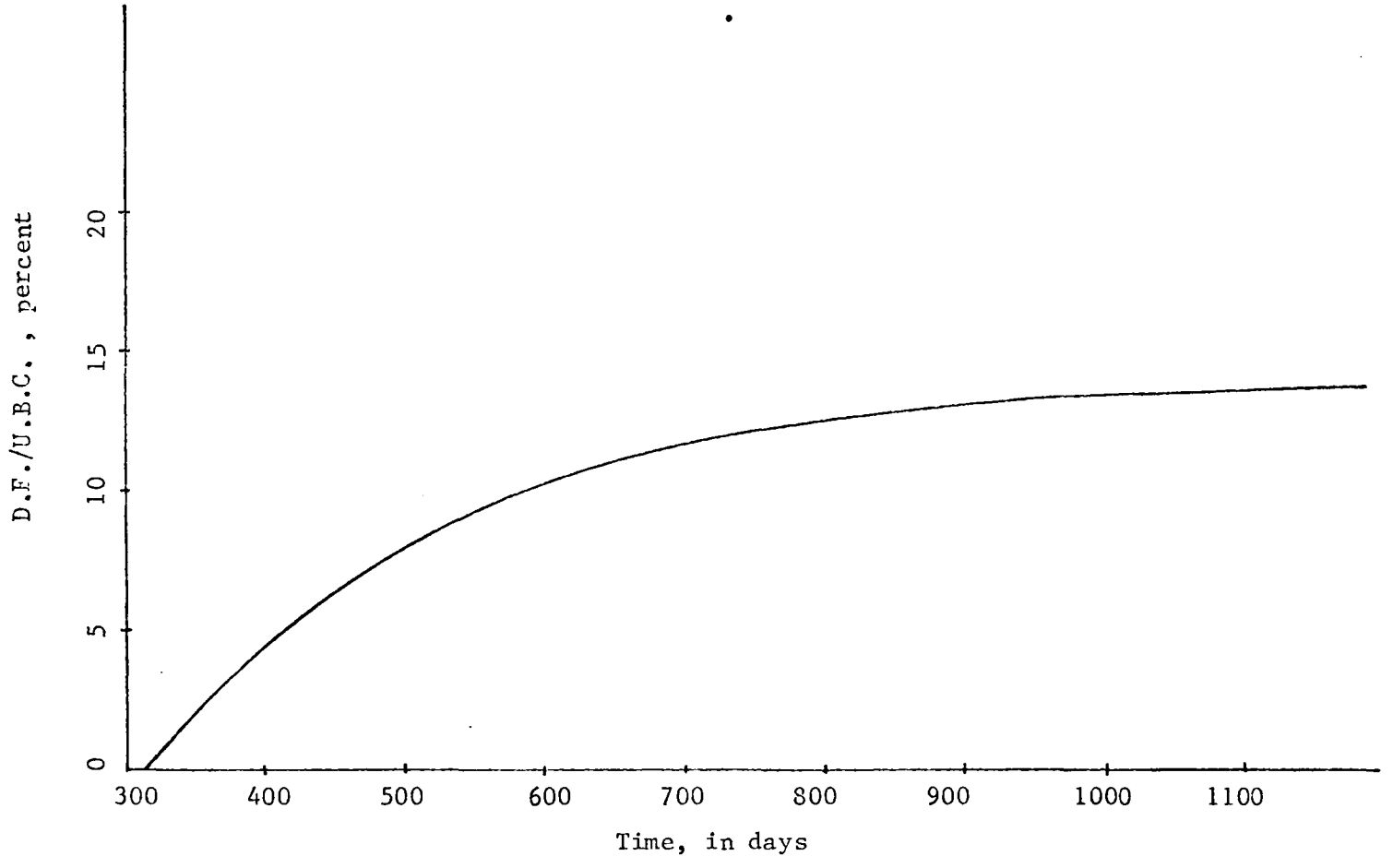

Fig. 33b. D.F./U.E.C. vs. Time (21000psf Time Loading)

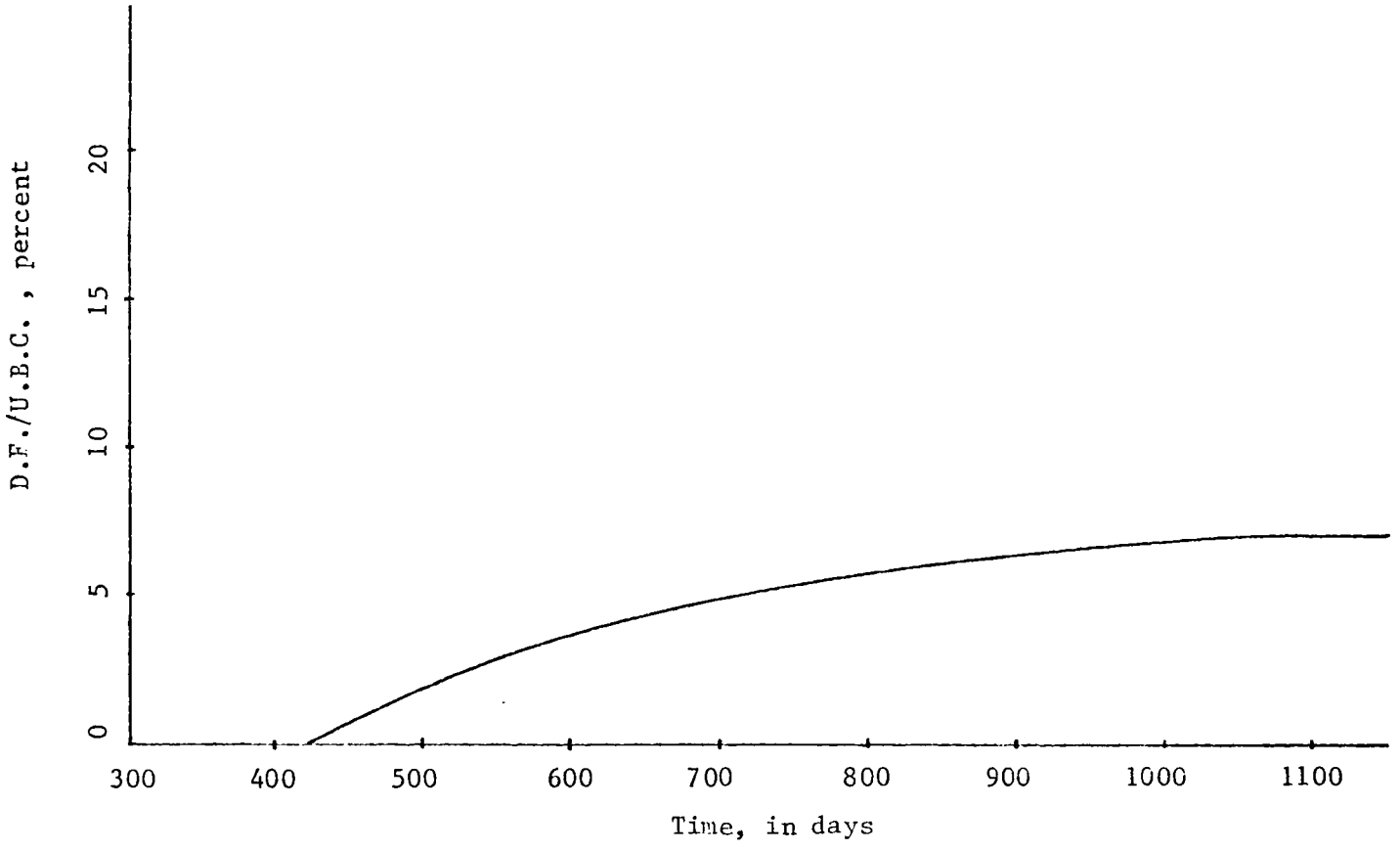

Fig. 33c. D.F./U.B.C. vs. Time. (35000psf Time Load)

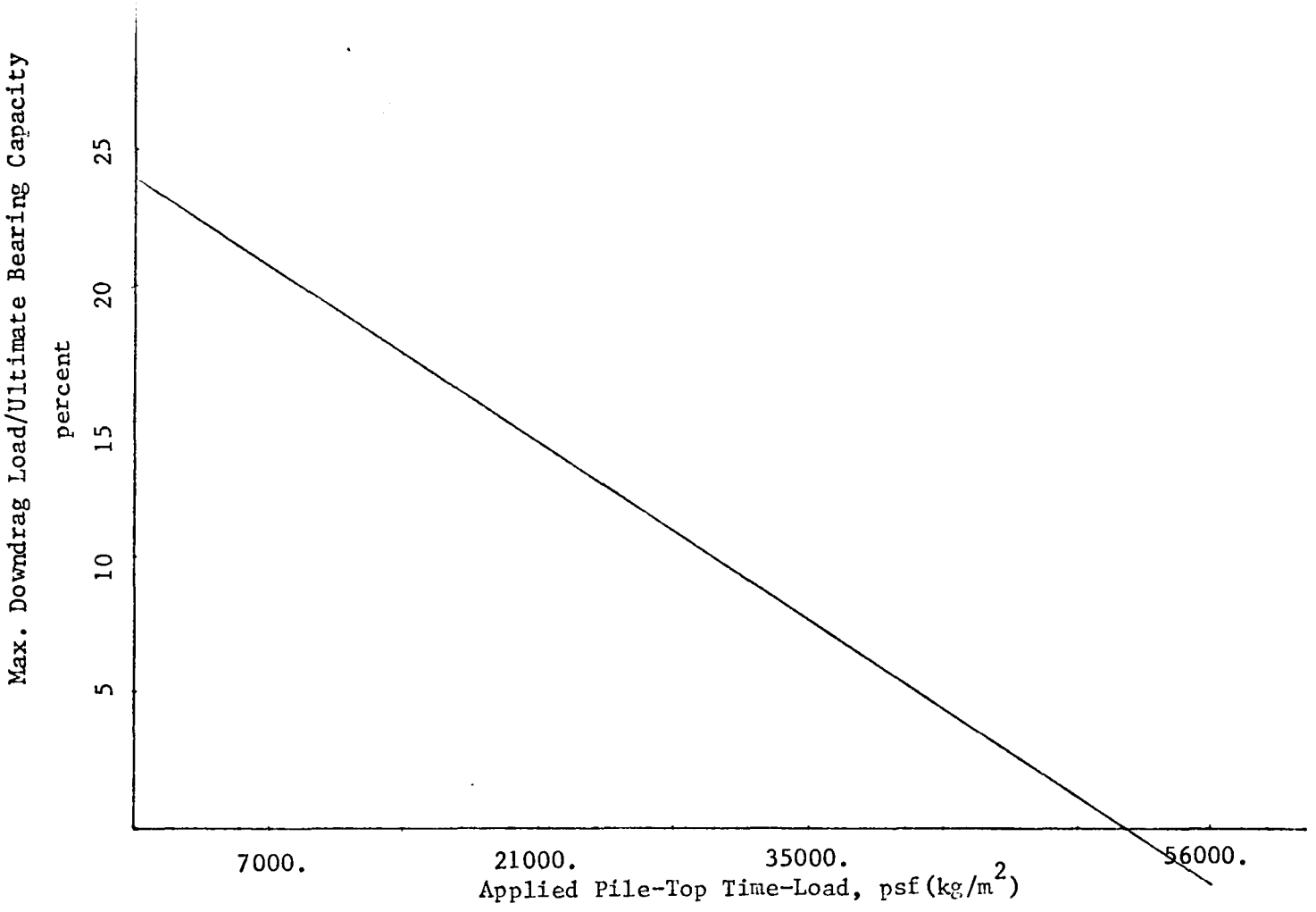

Fig.33d. The Maximum Downdrag Load vs. Applied Pile-Top Time-Load.

Chapter VI

SUMMARY, CONCLUSIONS AND RECOMMENDATIONS

Summary

The purpose of this study was to predict settlement, rate of settlement and negative skin friction effects and downdrag force on a pile caused by consolidation of the surrounding soils. This was done by FE.

The finite element method was based on axisymmetric idealization. It was applied for a number of cases that can cause negative skin friction.

The influence of negative skin friction caused by consolidation due to gravity, due to backfill and due to backfill with external load were investigated. The results in terms of downdrag force as a percentage of ultimate bearing capacity total amount of downdrag force and location of neutral point compared well with results from conventional method and field observations. An interesting finding was that for a given backfill loading, the downdrag effects are negligible if the pile loading was high, somewhere around 0.6 of the ultimate bearing capacity. The inclusion of time history influences the rate of settlements and variation of skin friction but not the ultimate settlements.

Conclusions and Recommendations

The results of this investigation have shown that the Finite Element procedure can be very useful in predicting the maximum

downdrag load on the pile structure. From the analysis, the following conclusions and remarks can be made:

1. The relative displacement between the pile and the soil controls the skin friction effects; negative skin friction occurs as the soil settles more than the pile; otherwise positive skin friction occurs.
2. A neutral point exists where the axial stress in a pile is maximal. The ratio of the depth to the neutral point in relation to the length of the pile is found to be around 0.6 in this investigation.
3. A predicted maximum downdrag load (assuming the negative skin friction to be the average shear stress near the pile-soil interface) is in agreement with the formula given by Endo et al. (31) based on field data. The two methods compared above are more reasonable than the -method which overestimates the downdrag load by assuming that negative skin friction occurs along the whole pile.
4. A long time is required for the negative skin friction to fully develop when the relative velocity of the pile-soil settlement is small. After the negative skin friction is fully developed, it has no tendency to get smaller with a decrease in the relative velocity between the pile and soil. Maximum negative skin friction usually occurs at a relative displacement of 0.4 (1.0 cm) to 0.5 inches (1.27 cm). Even if the relative displacement increases further, the

negative skin friction will remain essentially constant.

5. However, there is a tendency for the negative skin friction effect to get smaller with an increase in the applied pile-top load.
6. The backfill plays an important role in the negative skin friction effect but could be ignored when the applied pile-top load is large. This conclusion will require additional study.
7. The time-load history has an influence only on the intermediate characteristics of the settlements and skin frictions. The final results in terms of settlements are the same no matter whether the load is fully applied and kept constant or is increased gradually.
8. The final settlements of the soil under the same backfill but with different applied pile-top loads are almost the same.

Finally, the analysis presented herein with some modifications can be extended to problems with layered media and initial applied porepressures.

BIBLIOGRAPHY

1. Terzaghi, K. and Peck, R. B., Soil Mechanics in Engineering Practice, John Wiley and Sons, Inc., New York, 1968.

2. Rendulic, L., "Porenziffer und Porenwasserdruck in Tonen", Der Bouingenieur, vol. 17, no. 51/53, 1936, pp. 559-564.

3. Schiffman, R. L., "An Analysis of Consolidation Theories", Journal of Soil Mechanics and Foundations Division, ASCE, vol. 95, no. SM1, 1969, pp. 285-312.

4. Biot, M. A., "Consolidation Settlement of a Soil with an Impervious Top Surface", Journal of Soil Mechanics and Foundation Division, vol. 12, 1941, pp. 578-582.

5. Desai, C. S., "Analysis of Consolidation by Numerical Methods", Proc. Symp. on Recent Developments in the Analysis of Soil Behavior and Their Application to Geotechnical Structures, University of NSW, Australia, July, 1975.

6. Sandhu, R. S., Fluid Flow in Saturated Porous Elastic Media, Ph.D. Thesis, University of California, Berkeley, 1968.

7. Sandhu, R. S. and Wilson, E. L., "Finite Element Analysis of Seepage in Elastic Media", Journal of Engineering Mechanics Division, ASCE, vol. 95, 1969, pp. 641-652.

8. Sandhu, R. S., "Finite Element Analysis of Soil Consolidation", Geotechnical Engineering Report No. 6, The Ohio State University Research Foundation.

9. Biot, M. A., "Theory of Elasticity and Consolidation for a Porous Anisotropic Solid", Journal of Applied Physics, vol. 26, no. 2, Feb. 1955.

10. Biot, M. A., "Consolidation Settlement Under a Rectangular Load Distribution", Journal of Applied Physics, vol. 12, 426-430, (1941).

11. Biot, M. A., "Theory of Deformation of a Porous Viscoelastic Anisotropic Solid", Journal of Applied Physics, vol. 27, no. 5, pp. 459-467, (1956).

12. Biot, M. A., "The Elastic Coefficients of the Theory of Consolidation", J. App. Mech., Am. Soc. of Mech. Engrs., pp. 594-601, (1957).

13. Schiffman, R. L., Chen, A. T. F. and Jordan, J. C., "An Analysis of Consolidation Theories", ASCE, vol. 95, 1969, pp. 285-312.

14. Desai, C. S. and Johnson, L. D., "Evaluation of Some Numerical Schemes for Consolidation", International Journal of Numerical Methods in Engineering, vol. 7, 1973, pp. 243-254.

15. Yokoo, Y., Yamagata, K. and Nagaonka, H., "Finite Element Analysis of Consolidation Following Undrained Deformation", Soils and Foundations, vol. 11, no. 4, 1971, pp. 37-58.

16. Yokoo, Y., Yamagata, K. and Nagaonka, H., "Variational Principles for Consolidation", Soils and Foundations, vol. 11, no. 4, 1971, pp. 25-35.

17. Christian, J. T. and Boehmer, J. W., "Plane Strain Consolidation by Finite Elements", ASCE, Journal of Soil Mechanics and Foundations Engineering Div., vol. 96, no. SM4, 1970, pp. 1435-1457.

18. Christian, J. T., Boehmer, J. N. and Martin, P. P., "Consolidation of a Layer Under a Strip Load", Proceedings, ASCE, J. Soil Mechs. and Found. Engrg. Div., vol. 98, no. SM7, 1972, pp. 693-707.

19. Desai, C. S., "Analysis of Consolidation by Numerical Methods", Proc. Symp. on Recent Developments in the Analysis of Soil Behavior and Their Application to Geotechnical Structures, University of NSW, Australia, July, 1975.

20. Asproudas, S. A. and Desai, C. S., "Analysis and Applications of a Finite Element Procedure for Consolidation", M.S. Thesis, VPI & SU, 1975.

21. Desai, C. S. and Saxena, S. K., "Consolidation Analysis of Layered, Anisotropic Foundation", Int. J. Num. Analy. Methods in Geomech., vol. I, no. 1, 1977.

22. Martin, H. L., "Implementation and Comparison of the Biot and Terzaghi-Rendulic Theories of Consolidation", Ph.D. Thesis, University of Colorado, Boulder, Colorado, 1976.

23. Ghaboussi, J. and Wilson, E. L., "Flow of Compressible Fluid in Porous Elastic Media", Int. J. Numer. Meth. in Engrg., vol. 5, no. 3, 1973, pp. 419-442.

24. Valliappan, S., Lee, I. K. and Boonlualohr, P., "Finite Element Analysis of Consolidation Problems", Finite Element Methods in Flow Problems, Ed. Oden, J. T., Zienkiewicz, R. H., Gallagher, R. H. and Taylor, C. University of Alabama at Huntsville Press, Alabama, (1974).

25. Miller, R. M., "Soil Reactions in Relation to Foundations on Piles", Trans. ASCE, vol. 103, 1938, pp. 1193.

26. Baligh, M. M. and Vivatrat, V., "A Manual on Precition of Pile Downdrag on End Bearing Piles", M.I.T., Nov. 1975, M.I.T. Geotechnical Publication no. 518, pp. 2-5.

27. Poulos, H. G. and Davis, E. H., "The Development of Negative Skin Friction with Time in End Bearing Piles", Research Report #R121, University of Sydney, 1969.

28. Begemenn, H. K. S., "Negative Skin Friction of a Single Pile", Proc. 7th ICSMFE, Mexico, 1969, Specialty Session 8.

29. Fellenius, B. H. and Broms, B. B., "Negative Skin Friction on Long Piles Driven in Clay", Proc. 7th ICSMFE, Mexico, 1969, Specialty Session 8.

30. Lambe, T. W., Garlanger, J. E. and Leifer, S. A., "Prediction and Field Evaluation of Downdrag Forces on a Single Pile", April, 1974, M.I.T. Publication no. 339, pp. 19.

31. Endo, M., Kawasaki, T. and Shibata, T., "Negative Skin Friction Acting on Steel Pipe Pile in Clay", Proceedings of 7th International Conference on Soil Mechanics and Foundation Engineering, Session 2, pp. 85-92, 1969.

32. Winterkorn, H. F. and Fang, H. Y., Foundation Engineering Handbook, Van Nostrand Reinhold Company, New York, 1975, pp. 572.

33. Fellenius, B. H., "Downdrag on Piles in Clay due to Negative Skin Friction", Canadian Geotechnical Journal, vol. 9, no. 4, Nov. 1972, pp. 336.

34. Terzaghi, K. and Peck, R. B., Soil Mechanics in Engineering Practice, 2nd Edition, John Wiley and Sons, Inc., New York, 1967.

35. Garlanger, J. E. and Lambe, T. W., "Proceedings of a Symposium on Downdrag of Piles", Research Report no. 73-56, Soil Publication no. 331, M.I.T., 1973.

36. Desai, C. S. and Abel, J. F., Introduction to the Finite Element Method, 1972, New York, Van Nostrand Reinhold Co.

The vita has been removed from the scanned document

FINITE ELEMENT ANALYSIS OF TIME DEPENDENT SETTLEMENTS AROUND PILE STRUCTURES

by

Lawrence Lo Chow

(ABSTRACT)

The purpose of this thesis is to use a finite element procedure for predicting settlement, rate of settlement and negative skin friction effects and downdrag force on a pile caused by consolidation of the surrounding soils.

The influence of negative skin friction caused by consolidation due to gravity, due to backfill and due to backfill with external load are investigated. The inclusion of time history is also evaluated.